

MSc Sustainable Energy Technology
Master Thesis

**Modelling the yield of building
integrated photovoltaic systems
employing free space
luminescent solar concentrators**

Anne Rikhof

Graduation Committee:
Prof.dr. Rebecca Saive
Prof.dr. André Ten Elshof
dr. Laura Franco Garcia

July, 2023

Department of Inorganic Materials Science,
Faculty of Science and Technology,
University of Twente

UNIVERSITY OF TWENTE.

Abstract

Solar panels generate electricity by absorbing the freely-available incoming solar irradiance, thereby playing an important role towards the renewable energy transition. Bifacial cells accept light from both faces, the front and rear, generating a higher output compared to their monofacial counterparts. If optimal reflectors are installed around a bifacial solar plant, the yield of the rear face can be enhanced even further. This combination of bifacial solar cells and reflectors also opens doors for new building-integrated photovoltaic (BIPV) designs. A novel material called the free space luminescent solar concentrator (FSLSC) can concentrate diffuse light, i.e. a wide range of wavelengths coming from different directions, into a narrow cone, which can be directed towards a solar cell to increase its PV yield. This thesis aims to enhance the annual yield of the system by optimizing the cone size of the FSLSC. This is done by extending a reverse ray tracing model with a model of the properties of an FSLSC.

When a bifacial module is placed in front of an FSLSC and the module's tilt and distance to the FSLSC are varied, the results indicate that a cone size of approximately 40 degrees yields the highest short-circuit density, assuming realistic loss properties of the material. At this angle, there is an optimal balance between the yield increase due to the concentration factor and the yield decrease due to the increasing loss mechanism occurrences as result of the light being trapped longer in the FSLSC. Applying an FSLSC on a house's façade, redirecting the light to a solar fence, shows an annual yield increase of the solar fence of 39.3%, outperforming an optimally tilted monofacial solar panel up to 58% in winter. Comparing this to a specular (mirror-like) and diffuse reflector, the annual yield of the solar fence can be increased to 47,1% and 20.9%, respectively. Safety risks concerning specular reflectors eliminate this from being a socio-economically acceptable option, showing that the FSLSC is the reflector with the largest increase in yield while limiting the negative socio-economic impact of the studied reflectors. Future research should be aimed at further enhancing the FSLSC's yield by optimizing the cone tilt for which a methodology is proposed.

Keywords: Solar Energy, Light Concentration, Bifacial Solar Cells, Spectro-Angular Emission, Reflectors

Acknowledgements

During the time of my master's assignment, I was supported by many people, to whom I would like to express my gratitude. First of all, Rebecca, thank you for giving me the opportunity to do this assignment. I remember when we first talked about a possible assignment, I mentioned that I would like to learn more about simulation and modelling and I think you came up with an assignment where I could really grow in this regard. So thank you!

I would also like to thank André and Laura for being my committee members.

Furthermore, I would like to thank everyone in the group. First of all, Shweta, thank you for starting with the code and spending countless hours explaining the reverse ray tracing code to me or answering any other questions. Then, of course, Leonie, for being there during every baby step that I took during this project. I will definitely miss sitting across from you and staring at your face for 40+ hours per week. I really had a great time! Thanks to Jelle, for the physics classes that you gave me and the feedback on the report. Also, a thank you to Mathis and George for your feedback on the report, and to Jian-Yao and Zeinab for your input during group meetings. Although not part of the group, also Daan is thanked for reviewing this report.

Also a big thanks to Wout, for the early-morning and late-evening discussions on the project, giving feedback on the report, and your endless support.

Contents

1	Introduction	1
1.1	Solar Panels	1
1.1.1	Monofacial and Bifacial Solar Cells	2
1.1.2	Building Integrated Photovoltaic Designs	2
1.2	Free Space Luminescent Solar Concentrators	3
1.2.1	Possible Use-cases	4
1.2.2	Knowledge Gap	5
1.3	Focus and Outline of Thesis	6
2	Theoretical Framework	7
2.1	Solar Definitions	7
2.2	Reflectors	8
2.3	Bidirectional Reflectance Distribution Function	9
2.4	Influencing Factors to Reflection	9
2.5	Free Space Luminescent Solar Concentrators	11
2.5.1	Nanophotonic Coating	12
2.5.2	Luminophore-Embedded Waveguide	13
2.5.3	Ideal Case	14
2.5.4	Non-Ideal Case	15
2.6	Optimizing Reflectors	16
2.6.1	Calculation Yield	16
2.6.2	Multi-Criteria Analysis	17
2.7	3D Reverse Ray Tracing Model	18
2.7.1	Part A: Calculation of Geometry	18
2.7.2	Part B: Calculation of Short-Circuit Current Density	18
2.7.3	Results Tilt vs Height	21
3	Model Description	24
3.1	FSLSC Model	24
3.1.1	Short-Circuit Current Density Directly from the Sky	26
3.1.2	Short-Circuit Current Density from Specular Reflection	27
3.1.3	Short-Circuit Current Density from Ideal Cone Emission	27
3.1.4	Short-Circuit Current Density from Real Emission Cone	28
3.1.5	Validation of the Model	29
3.1.6	Usage of the Model	30
3.2	Calculation Annual Yield	31
3.2.1	Calculation Power	31
3.2.2	Irradiance	32
3.2.3	Annual Yield from Direct Irradiance	32

3.2.4	Annual Yield from Diffuse Irradiance	33
3.3	Multi-Criteria Analysis	33
4	Results & Discussion of a Generic FSLSC	35
4.1	Case setup	35
4.2	Ideal Properties	36
4.3	Real Properties	39
5	Case Study: FSLSC on Façade	43
5.1	Case setup	43
5.2	Azimuth & Elevation Occurrences	44
5.3	Front & Specular Reflection on FSLSC	45
5.4	Ideal Properties	45
5.5	Real Properties	48
5.6	Comparison between Real FSLSC, Specular, and Diffuse Reflector	50
5.6.1	Short-Circuit Current Density Comparison	50
5.6.2	Yield Comparison based on Direct Irradiance	53
5.6.3	Yield Comparison based on Diffuse Irradiance	55
5.6.4	Annual Yield Comparison	56
5.6.5	Multi-Criteria Analysis	60
6	Discussion of Model	63
6.1	FSLSC Model	63
6.2	Yield Calculation	64
6.3	Possible Extension of the Model	65
7	Conclusion	66
	Bibliography	67
A	Model	72
A.1	Tips for running the model	72
A.2	Required Files to Run Code	73
B	Elaborated Results	74
B.1	Occurrences Azimuth and Elevation	74
B.2	Façade Case - Angles	75
B.3	Façade Case - Emission Cone	75
B.4	Monthly Yield	76
B.5	Comparison Reflectors - Every Angle	77
C	Code	79
C.1	FSLSC Code - Parameter Document	79
C.2	FSLSC Code - Looping over azimuths & Elevations	89
C.3	FSLSC Code - Subfunctions	100
C.3.1	CurrentOneModule	100
C.3.2	EmissionConePlotter	101
C.3.3	FluxToCurrentOneModulePixel	102
C.3.4	Illumination	103
C.3.5	IncomingUsefulFluxComputer	104
C.3.6	interpolateCone	105

C.3.7	Polygon	105
C.4	Yield Calculation Code	106
C.4.1	DiffuseYieldCalculator	110
C.4.2	DirectYieldCalculator	111
C.5	Data Analysis Codes	112
C.5.1	Extracting Occurance Matrix	112
C.5.2	Extracting Irradiance Data	115

List of Abbreviations

AM - Air mass
BAPV - Building adopted photovoltaics
BIPV - Building integrated photovoltaics
BRDF - Bidirectional reflectance distribution function
DHI - Diffuse horizontal irradiance
DNI - Direct normal irradiance
EQE - External quantum efficiency
FSLSC - Free space luminescent solar concentrator
GHI - Global horizontal irradiance
MCA - Multi-criteria analysis
NL - Netherlands
PV - Photovoltaics
QY - Quantum yield of luminophores
RRT - Reverse ray tracing

List of Parameters

Symbol	Description	Unit
δ	Kronecker delta	-
η	Efficiency	-
θ	Elevation or zenith	deg
λ	Wavelength	m
ϕ	Azimuth	deg
Ω	Solid angle	sr
$d\omega$	Differential solid angle	sr
A	Area	m ²
C	Concentration factor	-
E	Irradiance	W m ⁻² ^a
f	BRDF function	sr ⁻¹
FF	Fill factor	-
j	Current density	mA cm ⁻²
L	Radiance	W m ⁻² ^a
M	Matrix	-
n	Refractive index	-
\dot{n}	Number of photons	-
P	Power	W
q	Charge	C
r	Radius	m
V	Voltage	V

^aDepends on the situation, can also be number of photons or per solid angle

List of Subscripts

subscript	Description
<i>ac</i>	acceptance cone
<i>es</i>	escape cone
<i>i</i>	incoming light
<i>id</i>	ideal
<i>m</i>	module
<i>MP</i>	maximum power
<i>oc</i>	open-circuit
<i>out</i>	outgoing light
<i>pix</i>	per pixel
<i>r</i>	reflected light
<i>rt</i>	reflector
<i>sc</i>	short-circuit
<i>tot</i>	total system

Chapter 1

Introduction

One of the sustainable development goals of the United Nations is "to ensure access to affordable, reliable, sustainable and modern energy for all" [1]. This highlights the importance of transitioning from fossil fuels towards renewable energies. Solar cells are one of the technologies which can generate electricity from the incoming solar irradiance, which is a freely-available renewable source. Solar energy therefore plays an important role towards the renewable energy transition.

In this chapter, the basics of solar panels will be explained in Section 1.1. Two types of solar panels, bifacial solar panels and building integrated photovoltaics, will be considered. In Section 1.2, a novel material system called free space luminescent solar concentrators will be introduced as a way to capture light and redirect this to solar panels. This could increase the yield of solar panels and expand the possibilities to integrate solar materials into buildings. Lastly, Section 1.3 presents the outline and the aims of this thesis.

1.1 Solar Panels

Solar panels are based on the photovoltaic (PV) effect, discovered by Becquerel in 1839 [2], where a voltage is generated in certain materials when they are illuminated. When this material is connected to an external circuit or load, an electrical current and thereby power can be generated.

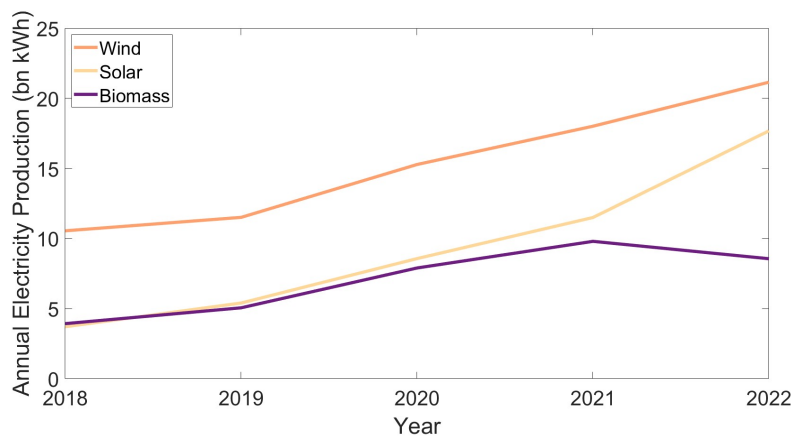


FIGURE 1.1: Renewable electricity production per source in the Netherlands from 2018 to 2022 [3]

Currently, solar energy plays a significant role in the renewable energy transition. Figure 1.1 illustrates the annual electricity production per renewable energy source from 2018 to 2022, showing that solar energy is becoming increasingly important in the Dutch electricity system and comprises a substantial part of the Dutch renewable electricity production [3]. Specifically, in 2022, a total of 118 TWh of electricity was generated in the Netherlands, of which solar energy accounted for 14.9% of the total electricity [3]. The Dutch renewable energy goal is to reach annually 55 TWh of renewable electricity by 2030, of which at least 35 TWh consists of a combination of solar and wind energy [4].

1.1.1 Monofacial and Bifacial Solar Cells

Monofacial solar cells are solar cells which accept light on one side and have been used most in the past [5]. Currently, bifacial solar cells are used more often [6], which are solar cells that accept light from both faces, the front and rear. In this manner, by capturing more light, they generate a higher output compared to their monofacial counterparts [7]. By optimizing reflectors or reflective properties of surrounding elements installed around a bifacial solar plant, the yield of the rear face can be enhanced further, leading to even more yield compared to a monofacial solar cell [8]. This also opens the doors for novel building integrated photovoltaic designs, as will be explained in the upcoming section.

1.1.2 Building Integrated Photovoltaic Designs

In the Netherlands, the majority of solar panels are currently placed on the roofs of buildings, although Dutch roofs do not provide enough space for solar panels to reach the Dutch renewable energy goals [9]. According to the Dutch NOVI policy, new PV systems should preferably be attached to buildings, specifically roofs and façades, and other locations are only considered afterwards [9]. Therefore, a lot of research is being done into new configurations to install solar cells onto buildings [10, 11, 12, 13].



FIGURE 1.2: BIPV applied as A) frameless modules, B) tiles, C) shingles to roofs and D) to façades. Figures from [14]

In building integrated photovoltaics (BIPV), solar panels are an integral component of the building. The solar panels are not only generating electricity, but also a functional unit in the building structure or architecturally integrated into the building's design [11, 14]. By contrast, building adopted photovoltaics (BAPV) describe a situation where a PV system is added to an already finished building [14]. BAPV are currently the most common [14], conversely, BIPV have many advantages. It provides opportunities to save costs in building materials and labour [11, 13] and can contribute comfort to the building, by adding amongst others weather protection [14], thermal isolation [12, 14], electromagnetic shielding [14] and noise protection [14]. One of the key market drivers of BIPV is the European Directive 2010/31/EU [15], as according to this directive, all newly build residential and utility buildings should be 'nearly zero energy' after 2018 [13].

Two main categories of BIPV applications have emerged in the past, besides smaller sub-categories like shading devices or semi-transparent elements of fenestration [11]. Around 80% of the BIPV market is the application of rooftop mounted BIPV [10], where the PV modules replace the need for tiles [14]. In a well-integrated system, frameless modules are often used, as can be seen in Figure 1.2A. It is also possible to use either solar tiles or solar shingles to stay closer to the appearance of ordinary roof tiles [14]. For example, to meet with the Mediterranean roof traditions, solar tiles can also be used as shown in Figure 1.2B. For shale roofs, solar shingles like in Figure 1.2C can be used, offering a lot of options to integrate solar panels into the roof.

Another major field of BIPV application is on façades, which covers around 20% of the BIPV market [10]. An example can be seen in Figure 1.2D, here solar cells are added to the façade of a building. In addition to applying BIPV to new buildings, a large market potential lies in the renovation of urban buildings to new energy standards [12, 13].

Another perspective on BIPVs, and the subject of this thesis, is to use the building's surface to reflect solar irradiance to a bifacial solar module. This could be done by free space luminescent solar concentrators as will be explained in the upcoming section.

1.2 Free Space Luminescent Solar Concentrators

Whereas some solar rays can reach a solar panel directly, also a significant fraction of rays undergo reflection and refraction due to clouds, water vapour or dust particles [16]. This latter is called diffuse light and comes from all different directions, as can also be seen in Figure 1.3. In the Netherlands, the fraction of diffuse light can be as high as 55% of the total irradiance [17]. The intensity of this diffuse light is less than light falling directly on the panel, thereby reducing the output of the solar cell [16]. Being able to concentrate this diffuse light onto the solar panel, would increase the yield of the solar cell and a free space luminescent solar concentrator (FSLSC) provides a way to do so as the FSLSC can accept light from all different directions in an acceptance cone and redirect this light into a smaller emission cone, as can also be seen in Figure 1.4A [8, 18, 19, 20].

Concentrating this disordered light means bringing order to a disordered system. This implies a need for a decrease in entropy, also called etendue for light, which poses a challenge. However, an FSLSC can accept light from all different directions in the acceptance cone and redirect this light in a smaller emission cone, while fulfilling the etendue requirements. This FSLSC can be used, such that the emission cone is directed towards a solar panel

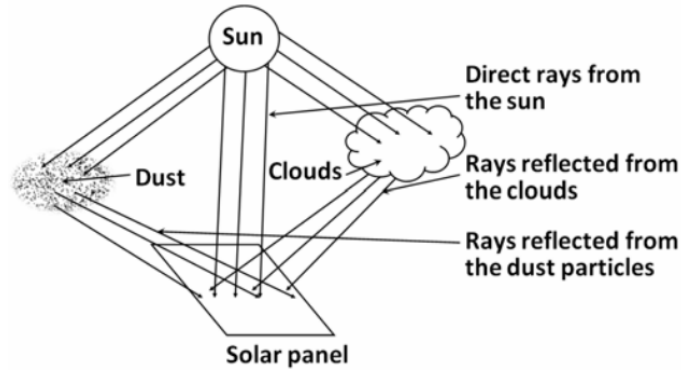


FIGURE 1.3: Diffuse light comes from all different directions due to clouds and dust in the sky, whereas direct irradiance comes directly from the sun. Figure from [16]

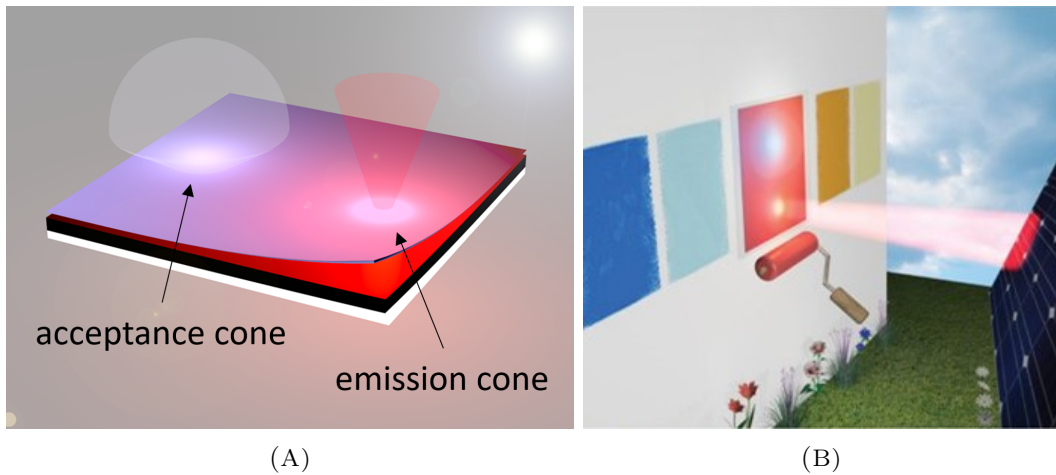


FIGURE 1.4: A free space luminescent solar concentrator, A) which accepts light from all different directions and redirects this light into a smaller emission cone and B) redirects this emission cone towards a solar panel to increase its yield. Figures from [20].

to increase the number of photons reaching the solar panel and thereby the panel's yield as can be seen in Figure 1.4B. A more detailed technical description of an FSLSC will be given in Section 2.5.

1.2.1 Possible Use-cases

Using FSLSCs in combination with bifacial solar panels for building integrated photovoltaic cells opens the doors for a variety of options. The FSLSCs should be positioned around a bifacial module, such that the cone emission reaches this module and the output of the solar cell can be increased. For instance, two possible combinations would be an FSLSC façade with either a vertical solar panel fence or a horizontal solar car park. Pal [8] explores two situations for the use of FSLSCs, both shown in Figure 1.5. These situations show the potential of using an FSLSC in new building configurations.



FIGURE 1.5: Applications of an FSLSC showing A) a two-story residential façade with a bifacial fence and B) a five-story façade with a bifacial car shed. Figures from [8].

1.2.2 Knowledge Gap

The goal of the FSLSC is to increase the number of photons reaching the module and thereby the module's yield. The maximum possible photon intensity within a desired emission cone largely depends on the size of the emission cone [20]. Ideally, the smaller this cone, the higher the photon intensity that can be achieved, also called a high concentration factor. This is due to the photons being spread over a smaller area and thus having a higher intensity, also shown in Figure 1.6. Nonetheless, the system's efficiency depends on the escape cone size. The narrower the escape cone, the longer the light will be trapped in the waveguide, leading to more loss mechanism occurrences and therefore a lower system efficiency [20]. As a consequence of these counter-acting effects of the cone size, there exists an optimal cone size for which the yield is maximized. This thesis aims to investigate which cone size is optimal taking system efficiency and concentration factor into consideration.

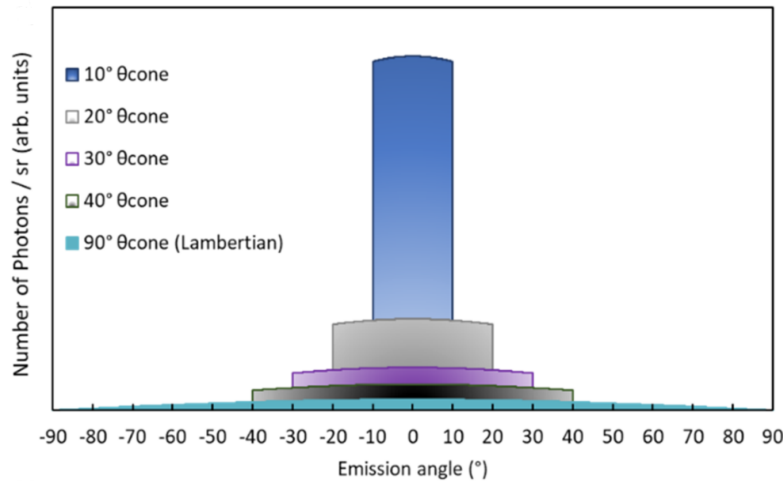


FIGURE 1.6: Angle-dependent photon emission distribution for five different emission cones in ideal systems. Figure from [20].

The objective of an FSLSC is to increase the yield of the bifacial solar module, nonetheless, currently it is not known to what extent the yield of a bifacial solar cell can be increased by using an FSLSC. That is why, another aim of this thesis is to calculate the yield of a

bifacial solar cell in the surrounding of an FSLSC. In this manner, the FSLSC can also be compared to other types of reflectors.

Lastly, it is known that the energy system plays an important role in the economic and social development of a region and the quality of living of the people in this region [21]. Therefore, a new sustainable energy technology should not only be looked at from a technical perspective, but also the economic, environmental, and social aspects should be taken into consideration [21]. A multi-criterial analysis (MCA) provides a way to look at these kinds of complex problems, with a mix of monetary and non-monetary objectives, to identify the best option or distinguish acceptable and unacceptable options [22]. It is currently unknown how an FSLSC scores on the economic, environmental, and social aspects and how this relates to other types of reflectors for yield enhancement of solar cells. Therefore, the last aim of this thesis is to do a multi-criteria analysis on the FSLSC compared to other reflectors.

1.3 Focus and Outline of Thesis

To achieve the aforementioned objectives, the cone size will be optimized to achieve the highest yield by considering the concentration factor and system efficiency in this master assignment. Afterwards, the annual yield of the optimized FSLSC will be calculated and compared to other available reflectors to see to which extent the FSLSC can enhance the output of solar cells. Lastly, a multi-criteria analysis will be performed to compare an FSLSC to other available reflectors based on socio-economical aspects.

This investigation and optimization of the concentration factor and system efficiency as a function of cone size are done by expanding the 3D reverse ray tracing model from Pal [23]. Furthermore, a new calculation approach will be made to calculate the annual yield of an FSLSC close to a bifacial solar panel. Based on this annual yield and the socio-economical aspects, a multi-criteria analysis will be performed. First, Chapter 2 describes the theoretical framework. The extension to the ray tracing model and the annual yield calculation are explained in Section 3. In Chapter 4, the cone size is optimized for a generic case. Chapter 5 studies a case of an FSLSC on a façade with a bifacial solar fence in front. In Chapter 6 the model will be discussed, after which Chapter 7 provides the conclusion.

Chapter 2

Theoretical Framework

This chapter lays the theoretical framework for the upcoming chapters. In Section 2.1, the solar angles and solar spectra will be defined. Moreover, in Sections 2.2 and 2.3, the different types of reflectors and their bidirectional reflectance distribution functions will be explained. Section 2.4 elaborates on the factors influencing the intensity, whereas Section 2.5 describes the FSLSC reflector. Section 2.6 describes methods for optimizing reflectors. Lastly, in Section 2.7, the 3D reverse ray tracing model from Pal [23] will be explained.

2.1 Solar Definitions

The position of the sun changes during the day and per day. Solar noon is the time of the day when the sun is highest in the sky [24]. The position of the sun can be described using the following angles, also shown in Figure 2.1A below:

- Zenith angle of the sun (θ) - The zenith angle is the angle between the sun's rays and the vertical plane. Therefore, the minimum zenith angle is reached at solar noon [24];
- Elevation angle of the sun (θ) - The elevation angle is the angle between the sun's rays and the horizontal plane. Therefore, the maximum elevation angle occurs at solar noon. This angle can also be called the altitude angle and can be seen as the opposite angle of the zenith, i.e. when the zenith angle is 0 degrees, the elevation angle is 90 degrees and the other way around;
- Azimuth angle of the sun (ϕ) - The azimuth angle between the sun's ray and the North, projected on the horizontal plane [24].

Another frequently-used angle is a solid angle, which is defined by Equation 2.1 and shown in Figure 2.1B. The solid angle Ω (steradian) is defined to be the ratio of the area covered by the sphere A (m^2) to the square of the radius of the sphere r (m).

$$\Omega = \frac{A}{r^2} \tag{2.1}$$

Another form of the solid angle is the differential solid angle ($d\omega$), which is defined in Equation 2.2. This shows that the differential solid angle is solely dependent on the azimuth (ϕ) and elevation (θ).

$$d\omega = \frac{dA}{r^2} = \sin \theta d\theta d\phi \tag{2.2}$$

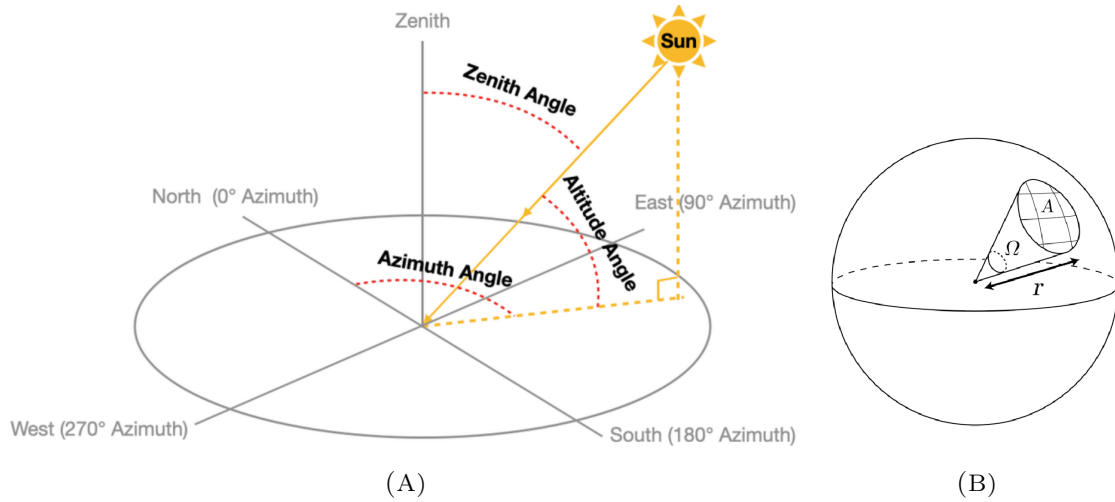


FIGURE 2.1: Definition of A) azimuth angle, zenith angle and altitude, also called elevation, angle, and B) solid angle. Figure A from [25], Figure B from [26]

Radiation from the sun can be classified into three different types of radiation [27]:

- Direct Normal Irradiance (DNI) - This is the part of the solar irradiance that directly reaches a surface, measured on a plane perpendicular to the sun;
- Diffuse Horizontal Irradiance (DHI) - This is the part of the solar irradiance, that is scattered by the atmosphere;
- Global Horizontal Irradiance (GHI) - This is the total radiation that is received on a horizontal surface at earth, including both direct and diffuse irradiance.

The air mass coefficient (AM) can be used to characterize a solar spectrum and is defined as the ratio of the path length which light takes throughout the atmosphere to the shortest possible path length [28]. AM 1.5 is the standard spectrum and aligns with a zenith of 48.2 degrees.

2.2 Reflectors

The solar module's yield can be increased by placing reflectors in such a way that additional irradiance falls on the bifacial module's surface. Reflectors can be categorized into three main categories, all displayed in Figure 2.2.

- Specular - Specular reflectance is characterized by the reflected light going into one single outgoing direction, often described as a mirror-like reflection;
- Diffuse - The light goes in all different directions, with equal probability;
- Glossy - A glossy reflector represents an intermediate case, where the reflection lobe is dependent on the surface roughness. With increasing surface roughness, the glossy reflection goes from specular to diffuse.

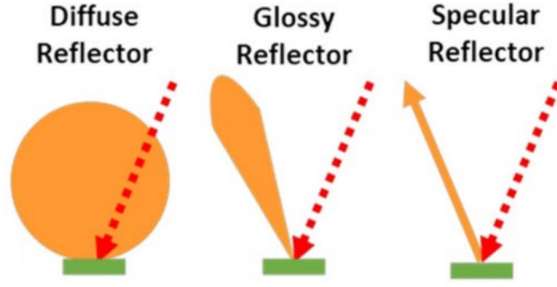


FIGURE 2.2: A diffuse, glossy, and specular reflector. Figure from [8]

2.3 Bidirectional Reflectance Distribution Function

Reflection properties of materials can be characterized by Bidirectional Reflectance Distribution Functions (BRDF), as defined by Nicodemus [29]. The BRDF (f) is a four-dimensional function with unit sr^{-1} , depending on the azimuth (ϕ) and zenith (θ) angles from the incoming (i) and reflected (r) light and is defined as follows:

$$f(\theta_i, \phi_i, \theta_r, \phi_r) = \frac{L(\theta_r, \phi_r)}{E(\theta_i, \phi_i)} \quad (2.3)$$

where L is the radiance or power per unit solid angle in the direction of the ray per unit projected area perpendicular to the ray and E is the irradiance or power per unit surface area [29].

Physically plausible simulations require physically plausible BRDFs. For this reason, the three following conditions should be obeyed:

1. Positivity: $f(\theta_i, \phi_i, \theta_r, \phi_r) \geq 0$
2. Symmetricity: $f(\theta_i, \phi_i, \theta_r, \phi_r) = f(\theta_r, \phi_r, \theta_i, \phi_i)$
3. Energy Conservation: $\int_0^{2\pi} \int_0^{\frac{\pi}{2}} f \cos(\theta_r) \sin(\theta_r) d\theta_r d\phi_r \leq 1$

Using these three conditions, the BRDF can be calculated for a diffuse and specular 3D case. Equations 2.4 and 2.5 give the BRDF for diffuse and specular reflection respectively, where δ is the Kronecker Delta, meaning that its value is one when the variables in the bracket are equal and zero in all other instances.

$$f_d = \frac{1}{\pi} \quad (2.4)$$

$$f_s = \frac{\delta(\theta_i - \theta_r) \delta(\phi_i - \phi_r)}{\cos(\theta_r) \sin(\theta_i)} \quad (2.5)$$

2.4 Influencing Factors to Reflection

The yield of a solar module can be increased by placing a reflector in the surroundings of a module, to ensure that more radiation can reach the module. There are several factors

influencing the reflection, also described by Pal [8], and these can either be based on an angular component or a distance component. Furthermore, these effects differ per type of reflection, thus can be different for specular, diffuse, and glossy reflection.

When looking into the influence of distance between the module and reflector, two important effects can be considered. First of all, the intensity of glossy and diffuse reflection decreases with distance, because the area over which the photons are spread will increase. Therefore, when increasing the distance between the module and reflector, the measured output in the module will decrease. Such an effect does not hold for specular reflection, as the area of the beam is independent of distance. Second, the shade that is induced by the module on the reflector plays a role as well. Generally, the closer the module is to the reflector, the larger the influence of the shaded area is and therefore the output will decrease. These two effects of shade and intensity are counter-acting for both diffuse and glossy reflection.

When looking at the angular influence of the rays, three different effects play a role. First of all, there is a so-called cosine influence, which equals the cosine of the incident elevation angle ($\cos(\theta_i)$), meaning that the intensity of the beam goes down by a cosine factor, also illustrated in Figure 2.3. This cosine influence happens twice for cases where a reflector is reflecting towards a solar module, once for the beam reaching the reflector and once for the angle of the reflector reaching the solar panel. For instance, for a horizontal solar module with incident radiation from an elevation angle of 30 degrees, the energy density will decrease by 50% solely due to this cosine term compared to a case where the radiation comes from perpendicular to the module.

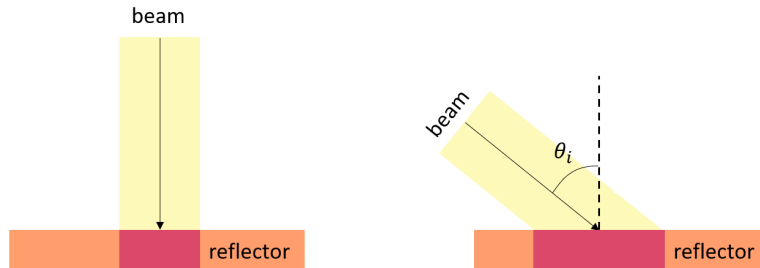


FIGURE 2.3: The cosine term ($\cos(\theta_i)$) decreases the ray's intensity at low elevation angles.

This cosine influence only depends on the elevation angle and not on the azimuth for vertical panels and reflectors, which can be explained with the following thought experiment: consider a horizontal module, changing the azimuth should equate rotating this module on the horizontal plane. When rotating the module, the shape of the beam will not change and therefore there is no dependence on the azimuth for the intensity. Nonetheless, changing the elevation equals tilting the module in a vertical direction. When tilting the module, the area does change and therefore also the intensity. Concluding, the intensity is dependent on the elevation angle but not on the azimuth for vertical surfaces.

Second, the differential solid angle ($d\omega$) influences the reflection of diffuse and glossy reflectors. The solid angle (Ω) is defined in Figure 2.1B, and based on this definition it can be seen that the larger the solid angle, the larger the area over which the photons are spread

and therefore the lower the intensity. Therefore the intensity decreases with an increasing differential solid angle.

Lastly, the external quantum efficiency (EQE) plays a role. The EQE is defined to be the ratio of the number of charge carriers collected by a solar cell to the incident number of photons on the solar cell, depending on the wavelength and angle of incidence. An example of an EQE of a bifacial solar cell can be seen in Figure 2.4 [30], where 0 degrees is defined to be the middle of the front face and the side edges of the panel are at 90 and 270 degrees. This shows that the angle of the incident light influences the number of charge carriers that are generated for angles close to parallel to the cell, i.e. in the range of 70 to 110 degrees and 250 to 290 degrees.

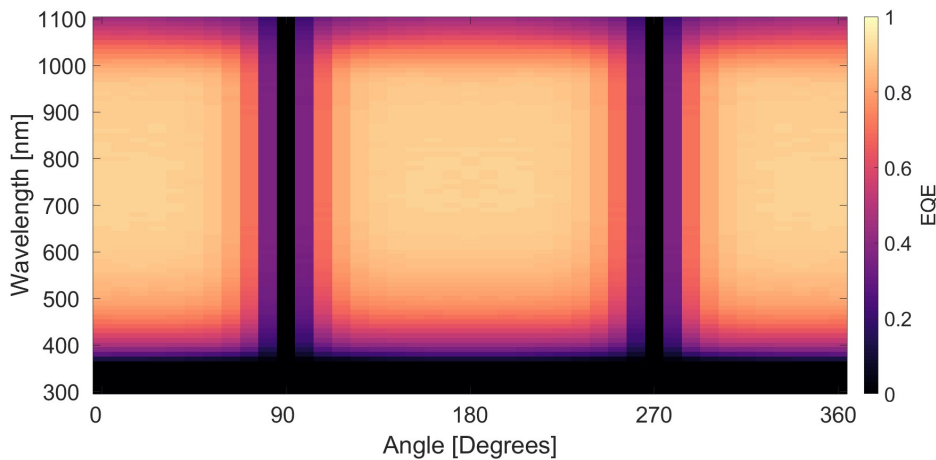


FIGURE 2.4: External quantum efficiency of a bifacial solar cell [30].

To repeat, the main effects influencing the intensity of the reflection are:

- Decrease in intensity of glossy and diffuse reflection with height;
- Shade depending on module's height and tilt;
- Cosine factor for angle corrections;
- $d\omega$ factor for solid angle corrections;
- External quantum efficiency.

2.5 Free Space Luminescent Solar Concentrators

One possible reflector to install next to a module is a free space luminescent solar concentrator. As explained in Section 1.2, an FSLSC provides a way to concentrate diffuse light which can be directed to a solar module to increase the module's yield. The FSLSC, as shown in more detail in Figure 2.5A, consists of a luminophore-embedded waveguide, with a nanophotonic coating on top and Lambertian walls on the sides and bottom. First, these different components of the FSLSC will be explained in more detail. Thereafter, the ideal and real conditions of an FSLSC are elaborated upon.

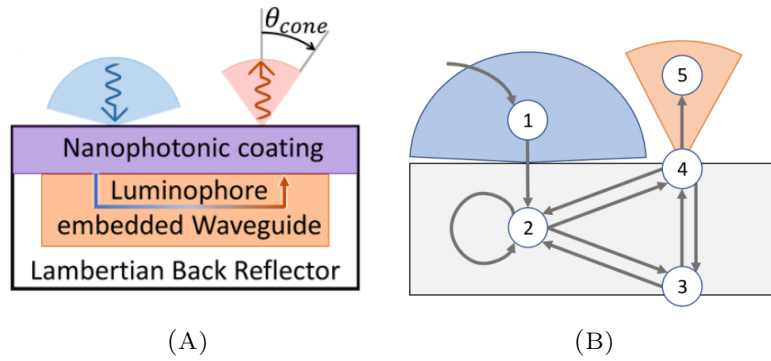


FIGURE 2.5: Schematics of a free space luminescent solar concentrator (FSLSC), showing A) the materials out of which the FSLSC consists and B) the possible paths of light in the FSLSC, where 1) is the acceptance cone, 2) the luminophores in the waveguide, 3) the Lambertian reflector at the sides and bottom, 4) the nanophotonic coating on top and 5) the emission cone. Figure A from [8], Figure B from [19].

2.5.1 Nanophotonic Coating

When a photon is approaching the FSLSC, it will first hit the nanophotonic coating, which is on top. The nanophotonic coating is a dielectric multilayer stack, meaning that it consists of thin layers of alternating high and low refractive index materials [18]. A refractive index is defined to be the ratio of the speed of light in a vacuum over the phase velocity of light in a medium, depending on the density of the medium [31]. This nanophotonic coating gives control over the reflection and transmission properties of the surface.

More specifically, the nanophotonic coating can be seen as a Bragg reflector, as it is a filter composed of periodic thin film stacks with alternating refractive indices [18]. However, a Bragg reflector generally has equal layer thicknesses, whereas the layer thicknesses of the nanophotonic coating vary. This nanophotonic coating can be tuned, by changing parameters like the number of layers, the thickness of layers, and the refractive index contrast, such that it fulfils the properties of transmitting photons with a certain wavelength and angle, while reflecting others. The nanophotonic coating of this FSLSC has been optimized by Einhaus [18] with the use of the software Lumerical.

For incoming photons, the nanophotonic coating ensures that photons that have high energy, and thereby low wavelength, are let through and go into the FSLSC material towards the waveguide. Photons that already have low energy, and thereby high wavelength, will be reflected in a specular manner on the material and not reach the waveguide. For reciprocity reasons, the photons with low energy that are already within the emission cone angle can enter the luminophore-embedded waveguide.

Figure 2.6 shows an example of reflection on the outside by a nanophotonic coating. For this example, a nanophotonic coating lets wavelengths below 600 nm through and these are absorbed in the luminophore-embedded waveguide.

For outgoing photons, the nanophotonic coating ensures that the photons can only exit the material inside the emission cone and therefore aims to provide angular control. The angle at which the photons can reach the nanophotonic coating from the inside is smaller than

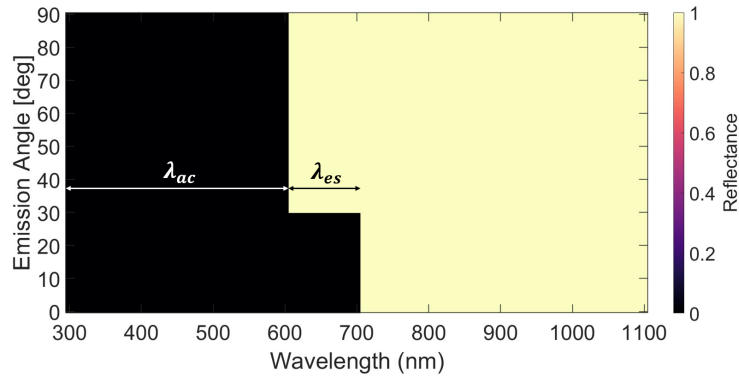


FIGURE 2.6: Example of the outside reflection of a nanophotonic coating, showing the acceptance wavelengths (λ_{ac}) and emission wavelengths (λ_{es}) of the nanophotonic coating

the angle at which the photons are emitted, due to the different refractive indices in the nanophotonic coating. Refraction can be described by Snell's law as is shown in Equation 2.6, where the difference in refractive indices between the materials (n_1 and n_2) leads to the angle of incidence (θ_1) being changed to a different angle (θ_2) [31]. Additionally, total internal reflection plays a role, meaning that the light from the waveguide is not refracted into the nanophotonic coating, but back into the waveguide due to the lower refractive index of the nanophotonic coating [32].

$$n_1 \sin \theta_1 = n_2 \sin \theta_2 \quad (2.6)$$

Continuing the example from Figure 2.6, the photons that reach the nanophotonic coating with properties where the nanophotonic coating has zero reflectance, these photons are transmitted to the luminophore-embedded waveguide. On the sides and the back, there is a Lambertian reflector ensuring the randomization of photons and preventing the loss of photons due to leakage. The photons can only leave the luminophore-embedded waveguide at the top. When the photons reach the top within a cone angle of less than 30 degrees, they can pass the nanophotonic coating and are emitted towards the bifacial module. When the photons do reach the top with a different angle, the photons are reflected back into the material and randomized by the Lambertian reflector. All the wavelengths that are not absorbed at the outer layer, as shown in the example with a wavelength larger than 600 nm and those that are outside of the emission cone, are reflected in a specular manner towards the bifacial module.

A loss mechanism associated with the nanophotonic coating is the emission cone loss [19], which are photons that pass through the nanophotonic coating outside of the desired emission cone.

2.5.2 Luminophore-Embedded Waveguide

After a high-energy photon has been let through by the nanophotonic coating, it reaches the luminophore-embedded waveguide. The photons are absorbed by the luminophores and re-emitted at a higher wavelength. Specifically, the luminophores enable Stokes-shifting, i.e. red-shifting, of the incoming light, meaning that the wavelengths are shifted from the absorption spectrum to a higher-wavelength emission spectrum [33]. For example, an

experimental FSLSC has been built based on Lumogen F Red 305 luminophores [19], its absorption and emission spectrum are shown in Figure 2.7. This shows that the spectrum of around 300 to 650 nm is shifted to a spectrum from 550 to 850 nm.

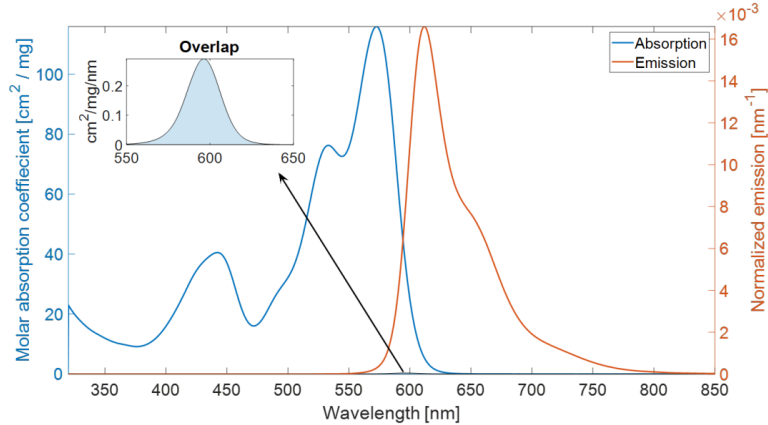


FIGURE 2.7: Molar absorption coefficient (blue) and normalized emission spectrum (red) of Lumogen F red 305 in toluene. Figure from [19].

Multiple loss mechanisms can occur in this process, of which the quantum yield of luminophores and reabsorption losses will be explained. Quantum yield losses of luminophores are losses due to non-radiative recombination, where there is no photon emitted during the recombination. The quantum yield of luminophores is defined as the number of photons that are emitted by the luminophores over the number of photons that are absorbed by the luminophores and is typically higher than 90% [19]. The reabsorption losses are losses due to overlap in the absorption and emission spectrum, which is for instance the case for Lumogen Red as can be seen in Figure 2.7. Photons which are already red-shifted by the luminophores are absorbed a second time [19] and in case the quantum yield of luminophores is not perfect, this reabsorption will lead to additional losses.

To summarize, the possible paths for light in the FSLSC can be seen in Figure 2.5B [19]. Light is accepted in the acceptance cone (1) or reflected specularly by the nanophotonic coating, depending on the wavelength and angle. The accepted light is absorbed by the luminophores (2). From the luminophores, the photons can either go to the bottom (3) or go to the top (4). When the photons go to the bottom, they are reflected by the Lambertian reflector and can go back to the luminophores or go to the top surface. When the photons go to the top surface, the photons can be reflected back into the material or transmitted through the nanophotonic coating and emit as an emission cone (5), depending on the angle at which the photons approach the top. After the photons have been absorbed by the luminophore once, they can get reabsorbed by the luminophores (2), this is related to the reabsorption losses. In the upcoming sections, a closer look will be taken at the properties of the FSLSCs in ideal and real conditions.

2.5.3 Ideal Case

When looking into the technical aspects, in the ideal cases, there are no losses in the free space luminescent solar concentrator. This means that all the incoming low wavelength photons can enter the luminophore-embedded waveguide and are converted into

higher wavelength photons, which corresponds to a 100% quantum efficiency of the luminophores. These photons will only leave within the desired escape cone. Furthermore, no re-absorption takes place, there is no transmission at the bottom, no transmission outside of the escape cone and also no scattering or absorption losses in the substrate. In this ideal case, the total incoming photon flux will equal the total emitted photon flux, which can be described using the following relation:

$$L_i \Delta\Omega_i = L_{out} \Delta\Omega_{out} \quad (2.7)$$

In this equation, $\Delta\Omega_i$ is the angular spread of the incoming light and $\Delta\Omega_{out}$ is the solid angle of the escape cone into free space. L_i and L_{out} are the radiance of the incoming and emitted light in photons per second per steradian, respectively. Multiplying the angular spread times the radiance will give the photon flux, which must be conserved in the ideal case.

The ideal concentration factor (C_{id}) is the ratio of the emitted radiance over the incoming radiance, thereby containing how much the light is concentrated compared to the incoming light. This equation can be derived using Equation 2.7 and is shown in Equation 2.8.

$$C_{id} = \frac{L_{out}}{L_i} = \frac{\Delta\Omega_i}{\Delta\Omega_{out}} \quad (2.8)$$

2.5.4 Non-Ideal Case

As explained above, there are multiple loss mechanisms which play a role in the non-ideal case. These include amongst others re-absorption, reflection on the top surface, emission outside of the cone and a non-ideal quantum yield of luminophores, leading to the number of emitted photons being lower than the number of absorbed photons. All these loss mechanisms are summarized in the total system efficiency (η_{tot}), which is the ratio of outgoing photons over incoming photons.

The performance of the concentrator can be determined using the concentration factor. The average radiance over a chosen escape cone needs to be determined, which is done by dividing the total amount of light emitted into the cone (I_i) by the size of the escape cone ($\Delta\Omega_i$) as is shown in Equation 2.9. Based on this and Equation 2.8, the concentration factor of FSLSC can be determined using Equation 2.10.

$$L_i = \frac{I_i}{\Delta\Omega_i} \quad (2.9)$$

$$C = \frac{L_{out}}{L_i} = \frac{\frac{I_{out}}{\Delta\Omega_{out}}}{\frac{I_i}{\Delta\Omega_i}} = \frac{I_{out}}{I_i} C_{id} = \eta_{tot} C_{id} \quad (2.10)$$

This shows that the performance of the concentrator is a function of the system efficiency and the ideal concentration factor. On the one hand, the ideal concentration factor increases with a decreasing cone size. On the other hand, the higher the concentration, the longer the light needs to be trapped inside the waveguide and the more loss mechanism occurrences will take place. The system efficiency will therefore decrease with decreasing

cone size.

The same trends can be seen in Figure 2.8, where the concentration factor and system efficiency are plotted for multiple quantum yields of luminophores. The quantum yield of luminophores is defined to be the number of photons that are emitted by the luminophores over the number of photons that are absorbed by the luminophores. This shows that the concentration factor decreases with increasing cone size and that the efficiency increases with increasing cone size. Consequently, an optimum exists between the system efficiency and concentration factor. This thesis aims to find this optimal cone size.

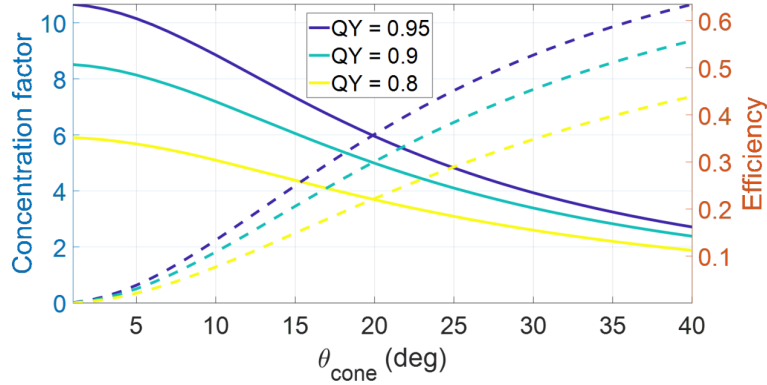


FIGURE 2.8: Concentration factor (solid line) and system efficiency (dashed line) depending on cone size for multiple quantum yields of luminophores. Figure from [19].

2.6 Optimizing Reflectors

Reflectors can be optimized for different objectives. For instance, the reflector can be optimized to get the highest yield or to be the most economically effective. That is why, first the additional yield generation of a module close to a reflector will be elaborated upon. Thereafter, a multi-criteria analysis will be elaborated upon as a way to incorporate the socio-economical effects into the comparison.

2.6.1 Calculation Yield

A basic calculation of the power of a solar panel can be done based on the open-circuit voltage (V_{oc}) and the short-circuit current (I_{sc}). The short-circuit current is the current through the solar cell when the voltage across the solar cell is zero [34]. This quantity is still dependent on the solar cell area, so that is why it is common to use the short-circuit current density (j_{sc}) as well. The open-circuit voltage is the maximum voltage from a solar cell, which occurs at zero current [34]. The open-circuit voltage is known to decrease with temperature [34].

The power can be calculated by multiplying the voltage and current as can also be seen in Figure 2.9. When operating at both the short-circuit current density as well as the open-circuit voltage, the power in the solar cell is zero. The fill factor determines the maximum power (P_{MP}) of a solar cell and is defined as the ratio of the maximum power from the solar cell to the product of the short-circuit current and the open-circuit voltage as can be

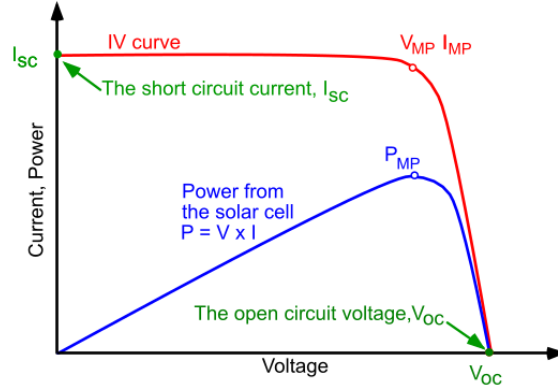


FIGURE 2.9: Overview of the IV curve of a solar cell, showing the short-circuit current density, open-circuit voltage and power generated by the solar cell. Figure from [34].

seen in the equation below [34].

$$FF = \frac{P_{MP}}{V_{oc} \cdot I_{sc}} \quad (2.11)$$

The power of solar cell can be calculated using Equation 2.12, where P is the power per module area [W/cm^2], J_{sc} is the short-circuit current density [A/cm^2], V_{oc} is the open-circuit voltage [V] and FF the fill-factor [-]. It should be noted that this is a basic estimation of the power output and does not take into account dependencies on aspects like temperature.

$$P = J_{sc} \cdot V_{oc} \cdot FF \quad (2.12)$$

2.6.2 Multi-Criteria Analysis

A multi-criteria analysis (MCA) provides a way to evaluate different options, and even make decisions, while accounting for the complex and evolving socio-economic system that technology functions in [21]. Whereas traditional single-criteria approaches are normally aimed at identifying the most efficient options at low costs, the MCA generally takes technical, economic, environmental, and social aspects into consideration [21].

Based on the objective of the MCA, different levels of detail and depth can be taken and the general approach will be described based on the manual from the UK's Department for Communities and Local Governments [22]. First of all, the objective of the MCA needs to be specified. Second, the to-be-considered options have to be listed. Third, the criteria on which the options are scored have to be determined. Afterwards, the options are scored on the criteria based on careful analysis. This concludes a basic MCA, after which a so-called performance matrix is made where the different options are ranked on the different criteria. For a more elaborate analysis, numerical analysis is performed on the performance matrix in the form of scoring and weighing. The process of scoring means that the criteria are given a numerical value for each option. Weighing means that the weights are assigned for each criterion to indicate a difference in the importance of the criteria. Based on either the basic or extensive analysis, multiple options can be compared.

2.7 3D Reverse Ray Tracing Model

In this section, the 3D reverse ray tracing (RRT) model from Pal [23] will be explained. This model aims to calculate the short-circuit current density of a bifacial solar cell, when the module is close to a reflecting surface by means of ray tracing simulation.

For ray tracing simulations, generally a source, objects, and a detector are defined, which are divided into pixels of which the orientation, dimensions and other characteristics are determined. To limit the computational effort, the light is traced in reverse order, such that it goes from the detector via the object to the source, i.e., from the solar module via the reflector to the solar source.

The code is subdivided into two parts. Part A of the code initializes the geometry and computes the solid angles between the pixels of the module and reflector. Differential solid angles are defined to be $d\omega$ in Figure 2.11, where they go from each centre of a reflector pixel to every module pixel. Part B uses those differential solid angles to calculate the number of reflected photons to determine the short-circuit current density generated in the solar cell due to the reflecting surface. This can be combined with the short-circuit current density directly from the source to get the total short-circuit current density of the solar cell. Both parts will be discussed in more detail below. An overview of the final code can be seen in Figure 2.10.

2.7.1 Part A: Calculation of Geometry

Part A of the code aims to capture the geometry and calculate the solid angles for every pixel between the module and reflector. To set the initial situation, the centre coordinates, length, breadth, height, tilt and surface roughness need to be specified for the module and/or reflector. The source's elevation angle and azimuth should be specified. The number of pixels per unit is of importance for the convergence of the model and should be set around 10 pixels for converged results, as will be explained in more detail in Section 2.7.3.

Alternative data that requires to be specified include the used solar cell, its EQE and the solar spectral irradiance. The solar cell that is used is a bifacial silicon heterojunction solar cell based on research from Saive [30], its exact composition can be seen in Figure 2.10. The EQE was computationally simulated using SunSolve, developed by PV lighthouse. The spectral irradiance is also based on SunSolve simulations.

Based on this input data, the edges of the reflector and module can be calculated. These can be divided into pixels and when using geometric rules, the solid angles between the different pixels can be determined. This is the input for the next part of the code.

2.7.2 Part B: Calculation of Short-Circuit Current Density

Part B of the code calculates the short-circuit current density output on the bifacial solar cell coming from the reflecting surface or directly from the source. The reflecting surface can be specified to be either diffuse, glossy, or specular reflectance as described in Section 2.2. The different behaviours of the surface are specified in the Bidirectional Reflectance Distribution Functions (BRDF).

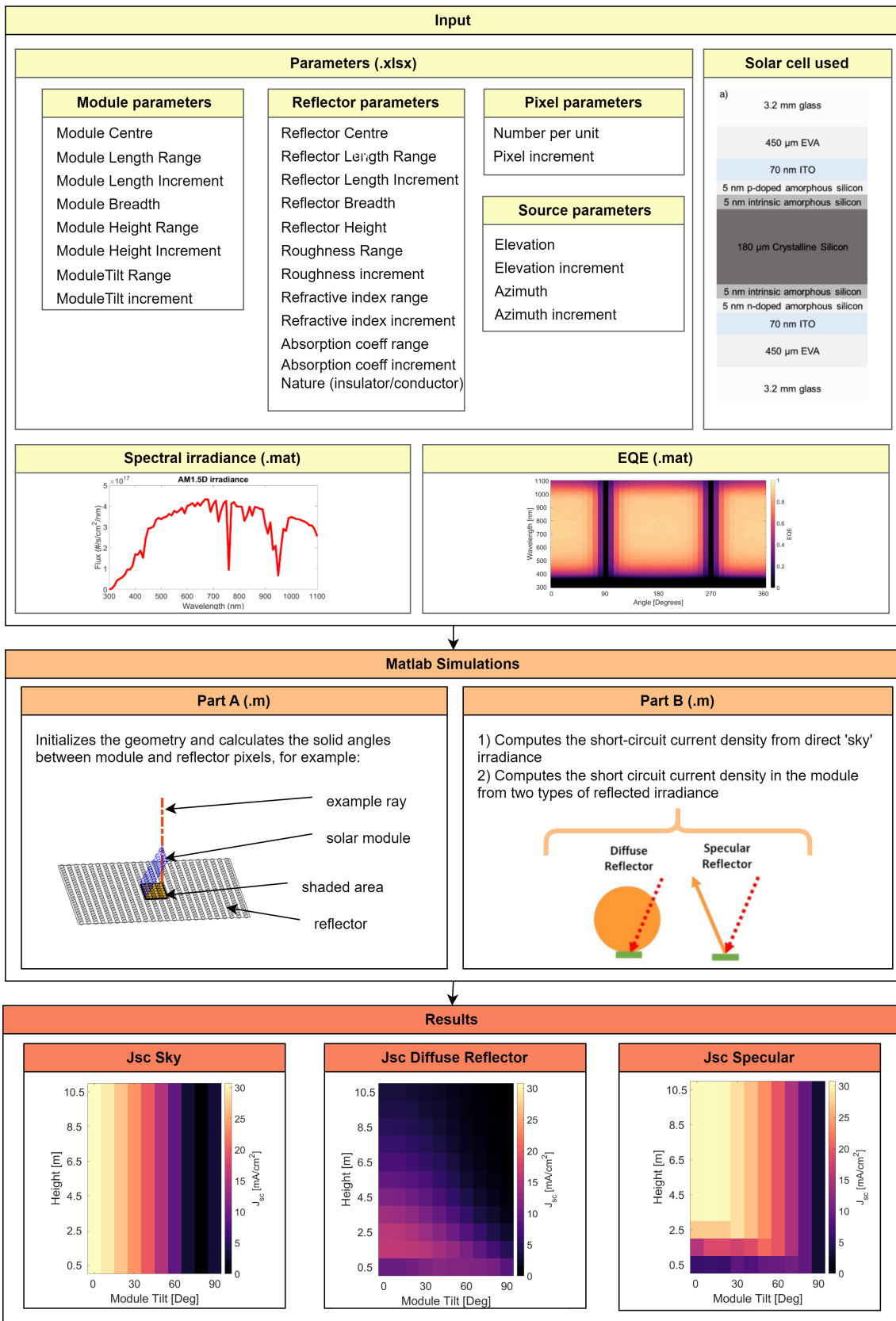


FIGURE 2.10: Overview of the Reverse Ray Tracing (RRT) Code as made by Pal [23]

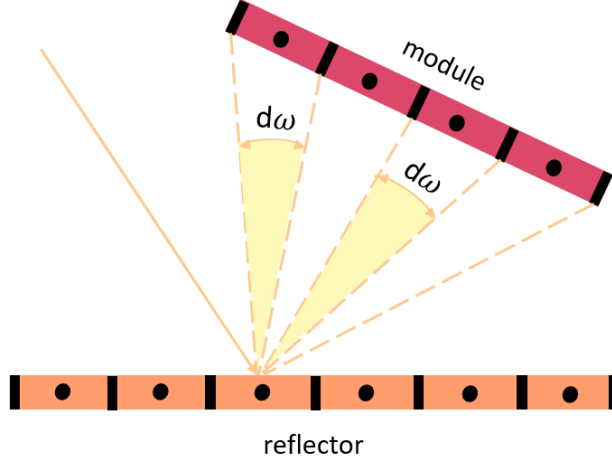


FIGURE 2.11: Definition of reverse ray tracing code setup, where both the module and reflector consist out of three pixels and $d\omega$ is the solid angle.

Using the solid angles and other input data from part A of the code, the number of photons received by the module pixels can be calculated using Equation 2.13. Term I describes the incoming flux, where \dot{n} is the number of photons per area per second and θ_i is the angle of incoming light relative to the module's normal. Term II describes the light that is reflected, where f_x is the Bidirectional Reflectance Distribution Function (BRDF) for a reflector x , θ_r the angle of the reflection, and $d\omega_r$ is the differential solid angle. Term III includes the part of the photons that is accepted by the module, by multiplying this by the angle to the module (θ_m).

$$\dot{n}_{pixel} = \underbrace{\dot{n} \cos \theta_i}_{\text{I}} \cdot \underbrace{f_x \cos \theta_r d\omega_r}_{\text{II}} \cdot \underbrace{\cos \theta_m}_{\text{III}} \quad (2.13)$$

The short-circuit current density (j_{sc}) received by the module can be calculated according to Equation 2.14. The number of incoming photons is multiplied by the external quantum efficiency (EQE_{θ_m}) to calculate the number of carriers per pixel. To compute the current density of one pixel, this is integrated over the wavelengths (λ) and multiplied by the charge (q). Summation over the pixels gives the total current density and division by the area of the module (A) gives the short-circuit current density.

$$j_{sc} = \sum_{pix} \frac{1}{A} q \int^{\lambda} \dot{n}_{pix} EQE_{\theta_m} d\lambda \quad (2.14)$$

Using this approach, the short-circuit current density of a module nearby a reflector can be calculated. Nonetheless, it should be noted that this is a purely optical model. This means that the model calculates how many photons reach the module and are converted into charge carriers according to the EQE, but does not take the electrical properties of the solar cell into account. For instance, a real solar cell consists of cells which are electrically in series connected to produce a sufficient voltage. This in-series connection can lead to a variety of interconnection effects, like losses due to mismatch losses [35]. These losses are incurred due to the fact that the module's output is determined by the solar cell with the lowest output, but these effects are not taken into consideration.

2.7.3 Results Tilt vs Height

To illustrate the relevant effects described in Section 2.4, when placing a reflector close to a bifacial solar cell, this section will elaborate on the short-circuit current density of the bifacial solar cell for a large range of heights and tilts.

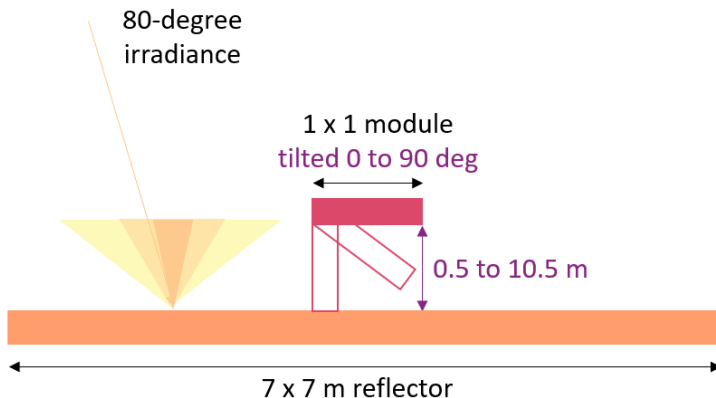


FIGURE 2.12: Test case for 3D for reverse ray tracing code, where a 1 by 1 m module is placed in the centre of a 7 by 7 m reflector, where the module is changed in height, from 1.0 to 10.5 m, and tilt, from 0 (horizontal) to 90 degrees (vertical).

The initial situation is displayed in Figure 2.12. The module is rotated in clockwise directions, as is shown in the figure, to closely examine the differences in reflectors, since rotating the module counter-clockwise would have resulted in a situation where the reflected beam never hits the module perpendicularly. Nonetheless, these perpendicular rays are important for some of the effects mentioned in Section 2.4.

A convergence test is run for this RRT code, as can be seen in Figure 2.13. Several cases have been tested, where convergence was reached at the highest number of pixels in case a reflector was installed perpendicularly to a module. Therefore a more detailed analysis has been done on these types of cases, of which the results of a diffuse reflector can be seen in Figure 2.13. This shows that the results are converged at 10 pixels, so this number of pixels is used. Note that for the convergence of a specular reflector, the ray either hits the module or it does not and therefore is less gradual than the trends for a diffuse reflector. Nonetheless, several tested cases show reasonable accuracy for 10 pixels per unit for specular reflection.

Figure 2.14 shows the short-circuit current for a variety of heights and tilts generated at the front of the module from direct sky irradiance (Figure 2.14A), at the rear of the module due to a diffuse reflector (Figure 2.14B) and at the rear of the module due to a specular reflector (Figure 2.14C). To get the total short-circuit current density of the module, the front and a rear of choice should be added together. A tilt of 0 degrees is defined to be parallel with the reflector, whereas a tilt of 90 degrees is defined to be perpendicular to the reflector.

Figure 2.14A shows that the short-circuit current density of the module's front is independent of height. The highest short-circuit current density is reached for a horizontal module, which is parallel with the reflector, whereas the lowest short-circuit current density is reached at a tilt of 80 degrees. The reason for this lowest short-circuit current

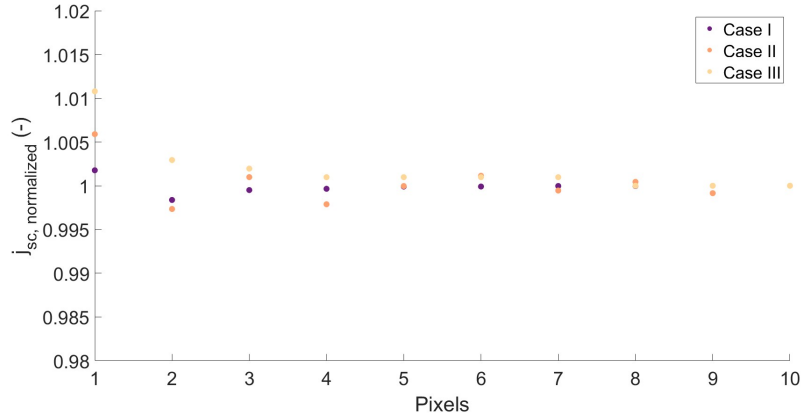


FIGURE 2.13: Convergence test for three cases, where a module is placed perpendicular to a diffuse reflector, where the output of the rear of the module is shown for different pixels.

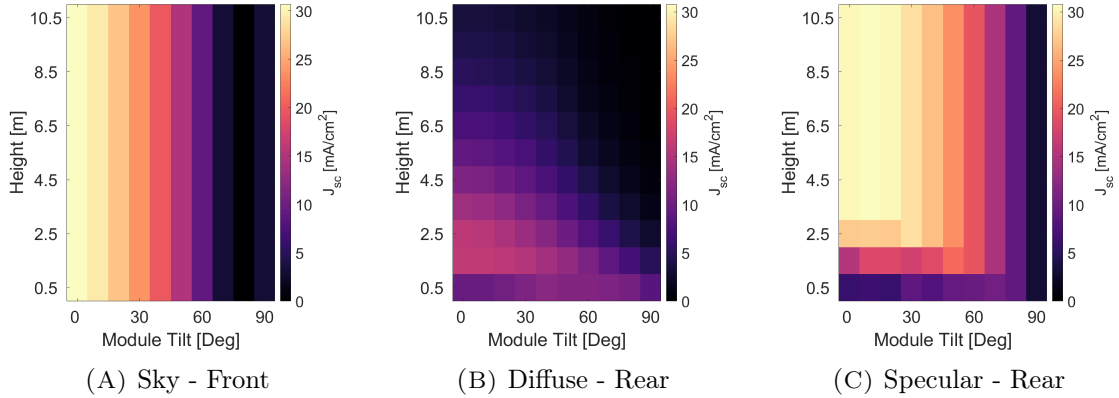


FIGURE 2.14: Short-circuit current density calculated for the front and rear of a bifacial solar cell for the setup described in Figure 2.12, where the height and tilt are varied for a specular and diffuse reflector.

density is that the module is parallel to the sun's rays and therefore no output is yielded. When solar rays hit the module perpendicularly, the highest yield is generated. That is why the 0-degree module tilt yields the most optimal short-circuit current density, since this is closest to the perpendicular incidence.

In Figure 2.14B, the short-circuit current density on the rear of the module due to a diffuse reflector is shown. It can be seen that the short-circuit current density on the rear of the module has a maximum of 16.3 mA/cm^2 , which is reached at a 1.5-meter height and 10-degree tilt. It decreases with increasing height and tilt, this is due to the decrease in intensity with increasing height for diffuse reflectors and a decreasing cosine effect with increasing tilt. Furthermore, the EQE amplifies this effect of decreasing with tilt. For a 0.5-meter height, the shade of the module on the reflector reduces the short-circuit current density.

As can be seen in Figure 2.14C, the height does not influence the short-circuit current density from a height of 3.5 m onwards. The tilt influences the short-circuit current density

for each tilt, therefore, the short-circuit current density is mainly dependent on the tilt of the module. In this setup, the light comes from 80 degrees elevation, leading to the highest output also being at 80 degrees, due to the most optimal properties in both EQE and cosine-term being at this angle. The height does not affect the short-circuit current density, given that the module is not too close to the reflector inducing shade on the reflector. It can also be seen that a horizontal module induces more shade than a vertical module, due to the height at which the output is affected up to 3.5 meters for a horizontal module, whereas there is no influence of shade for a vertical module.

Chapter 3

Model Description

In this chapter, the methodology of this thesis will be elaborated upon. A novel model will be presented that aims to calculate the short-circuit current density of a bifacial solar module due to an FSLSC. This model can then be used to optimize the cone angle of the FSLSC and the annual yield can be calculated based on this. First, in Section 3.1, a general overview of the model that can calculate the short-circuit current density will be presented, after which the detailed calculation approach is explained. Next, Section 3.1.5 elaborates on the validity of the model. Afterwards, in Section 3.1.6, aspects to keep in mind when using the model are elaborated upon. Section 3.2, the yield calculation based on this FSLSC model is elaborated upon. Finally, the methodology for the MCA is explained.

3.1 FSLSC Model

An overview of the model can be found in Figure 3.1 and the Matlab code is added in Appendix C. The Matlab model is based on the RRT model as explained in Section 2.7 and consists of two parts. The geometry is initialized in part A, whereas in part B the configuration is illuminated and the resulting short-circuit current densities are calculated.

First, the input parameters need to be defined. As can be seen in Figure 3.1, parameters regarding the properties of the module, reflector, pixels, emission cone and source need to be specified. New parameters compared to the existing model, as explained in Section 2.7, are the cone parameters, consisting of the cone size, the emission range and the wavelength at which the FSLSC exhibits specular behaviour. As can be seen in Figure 3.2B, it will be assumed that there is a wavelength where the properties of the FSLSC go from absorptive of photons (indicated in black) to specular reflective (indicated in yellow). Other input data are the spectral irradiance, solar cell, its EQE and the FSLSC efficiencies. Combining this data, the Matlab simulations can be run.

In part A of the Matlab code, using the input parameters, the planes of the geometry are defined and divided into pixels of the desired size. Furthermore, solid angles between the module's pixels and the reflector's pixels are calculated as shown in Figure 2.11. Part A of the RRT code from Pal, as described in Section 2.7.1, is designed to do these calculations and is for this reason used as a basis for this new model.

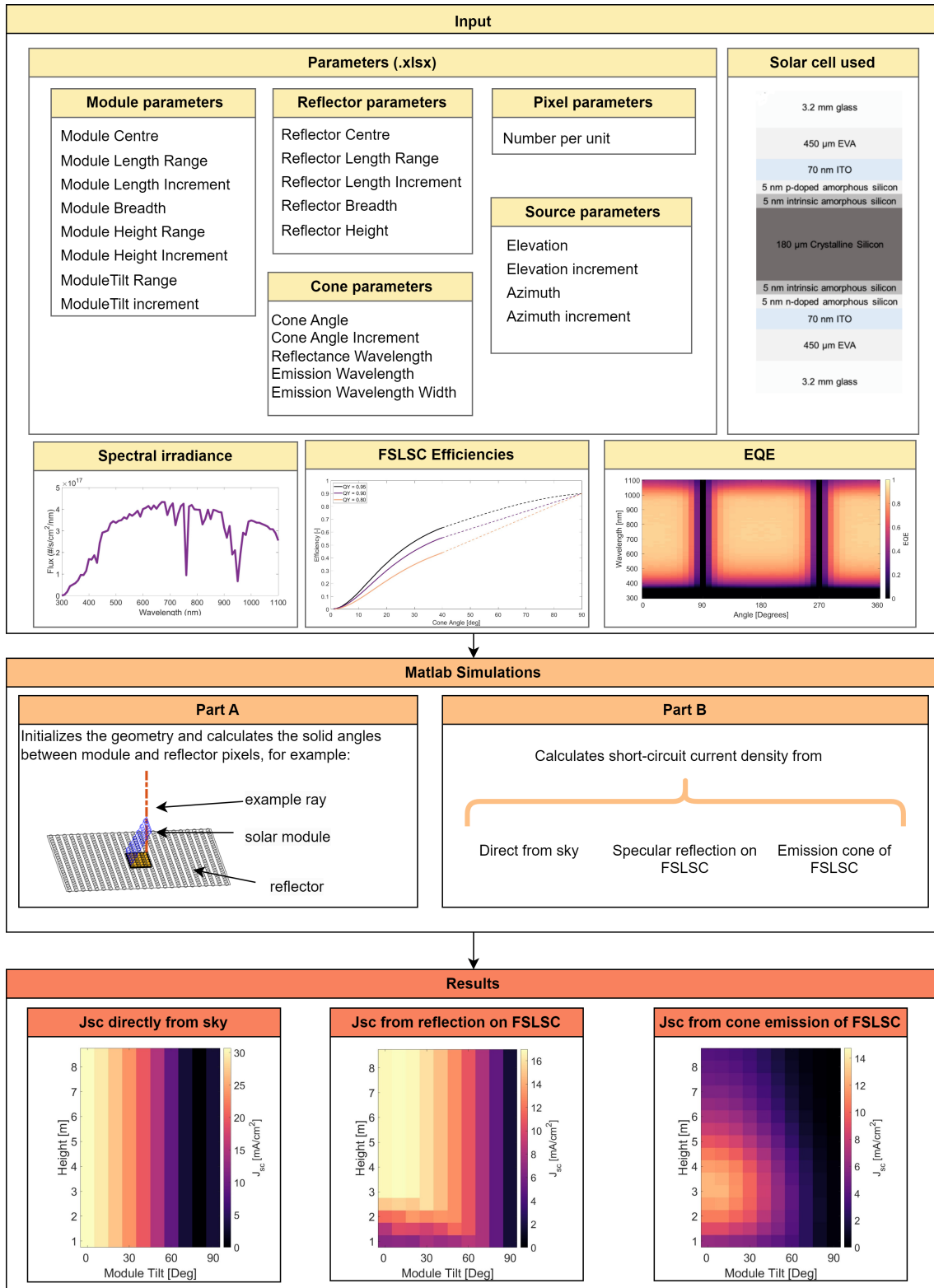


FIGURE 3.1: Overview of the FSLSC Code, showing the workflow of first defining the input parameters. Then running two parts of the Matlab model, for initializing the geometry (part A) and calculating the short-circuit current density (part B). Lastly, the results can be analyzed.

In part B of the code, the geometry is illuminated from a desired angle and the short-circuit current densities are calculated. The illumination used in the model is 1.5 AM GHI or 1.5 AM DNI. Based on reverse ray tracing, the shadow, the reflectance and the short-circuit current density induced on the module can be calculated. The short-circuit current density calculation is split into three different parts, which is also shown in Figure 3.2A. First, some of the irradiance of the source directly falls on the module generating a short-circuit current density. This will be referred to as short-circuit current density directly from the sky and is elaborated upon in Section 3.1.1. Second, some part of the irradiance falls on the FSLSC and has a wavelength above the absorption wavelength of the FSLSC. This is specularly reflected and referred to as the short-circuit current density from specular reflection and is elaborated upon in Section 3.1.2. In Figure 3.2B, this is indicated as the yellow part for an absorption wavelength of 600 nm. Lastly, some part of the irradiance falls on the FSLSC and has a wavelength below the absorption wavelength. This part of irradiance is absorbed by the FSLSC, red-shifted, and emitted as an emission cone afterwards. This is indicated as the black part in Figure 3.2B and referred to as short-circuit current density from cone emission. The method for computing these short-circuit current densities will be explained in the upcoming sections.

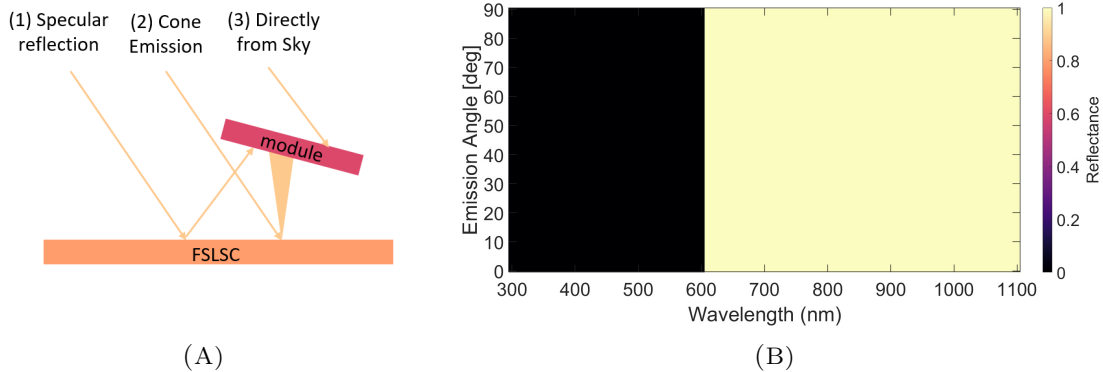


FIGURE 3.2: A) The three ways in which the light can reach the module; 1) specular reflection on the FSLSC for the light with a wavelength above the absorption wavelength, 2) cone emissions from the FSLSC for the light with a wavelength below the absorption wavelengths, and 3) light reaching the module directly. B) An example of wavelength dependency of an FSLSC, where 600 nm is the absorption limit. All photons with a wavelength below 600 nm are absorbed and emitted as a cone, whereas all photons with a wavelength above 600 nm are specularly reflected.

3.1.1 Short-Circuit Current Density Directly from the Sky

When placing an FSLSC oriented towards the rear of the module, the irradiance coming from the sky and reaching the front of the module is not influenced by the FSLSC. Therefore, the short-circuit current density calculation from the irradiance from the sky falling directly on the module is taken from the RRT code from Pal [23]. This means that the angle between the module's normal and the incoming light is calculated using the spherical cosine law and the EQE matrix is interpolated such that the value is obtained for the angle with which the ray hits the panel. Thereafter, Equations 2.13 and 2.14 are used to calculate the short-circuit current density.

3.1.2 Short-Circuit Current Density from Specular Reflection

When placing the FSLSC behind the module, part of the incoming rays on the FSLSC will reflect specularly (indicated by the (1) in Figure 3.2A as well as the yellow part in Figure 3.2B). The specular behaviour is similar to the existing RRT model, but wavelength dependence should be added as only a part of the spectrum is reflected in this way. Therefore, the short-circuit current density calculation from specular reflection is calculated in the same way as the short-circuit current density calculated from the sky, but an additional factor is added for wavelength dependence. This is implemented by changing the EQE matrix, which is dependent on wavelength and incidence angle as explained in Section 2.4. For the FSLSC, specular reflection only occurs above the absorption wavelength, meaning that no carriers are generated below this absorption wavelength since the photons are absorbed. That is why the EQE matrix for the specular reflection on the FSLSC can be set to zero for wavelengths below the absorption wavelength, thereby modelling the aspect of absorption, and therefore only the specularly reflecting part is considered.

3.1.3 Short-Circuit Current Density from Ideal Cone Emission

The short-circuit current density due to cone emission is indicated by (2) in Figure 3.2A and represented by the black area in Figure 3.2B. This part of the irradiance is absorbed by the FSLSC and redshifted to the emission wavelength. The absorption and emission ranges are defined in the parameters file of the model.

Redshifting is modelled by integrating the number of photons over the absorption wavelength and redistributing this number of photons equally over the emission cone width. For instance, Figure 3.3 shows the conservation of photons when redshifting the photons with an absorption range of 300 to 600 nm (indicated by the purple curve) to an emission range of 675 to 725 nm (indicated by the orange curve).

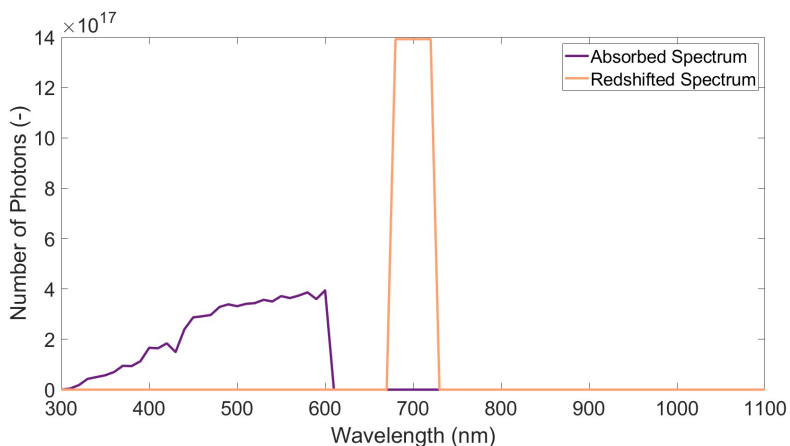


FIGURE 3.3: Redshifting photons with an absorption range of 300 to 600 nm to an emission range of 675 to 725 nm.

According to the properties of the FSLSC, these redshifted photons should be emitted in the shape of a cone. This cone shape emission is simulated by adapting the BRDF. As explained in Section 2.3, the BRDF characterizes the reflection properties of a material and has to fulfil the laws of positivity, symmetry, and energy conservation. The shape of the

cone emission can be produced by making a zero matrix with the azimuth and elevation angle as their axis and setting the BRDF to be one for angles inside the emission cone. The shape of a cone can be reproduced in a so-called BRDF matrix (M_{BRDF}). Examples of matrices and their resulting shape can be seen in Figure 3.4.

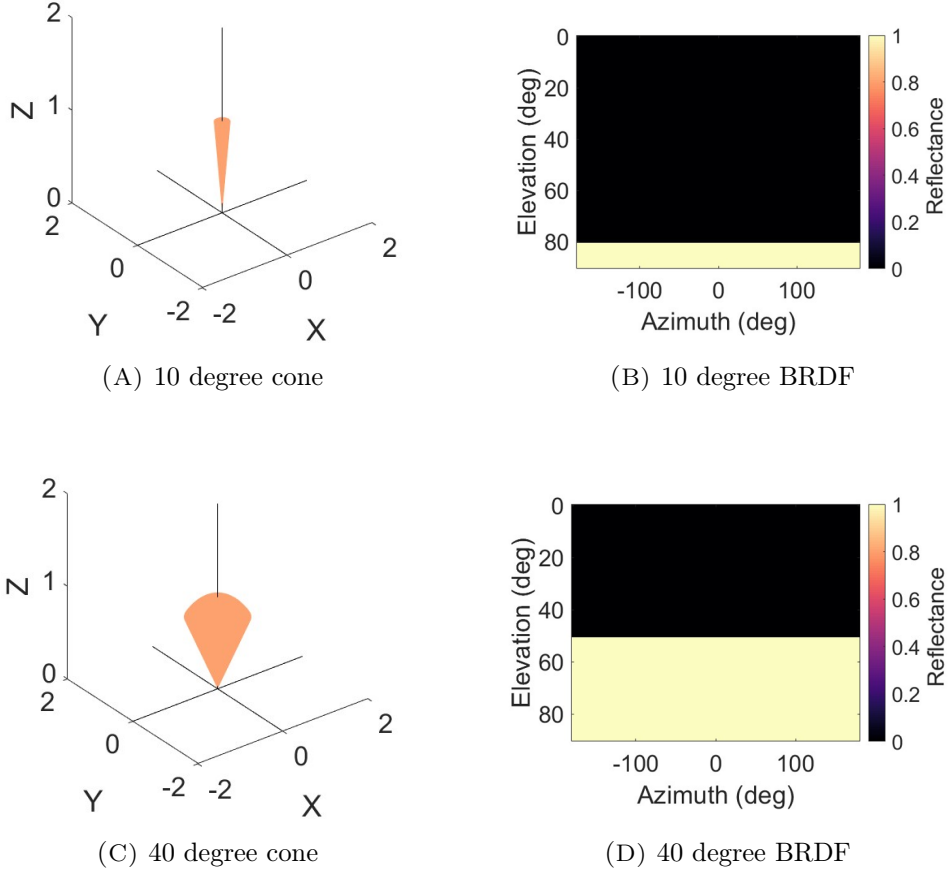


FIGURE 3.4: The shape and BRDF matrix of a 10 and 40-degree emission cone

Using the energy conservation law as mentioned below, the BRDF matrix can be normalized such that energy is conserved within the system. This will immediately result in an ideal concentration factor and therefore follows the trends as explained in Figure 1.6.

$$\int_0^{2\pi} \int_0^{\frac{\pi}{2}} M_{BRDF} \cdot \cos(\theta_r) \sin(\theta_r) d\theta_r d\phi_r = 1 \quad (3.1)$$

The final short-circuit current density from the emission cone can be calculated using Equations 2.13 and 2.14 from the existing RRT model.

3.1.4 Short-Circuit Current Density from Real Emission Cone

Up to this point, ideal properties of the emission cone have been assumed. When the real properties of the materials are taken into account, multiple loss mechanisms play a role. As explained in Section 2.5.4, the total photon efficiency (η_{tot}), i.e. the ratio of the number

of photons out to the number of photons coming in, should be taken into consideration as given in the following equation, where C is the concentration factor and C_{id} is the ideal concentration factor.

$$C = \eta_{tot} C_{id} \quad (3.2)$$

Consequently, the results should be multiplied by the total efficiency of the cone to determine the total short-circuit current density in a real case. This efficiency has been explained in Section 2.5.4 and depends on the quantum efficiency of the luminophores as shown in Figure 3.5, where the quantum yield is the number of photons that are emitted from the luminophores divided by the number of photons that are absorbed by the luminophores. The data of these efficiencies are determined by Heres [19] for cone angles up to 40 degrees, but to be able to compare higher angles as well, this data has been linearly extrapolated to a 90% efficiency for fully diffuse reflection. This 90% efficiency for a 90-degree cone is in line with common diffuse reflectors, like white paint [8]. The calculated short-circuit current density calculated for ideal cases can be multiplied by the efficiency of the cone size, for a given quantum yield of luminophores, to get the real short-circuit current density.

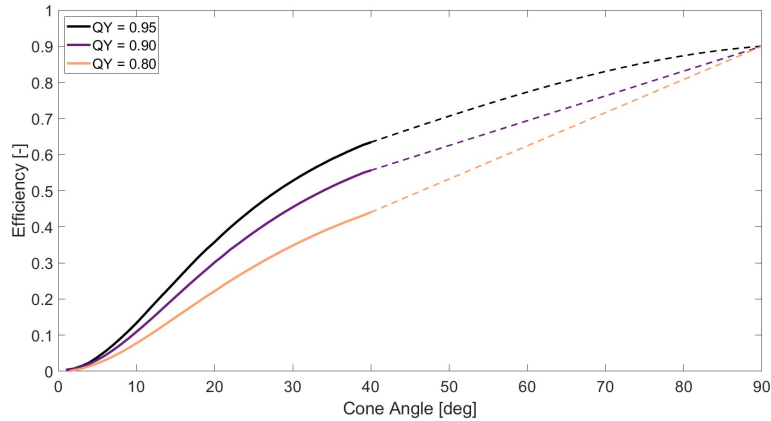


FIGURE 3.5: System efficiency of an FSLSC depending on cone size and quantum yield, given for range 5 to 40 degrees by [19] and extrapolated to 90 degrees based on a 90% efficiency of a diffuse reflector.

3.1.5 Validation of the Model

Extensive testing has been carried out to validate the model. The main validation criterium is the conservation of energy. The three different parts, short-circuit current density directly from the sky, short-circuit current density from specular reflection on the FSLSC and short-circuit current density from cone emission from the FSLSC have all been validated to conserve energy.

Specifically, the specular reflection has been validated using the following setup. The angle of incidence is set to be 90 degrees, such that the cosine factor does not influence the results. To get output from the module, the shading has to be turned off. To make sure the wavelength does not influence the results, the EQE is set to 1 for each wavelength, meaning that no photons are lost due to the EQE. In this case, the short-circuit current density generated from the sky is exactly equal to the short-circuit current density that enters the model. For specular reflection of the FSLSC, the output depends on the absorption

wavelength that is determined in the settings as can be seen in Figure 3.6. Once the reflection wavelength is set to be 300 nm, and thus all photons reflect on the FSLSC's surface, the calculated short-circuit current density exactly equals the input short-circuit current density of the global horizontal irradiance, showing that it fulfils the energy conservation law. When the wavelength is set to be at half of the spectrum (at 700 nm), 50% of the photons are reflected. If the wavelength is set at the end of the spectrum (1100 nm) and thereby all photons are absorbed and emitted in an emission cone, zero output is yielded for the specular reflection, as should be the case. Therefore, the specular reflection on the FSLSC fulfils the requirements of energy conservation.

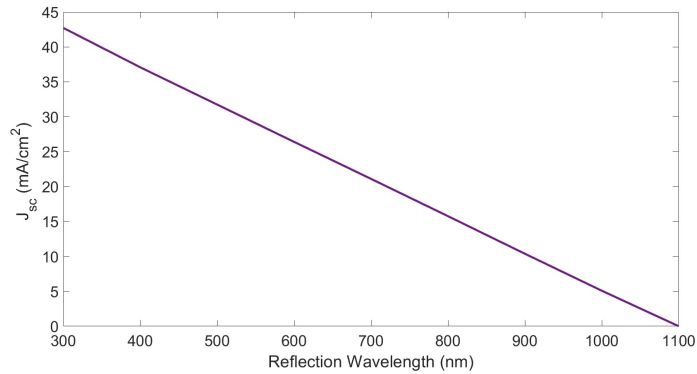


FIGURE 3.6: The calculated short-circuit current density of the specular reflection on the FSLSC for different reflectance wavelengths of the FSLSC, given the global horizontal irradiance spectrum.

All the photons that are not specularly reflected, are emitted in the shape of an emission cone. To test this emission cone, it will be compared to a known case, namely that of a diffuse reflector. By setting the emission cone to 90 degrees and having the EQE to be independent of wavelength, the diffuse calculation and emission cone should yield the exact same results. This has been tested for a variety of cases and holds in all these cases, showing that the energy conservation law is fulfilled.

3.1.6 Usage of the Model

To use the model, it is important that the convergence criteria are fulfilled. That is why these are explained in the upcoming section. In case other users would like to use the model, it is good to take certain aspects into account, that is why a list of tips for running the model has been included in the Appendix A.1. This also includes how one can run the code when looping over azimuths and elevations from another data file instead of the parameter document and how to run it for a common specular reflector and a common diffuse reflector.

Convergence

The convergence of the model has been tested in multiple scenarios, varying from horizontal, to tilted, vertical modules. An example graph can be seen in Figure 3.7. This shows that at 10 pixels per unit, convergence is reached. Given the above, 10 pixels per unit are used while using the model.

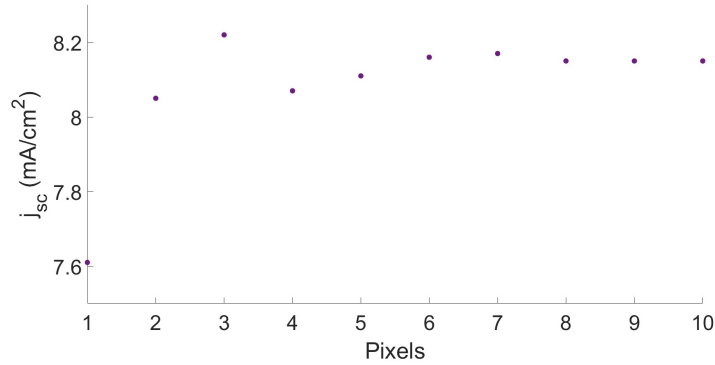


FIGURE 3.7: Short-circuit current density output for the rear of a module depending on the number of pixels per unit, showing convergence is reached at 10 pixels per unit

Angle Definitions

When using the model, it is important to keep the angle definitions into account. The geometry is initialized as is done by Pal as explained in Section 2.7.1, therefore the same angle definitions are used. The reflector is always defined to be horizontal in the Matlab script. When a horizontal reflector needs to be modelled, the elevation angle can be used. However, when a vertical reflector is modelled, the entire system is turned, meaning that it has to be simulated in such a way that the reflector is horizontal. This can be done by using the zenith angle instead of the elevation angle. Therefore for consistency in this report, in case the reflector is horizontal in the modelled situation, the elevation angle is used on the axis. When the reflector is vertical in the setup, the zenith angle is used on the axis.

3.2 Calculation Annual Yield

Using the previously explained FSLSC model, the short-circuit current density in the module can be calculated. To calculate the annual yield of the module, two different effects have to be taken into account. On the one hand, the short-circuit current density generated by the module depends on the azimuth and elevation of the sun and these change with the seasons. On the other hand, the irradiance spectrum also depends on the location and changes throughout the seasons. These two different effects will be explained below. The code calculating the annual yield can be found in Appendix C.4.

3.2.1 Calculation Power

As explained in Section 2.6.1, the power output of a solar cell can be calculated using Equation 3.3, where P is the power per module area [W/cm²], J_{sc} is the short-circuit current density [A/cm²], V_{oc} is the open-circuit voltage [V] and FF the fill factor [-].

$$P = J_{sc} \cdot V_{oc} \cdot FF \quad (3.3)$$

The FSLSC model is built on the solar cell properties from Saive [30], therefore the open-circuit voltage and fill factor of this solar cell are used, since both quantities are solar cell

dependent. For this reason, the open-circuit voltage of this cell is also used for calculations, which is 730 mV. In reality, the open-circuit voltage also depends amongst others on the temperature, but these are not taken into consideration and a constant open-circuit voltage is assumed. The fill factor is assumed to be 0.85 for the power calculations.

3.2.2 Irradiance

The irradiance varies during the year, depending on the time of the day and the day itself. The FSLSC model has three different options for irradiance, namely Extraterrestrial, 1.5 AM Global Horizontal Irradiance and 1.5 AM Direct Normal Irradiance. To change this irradiance to an annually varying irradiance, the following correction needs to be made:

$$\text{hourly yield} = \frac{\text{hourly yield with chosen irradiance}}{\text{chosen model irradiance}} \cdot \text{hourly actual irradiance} \quad (3.4)$$

Using the National Solar Radiation Database from the American National Renewable Energy Laboratory [36], the direct normal irradiance (DNI) and diffuse horizontal irradiance (DHI) can be extracted for a certain location. Using the PSM V3 Model, based on the Meoteosat Iodic satellite data, the radiation in the Netherlands can be found with a temporal resolution of 15 minutes and a spatial resolution of 4 km, for the years 2017 to 2019. The daily irradiance data for Enschede, averaged over three years, can be seen in Figure 3.8.

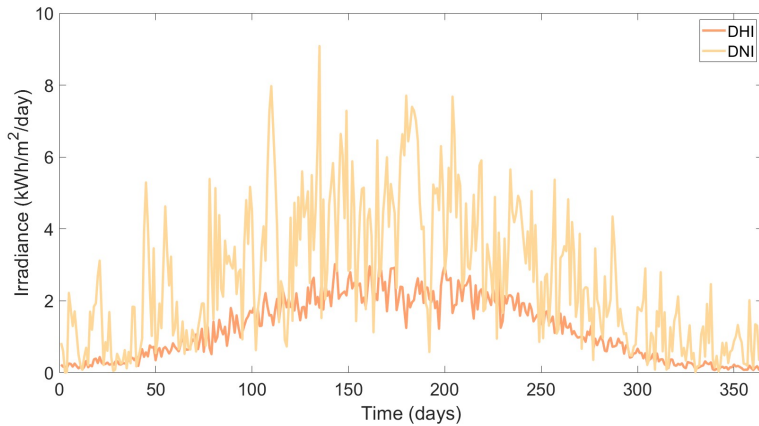


FIGURE 3.8: Daily diffuse horizontal irradiance and direct normal irradiance for Enschede (NL) as an average over 2017-2019 [36].

3.2.3 Annual Yield from Direct Irradiance

The annual yield from direct irradiance depends on the azimuth and elevation occurrences per day. These azimuth and elevation occurrences are taken from SunEarthTools [37]. The azimuth-elevation occurrences can be rewritten to a histogram, showing which azimuth-elevation occurrences happen and how often they happen on a certain day.

When multiplying this occurrence matrix, including the occurrences of each azimuth-elevation combination, with the calculated short-circuit current density for a given azimuth-elevation combination, the total current density can be calculated. In this data, some days have more 5-minute interval occurrences than other days, because the time between sunrise

and sunset is longer in summer than it is in the winter. However, as the difference in time is already taken into account in the hourly irradiance, the short-circuit current density needs to be divided by the number of occurrences per hour for normalization purposes.

3.2.4 Annual Yield from Diffuse Irradiance

Direct irradiance comes from all different angles and does not have an elevation-azimuth dependence. To calculate the yield from diffuse irradiance, it is assumed that the light comes from all different angles, i.e. 90-degree range in elevation and a 180-degree range in azimuth, with an equal probability. Therefore, the power can be calculated for all different azimuth-elevation combinations and then averaged over all azimuths and elevations. After correcting for the annual irradiance as is shown in Equation 3.4, the diffuse annual yield is given.

3.3 Multi-Criteria Analysis

As mentioned before, a multi-criteria analysis (MCA) is a decision-making procedure that explicitly considers multiple criteria to identify one best option, distinguish acceptable and unacceptable options, or rank options [22]. As was explained in Section 2.6.2, a basic analysis will result in a performance matrix, in which the different options are ranked on the different criteria which provides an overview of the socio-economic context of the technologies. The MCA aims to give such an overview in terms of a performance matrix of the different reflective technologies.

Specifically, this basic MCA will aim to assess the socio-economic aspects of the different reflectors, namely the specular reflector, diffuse reflector, and the FSLSC. The MCA will be performed on a case as described in Chapter 5. In short, a reflector is put on a façade with a solar fence in front of it. For this MCA, five different criteria have been chosen to assess the reflectors:

- Costs - How much does the reflector cost per area?
- Energy mix - When does the reflector induce a current on the solar module compared to the solar module?
- Safety - How safe is the reflector for humans and animals?
- Social Acceptance - To what extent are people expected to accept the look of the façade?
- Yield - How many additional kWh does the reflector induce on the solar panel?

First of all, the costs need to be considered while assessing the technology, as it is known that costs play a significant role when deciding on a certain sustainable energy technology [21]. Second, it will be considered how the reflector contributes to the energy mix. It would be most beneficial if the reflectors could induce electricity on the fence at the times the electricity is needed most and fits best into the current energy mix, which would mean that it generates electricity during winter [38]. Third, the safety of the façade is considered to be of major importance, as has also been shown by other MCA on façades [39]. Therefore, aspects like fire hazards are taken into consideration. Fourth, the expected social acceptance based on the visual appearance of the façade is of importance, since the aesthetics and visual comfort of a façade are decisive factors when choosing façades [39]. Lastly,

the additional yield that is induced on the solar panel by adding the reflector is assessed, as this is the main goal of installing the reflector and therefore a measure of its performance.

These criteria will be researched for the different reflectors and assessed on a scale from extremely unfavourable (- -), unfavourable (-), neutral (o), favourable (+), and extremely favourable (++) .

In this comparison, described in more detail in Chapter 5, a diffuse reflector, a specular reflector and an FSLSC are compared. For this comparison, a diffuse reflector can be considered to be white paint and a specular reflector can be seen as a mirror.

Chapter 4

Results & Discussion of a Generic FSLSC

In this chapter, a generic case is studied to examine the effects of changing the cone size of the FSLSC on the short-circuit current density output of the bifacial solar module. First, the setup is described. Subsequently in Section 4.2, the results assuming ideal FSLSC properties are discussed. In Section 4.3, loss mechanisms are taken into account and the real FSLSC properties are discussed.

4.1 Case setup

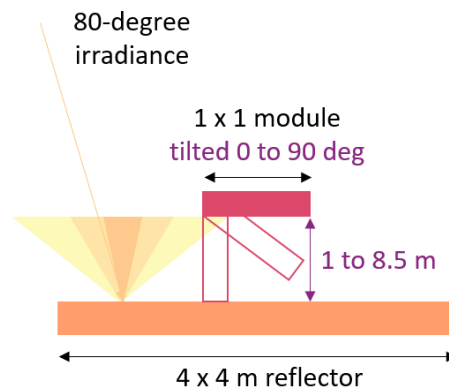


FIGURE 4.1: Generic setup where a 1 by 1 m bifacial solar module is placed in the centre and front of a 4 by 4 m reflector. The module is varied in position, both in tilt (from horizontal to vertical) and height (from 1.0 to 8.5 m).

The generic setup is described in Figure 4.1 and simulated for cases where the cone size is varied from 10 to 90 degrees, in steps of 10 degrees. The module is rotated counter-clockwise, to be able to examine the effects on the reflector. In this particular case, the absorption and emission spectra are set in the ranges of 300 to 700 nm and 875 to 925 nm, respectively. This choice is based on possible luminophore properties. For incoming radiation, the 1.5 AM direct normal irradiance (DNI) spectrum is used.

Figure 4.2 shows the short-circuit current density generated by the front of the module and the specular reflection on the FSLSC to the rear of the module. Please note that this short-circuit current density is per area of the module. The specular reflection is assumed to have a 100% efficiency in this case, meaning that all the photons with a wavelength above 700 nm that reach the FSLSC are reflected, based on the assumptions of the FSLSC model. The wavelength of the photons during specular reflection is conserved and the angle is changed according to specular reflection. The short-circuit current density generated by the front and specular reflection on the rear of the FSLSC are independent of the properties of the FSLSC, given the reflection range and reflection properties of the FSLSC.

Figure 4.2 also shows that the short-circuit current density generated at the front of the panel is solely dependent on the module's tilt and is independent of the height. A similar trend can be seen for the specular reflection on the rear, given that the height is at least 3 meters. This is expected since shade is induced on the reflector at low heights, depending on the module's tilt. When the shade does not play a role, which is the case for the front of the panel and the specular reflection at the rear above 3 meters, the short-circuit current density only depends on the tilt. The reason for this is that the specular reflection and incoming ray beams do not diverge, i.e. the area of the beam is constant, meaning that the height does not play a role.

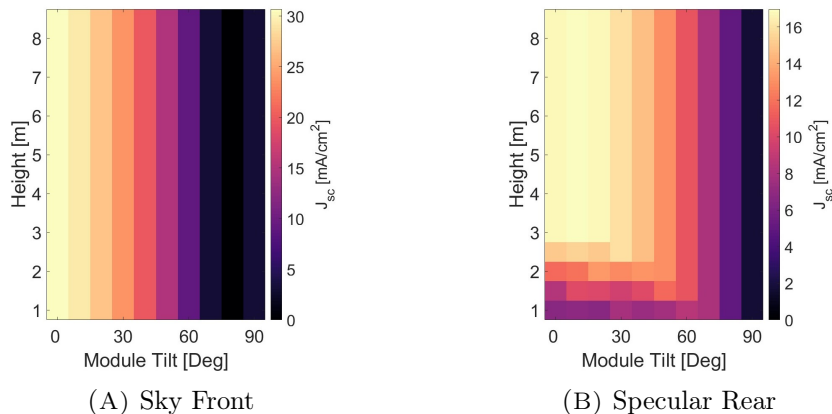


FIGURE 4.2: Short-circuit current density generated from A) the direct irradiance from the sky on the front of the module and B) the specular reflection of the FSLSC to the rear of the module in the generic setup. Both depend on the module's height above the reflector and the module's tilt.

4.2 Ideal Properties

When ideal properties are assumed, the quantum yield of luminophores is taken to be 100% and all the other loss mechanisms are not taken into consideration, meaning that all the photons entering the device also leave the device. An overview of the ideal results from the cone emission for several cone sizes can be seen in Figure 4.3. Please note, the upcoming figures do not include the short-circuit current density generated by specular reflection towards the rear of the module or the short-circuit current density directly from the sky on the front of the module, but solely focus on the emission of the cone. Furthermore, note that all short-circuit current densities are per area of the module, not of the reflector.

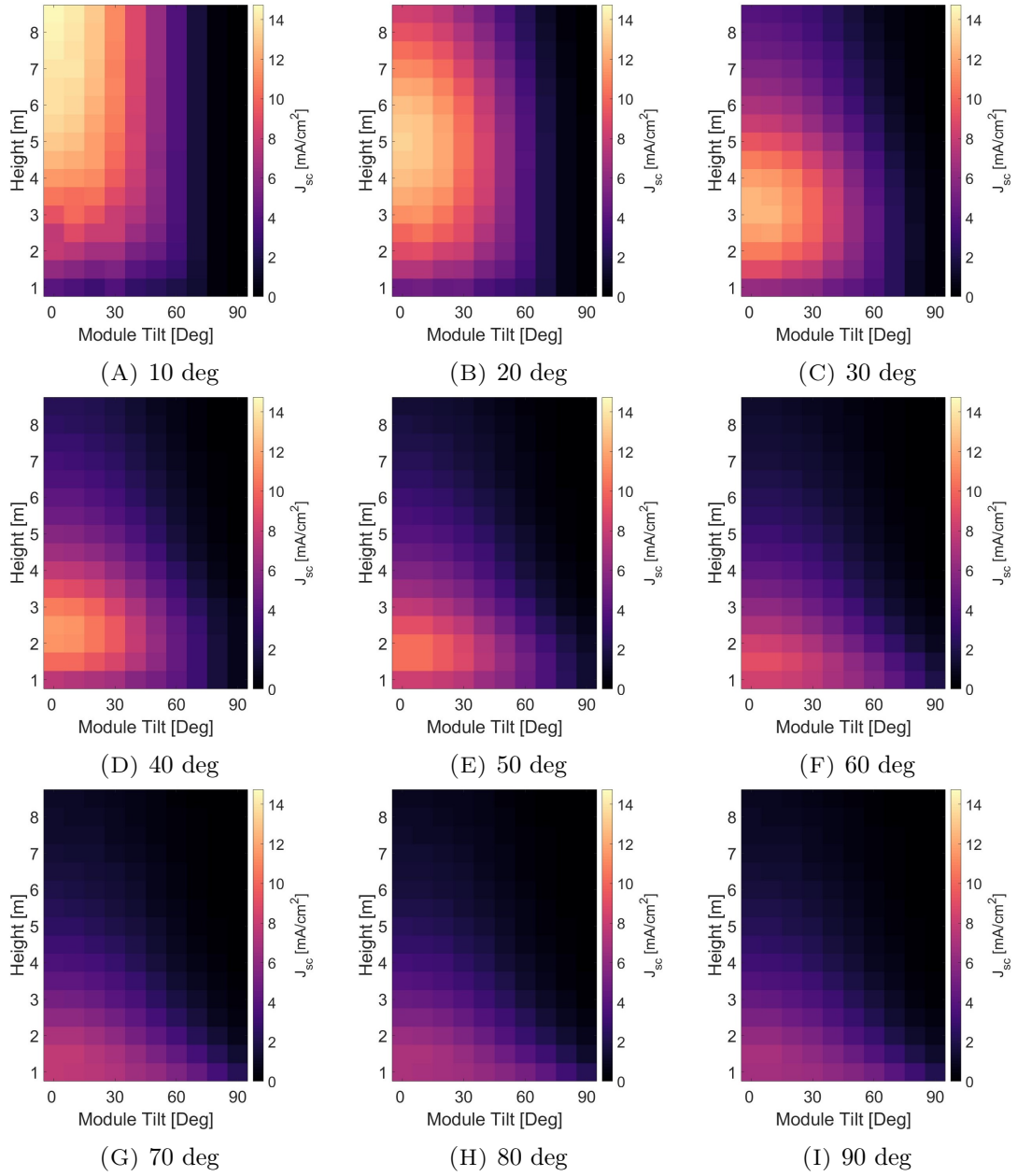


FIGURE 4.3: Short-circuit current density generated in the generic set-up from ideal cone emission to the rear of the module, for a variety of emission cone angles depending on the module's height and tilt.

For every cone size, two effects are of main influence of the height of the module. On the one hand, the larger the distance between the module and the reflector, the larger the area of the reflector that can contribute to reflection. This is also described in Figure 4.4A, where the emission at the edge of the reflector can reach the middle of the module at a 1 m height, given that the emission cone is larger than 63.4 degrees. With decreasing cone size, the height, at which this full reflector area is used, is increasing. For instance, the required height to use the entire reflector is 2.38 m for a 40-degree cone size as is displayed in Figure 4.4B. This distance increases even further with decreasing cone size, to 3.46 m, 5.49 m, and 11.34 m for 30, 20, and 10-degree cones, respectively, for the given system dimensions. Similarly, the larger the distance between the module and the reflector, the smaller the effect of shading is, since the shaded area will be further away from the centre of the module for higher heights, given that the irradiance is not coming from 90 degrees. On the other hand, the intensity of the cone decreases with height. When the cone is captured at a higher height, less short-circuit current density will be captured, because the photons are spread over a larger area.

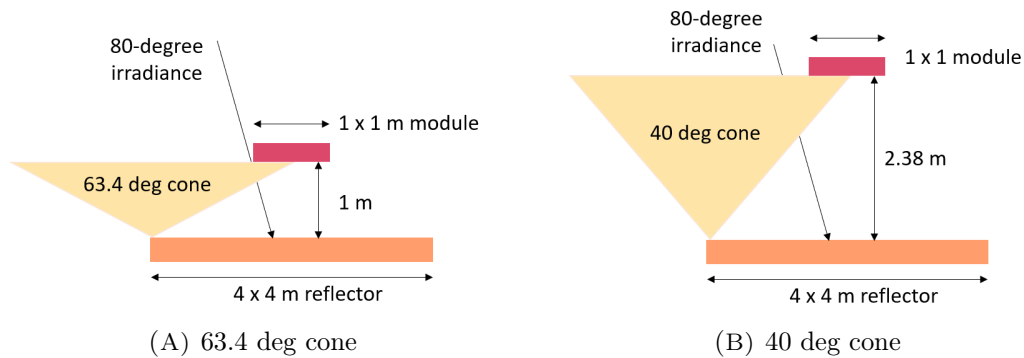


FIGURE 4.4: The angle at which the emission from the edge of the reflector can reach the middle of the module for different module heights for A) a module at 1 m height and B) for an emission cone of 40 degrees.

These two counteracting effects lead to an optimum height for each cone angle, where the entire area of the reflector is used and the intensity of the cone is as high as possible. Since the intensity of the cone is highest for a 10-degree cone, this specific case yields the highest short-circuit current density. The simulated maximum short-circuit current density decreases with an increasing cone size, due to the lower intensity with increasing cone size.

This influence of decreasing photons intensity with an increasing area over which it is spread can also be seen in cone sizes larger than 63.4 degrees, where the entire reflector area is used. Therefore, in these cases, the influence of the reflector's area contributing to reflection based on height is eliminated and only the dependence on photon intensity is shown. As can be seen in Figure 4.5, where these larger cone sizes have been plotted on a different scale, the larger the cone size, the lower the photon intensity, and therefore the lower the short-circuit current density. Whereas the maximum for a 70-degree cone size is 7.79 mA/cm^2 , the maximum short-circuit current density for 80 and 90-degree cones are only 7.06 mA/cm^2 and 6.83 mA/cm^2 , respectively.

In general, when looking into the tilt of the module, two other counteracting effects play a role. First, the more tilted the module is, the more light reaches the module at shallow

angles. Due to the cosine factor, the light at shallower angles produces less short-circuit current density than light when it would have hit the module perpendicularly. This leads to the optimum always being at a horizontal module and a decrease in output when tilting the module. Second, the wider the cone is, the more the light is spread over all directions and the less light is directed in a vertical manner. In case the module is tilted, the light in the horizontal direction can be captured and therefore the output for wider cone sizes in fully tilted modules (vertical module with 90-degree tilt) is higher than for smaller cone sizes.

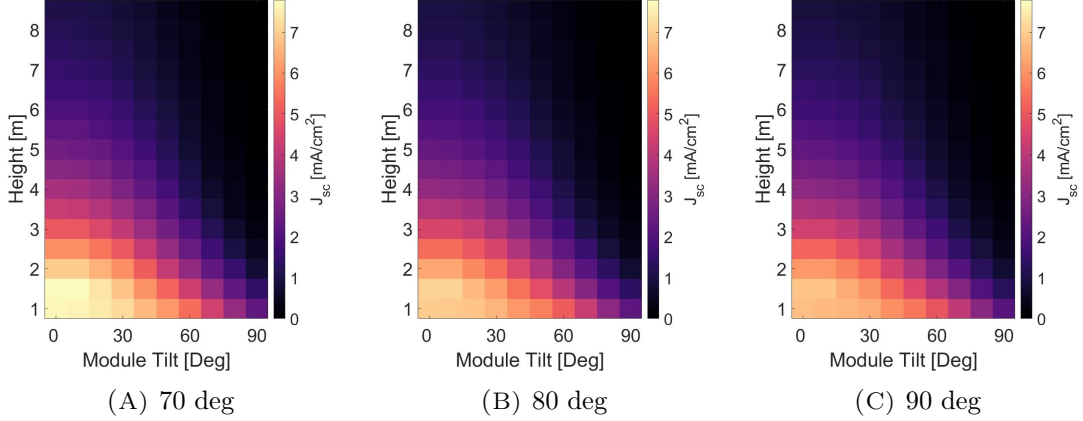


FIGURE 4.5: Short-circuit current density from ideal cone emission for cones sizes of 70, 80, and 90 degrees on a lower short-circuit current density scale compared to Figure 4.3.

Concluding, multiple different effects play a role in determining the output of the cone emission of an FSLSC. Regarding the distance between the module and the reflector, the short-circuit current density increases with an increasing distance up to the point where the edges of the reflector can emit to the middle of the module. After this point, the short-circuit current density decreases with increasing distance due to a decrease in photon intensity as the photons are spread over a larger area. Regarding the module's tilt, the optimum is always when the module and reflector are parallel to each other.

4.3 Real Properties

In the previous section, the ideal properties of an FSLSC were assumed. In reality, the system's efficiency is not 100% as explained in Section 3.1.4, where the efficiency is given for multiple quantum yields of luminophores (QY) extrapolated to angles of 90 degrees. In this section, the influence of taking these quantum yields of luminophores into consideration will be explained.

Figure 4.6 shows the short-circuit current density when taking into account a quantum yield of luminophores of 95%. Based on this, the maximum short-circuit current density is obtained for a 40-degree cone angle, where the maximum short-circuit current density is 7.32 mA/cm². This maximum short-circuit current density decreases for smaller cone sizes, it is still 6.57 mA/cm² for a 30-degree cone, but it reduces even further for 20- and 10-degree cones. The maximum short-circuit current density for a 50-degree cone is comparable to the 40-degree cone, with the 7.29 mA/cm² output, but the short-circuit current

density decreases when further increasing the cone size.

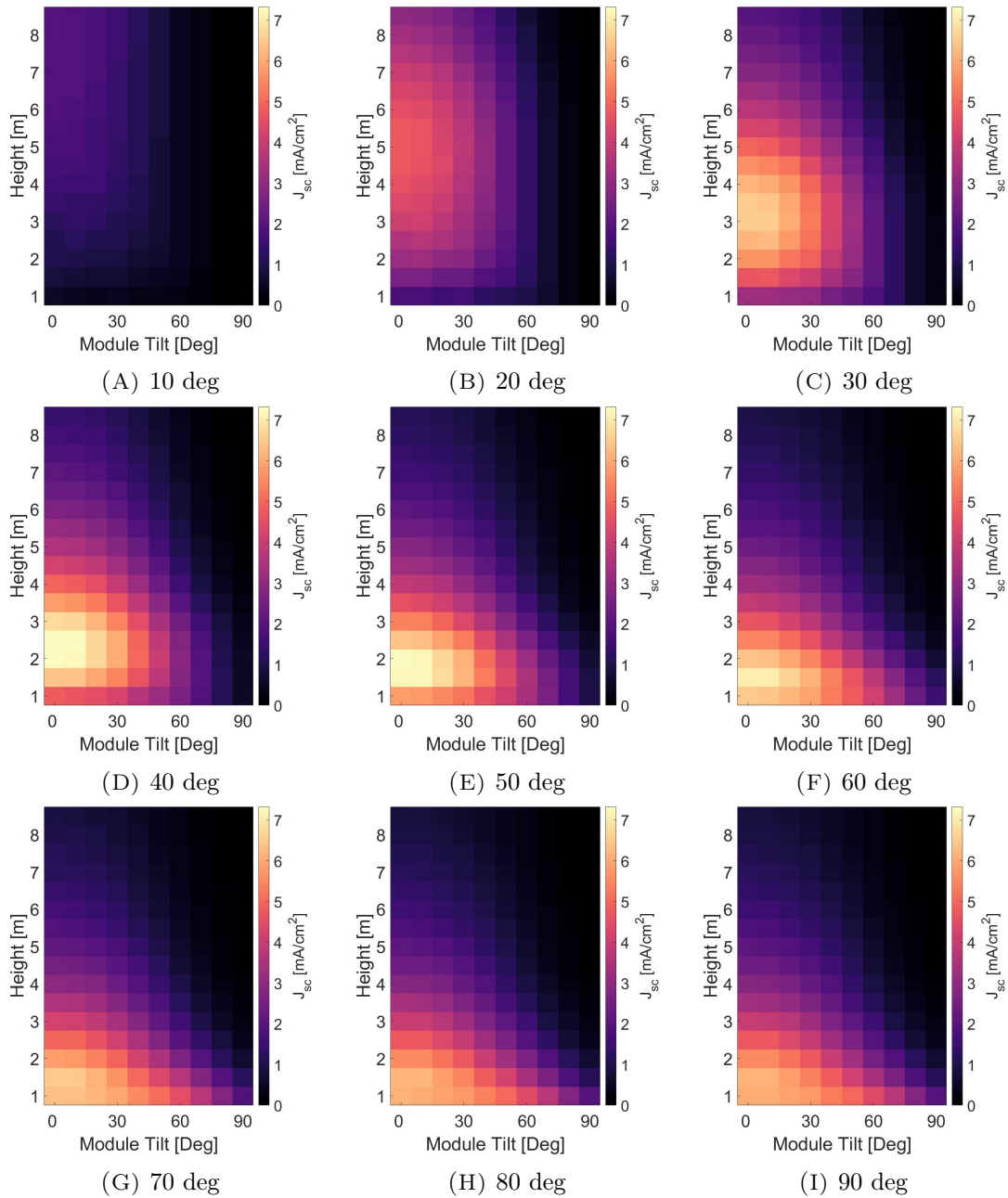


FIGURE 4.6: Short-circuit current density in the generic set-up for varying the cone emission angles with a quantum yield of luminophores of 95%, depending on the module's height and tilt.

Furthermore, Figure 4.6 shows that in case the distance between the module and FSLSC can be freely chosen, the 40-degree cone angle would result in the highest short-circuit current density from the cases that have been run, given that the quantum yield of luminophores is 95%. Nonetheless, a 50-degree cone angle yields comparable results with a small difference of 0.03 mA/cm^2 , therefore the entire range between 40 and 50-degree cone angles seems to yield high short-circuit current densities, when looking at a quantum yield

of luminophores of 95%.

Figure 4.7 shows a comparison between multiple quantum yields of luminophores. The efficiency data for multiple luminophore quantum yields of an FSLSC is only known for 5 to 40-degree cone angles but has been linearly extrapolated to 90 degrees as well. Yet, this imposes a larger uncertainty, which is indicated by the dashed lines. Based on this figure, it can be seen that in the case of an ideal luminophore quantum yield, the output short-circuit current density is highest for a 10-degree cone and decreases with cone size. However, when taking quantum yields of luminophores into account, the trend reverses and the highest output is at 40 degrees. Due to the extrapolation and the used step size a specific cone angle with the highest short-circuit current density cannot be determined. Nonetheless, it can be seen that the short-circuit current density increases with increasing cone size for this given range.

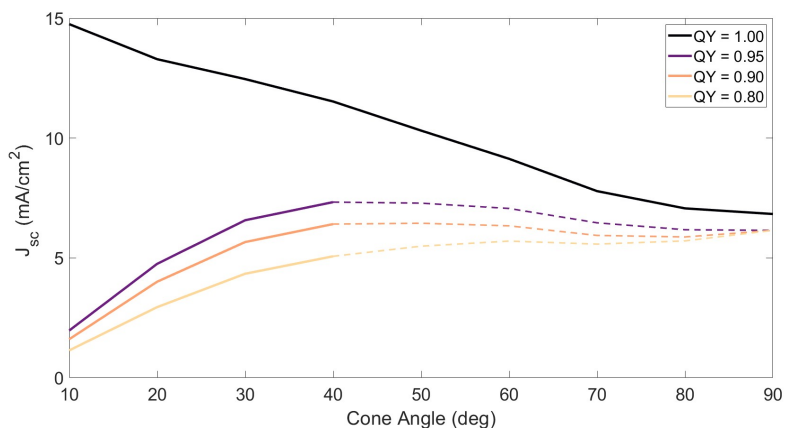


FIGURE 4.7: Comparison of maximum short-circuit current density reached, while varying module’s height and tilt, for multiple quantum yields of luminophores in the generic setup. Data on the quantum yields in known for the range of 10 to 40 degrees (solid line) and extrapolated for higher angles (dashed line).

The reason for this optimum being around 40 to 50 degrees is a result of two counter-acting effects. On the one hand, the maximum short-circuit current density decreases with increasing cone size due to a lower photon intensity, as was already explained in the previous section. On the other hand, when assuming real properties, the system efficiency now plays a role. For a small cone angle, the system efficiency is low. The photons can only go out of the material at a small angle, therefore, the optical path of a photon and the time that a photon is in the material is very long. This leads to all sorts of loss mechanism occurrences, like the combination of re-absorption with a non-ideal quantum yield of luminophores. The larger the cone, the shorter the optical path and the lower these losses. For example, whereas the number of photons that get out of the 10-degree cone is only 13.3% of the incoming photons, this is already 63.4% for a 40-degree cone, given a luminophore quantum yield of 95%.

When comparing the different quantum yields of luminophores, it is as expected that a higher quantum yield leads to a higher short-circuit current density output, as fewer photons are being lost during the Stokes-shifting by the luminophores and therefore the re-absorption losses are also less. Changing from a perfect quantum yield to a real quan-

tum yield seems to have the largest influence, as the additional factor of efficiency starts to play a role.

Concluding, when looking at the generic case of having a 1 by 1 m module in the centre of a 4 by 4 m reflector for ideal and real FSLSC properties, the system efficiency plays a significant role. When assuming ideal properties, the short-circuit current density in the module decreases with increasing cone angle due to the lower concentration factor. When taking loss mechanism occurrences into account, the short-circuit current density increases with increasing cone angle up to an optimum of around 40 degrees. Afterwards, the short-circuit current densities decrease again. Even though the case is chosen to be as generic as possible, the particular system design and its quantum yields do influence these results, which should be noted. Nonetheless, it serves as a good example of generic FSLSC behaviour and a good starting point for a practical application in the upcoming chapter.

Chapter 5

Case Study: FSLSC on Façade

In this chapter, a case study is performed on an FSLSC on a façade with a vertical bifacial solar fence placed in front. In Section 5.1, the setup of the case will be explained in more detail. In Section 5.2, the solar path for the chosen location, Enschede (the Netherlands), is shown. Afterwards, Section 5.3 will describe the short-circuit current density from the front of the module and the FSLSC's specular reflection towards the rear of the module. Sections 5.4 and 5.5 will describe the cone emission in ideal and real simulations, where the different cone sizes are compared. In Section 5.6, a diffuse reflector, a specular reflector and an FSLSC with optimal cone size are compared based on the short-circuit current density, the annual yield and the socio-economic aspects.

5.1 Case setup

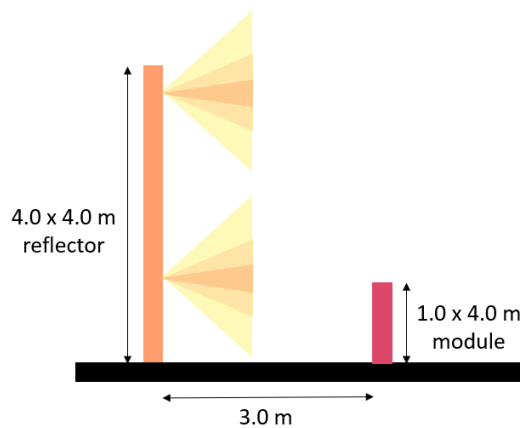


FIGURE 5.1: Case with a 4 by 4 m FSLSC on a façade and a 1 by 4 m bifacial solar fence in front, the cone sizes of the FSLSC will be varied to study the influence and calculate the annual yield. This setup is located in Enschede, the Netherlands.

In this case, a closer look will be taken at the possibility to put an FSLSC on a façade with a bifacial solar fence in front. An overview can be seen in Figure 5.1, which describes a situation where a 4 by 4 m reflector is put on the house's façade and a 1 by 4 m bifacial solar fence is put in front at a distance of 3 m. The façade and the front of the bifacial fence are oriented towards the south. The absorption and emission spectra of the luminophores are set to be from 300 to 700 nm and 975 and 1025 nm, respectively, in accordance with

the ranges of luminophores. The location for this system is Enschede, the Netherlands, and the 1.5 AM direct normal irradiance (DNI) is used to run the model.

5.2 Azimuth & Elevation Occurrences

To compare the application of an FSLSC for different cone angle sizes, the location on earth is of importance as the solar elevation and azimuth influence the output of the FSLSC. Figure 5.2 shows a histogram of the different azimuth and elevation angles that occurred in 2022 in Enschede, sampled every 5 minutes. It also includes examples of the occurrences on one day, specifically for the 21st of June and the 21st of December. It can be seen that occurrences of an elevation angle above 63 degrees have not been reported for this location. In this figure, a 180-degree azimuth is defined to be south. For example, this means that when the sun comes from the south, the elevation angle is only between 12 and 63 degrees.

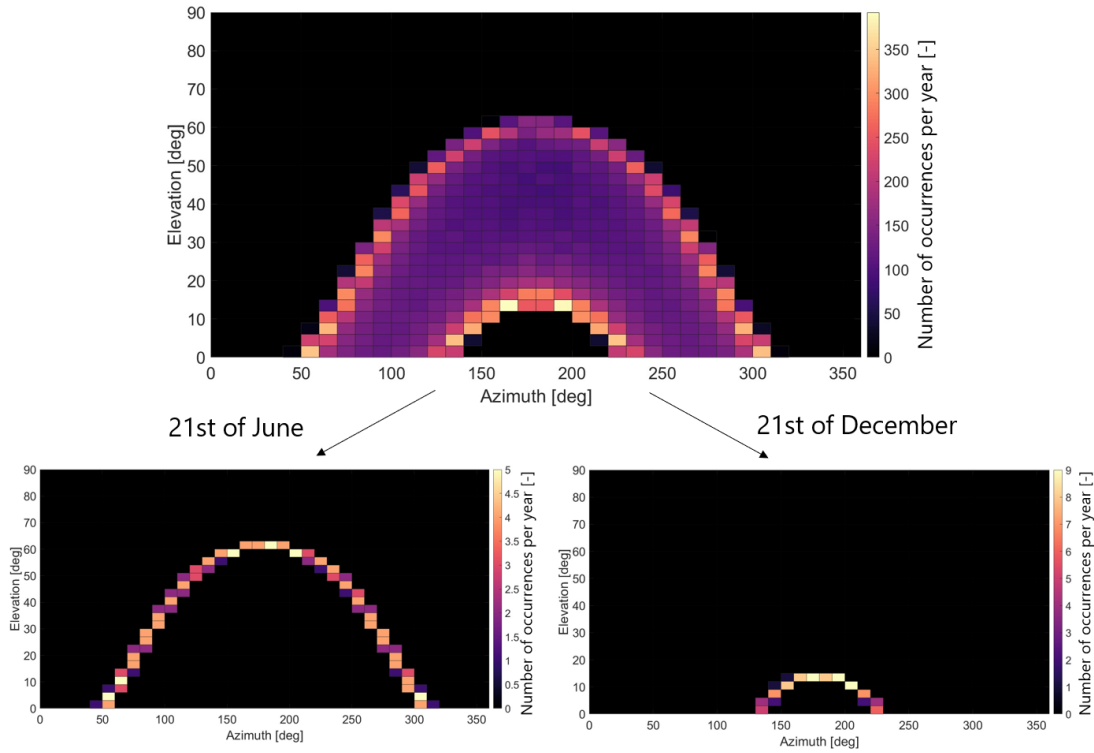


FIGURE 5.2: Annual azimuth and elevation occurrences in Enschede (NL)

To simulate this situation and to be able to compare the different cone sizes, it is assumed that the façade is located next to other buildings so only azimuths between 90 and 270 degrees can reach the solar panel. When symmetry is assumed, only the cases between 90 and 180-degree azimuth are simulated. The exact simulation parameters, according to the Matlab model, together with the number of occurrences of each azimuth-elevation combination can be found in Appendix B.1. The short-circuit current densities are obtained for these elevation-azimuth combinations and the results are discussed in the sections below.

5.3 Front & Specular Reflection on FSLSC

The properties of the FSLSC, like cone size, influence the output of the emission cone towards the bifacial solar module, given a certain reflection wavelength and reflection properties. Nonetheless, the output of the front of the module as well as the specular reflection of the FSLSC to the rear of the module are independent of the emission cone properties, given a certain absorption range. The output of the front of the module and specular reflection towards the rear of the module can be seen in Figure 5.3. Azimuth-elevation combinations that are marked as black, are instances which are not occurring for the chosen location and therefore the simulation did not run for these occurrences to save computational time.

Figure 5.3A shows that the short-circuit current density on the front of the module, based on direct irradiance, is only based on elevation angle. This is due to the fact that the cosine factor influences the area and thereby the intensity of the irradiance, as is explained in Section 2.4. In the same section is explained that the azimuth does not influence this cosine factor as long as the plane is perpendicular to the elevation plane. Therefore, a change in azimuth will not change the short-circuit current density output.

Figure 5.3B displays the short-circuit current density due to specular reflection on the FSLSC per module area. For this figure, a 100% efficiency of the specular reflector is assumed and the wavelengths are conserved. This shows again that output decreases with decreasing zenith, due to the cosine factor. For the specular reflection, the azimuth does influence the short-circuit current density received by the module, because for low and high azimuths, the reflection will be close to parallel to the module and therefore not able to reach the module.

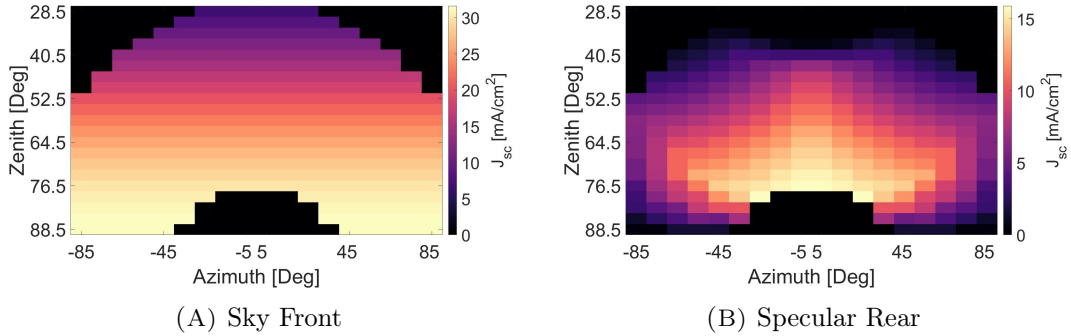


FIGURE 5.3: Short-circuit current density generated from the direct irradiance from the sky on the front of the module and the specular reflection of the FSLSC to the rear of the module in the façade case.

5.4 Ideal Properties

An overview of the short-circuit current density generated by cone emission can be found in Figure 5.4. In this case, the properties of the FSLSC are assumed to be ideal, meaning that loss mechanisms are not taken into account. Note that only the emission of the cone is considered and this does not include short-circuit current density generated by the front

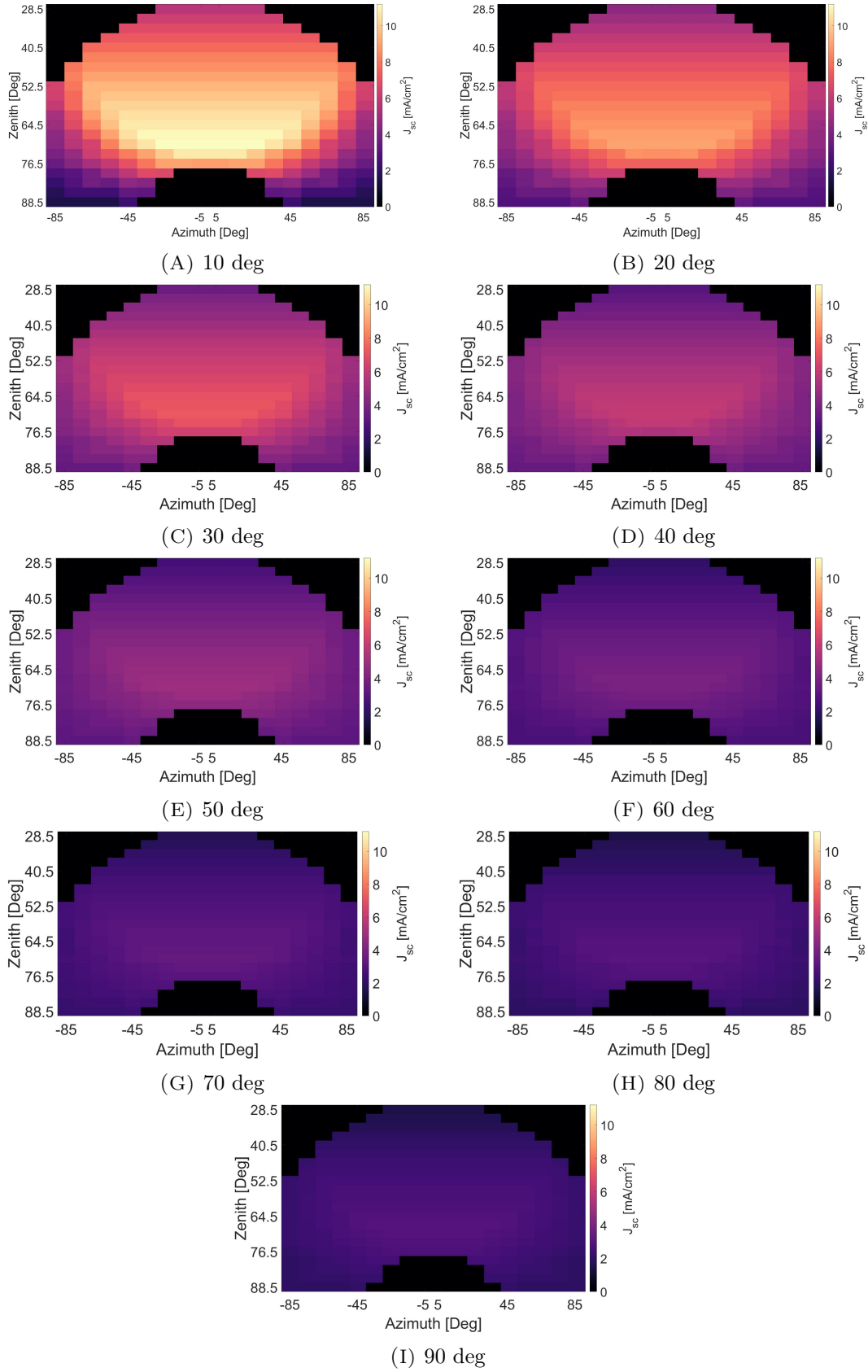


FIGURE 5.4: Emission cone short-circuit current density in the façade set-up for the occurring azimuth-elevation cases, for a variety of cone angles assuming ideal FSLSC properties.

of the module or by the rear of the module due to specular reflection on the FSLSC.

It can be seen that the highest short-circuit current density is reached for a 10-degree cone and decreases with increasing cone size. This can also be seen in Figure 5.5, where the maximum and minimum short-circuit current densities for a simulated azimuth-elevation case are shown. The reason for this decrease in short-circuit current density with increasing cone size is the fact that the concentration factor of the FSLSC also decreases with cone size. The photon intensity in a 10-degree cone is higher than for all other cone angles, hence the highest short-circuit current density can be reached for a narrow cone.

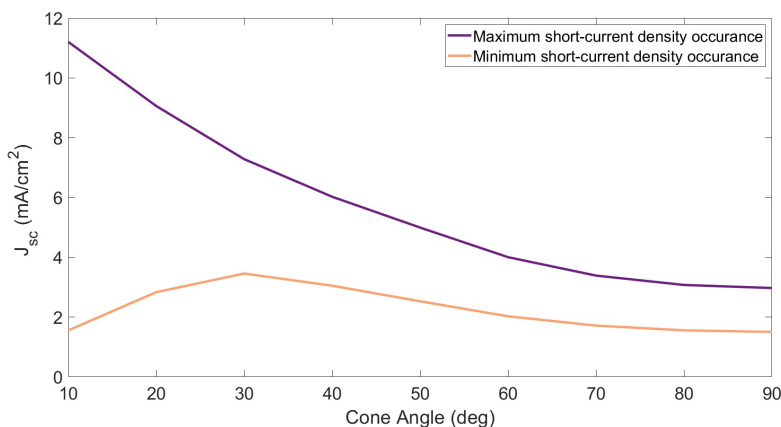


FIGURE 5.5: Comparison of the minimum and maximum short-circuit current density of the simulated azimuth-elevation occurrences, for different cone sizes assuming ideal FSLSC properties.

The minimum short-circuit current density, meaning the azimuth-elevation combination where the lowest short-circuit current density is given, varies with cone size as well. Up to a 30-degree cone angle, the minimum occurs at an azimuth of (-) 85 degrees and a zenith angle of 88.5 degrees (at the bottom corners of Figure 5.4). This value increases with cone size, since a larger part of the FSLSC will contribute to the reflection for a larger cone size. When the cone angle is 45 degrees, as can be seen in Appendix B.2, the entire area of the FSLSC is contributing to the module by means of cone emissions.

For a cone angle higher than 40 degrees, the minimum occurs at a zenith angle of 28.5 degrees (on the top of Figure 5.4). With increasing cone size, the generated short-circuit current density decreases at a low zenith angle, this leads to lower minima. The reason why the short-circuit current density decreases is that the photon intensity decreases with increasing cone size, meaning that the part of the emission cone that reaches the solar panel stays the same, but the photon intensity within this part of the cone is lower, since photons are now also going in other directions. In this way, fewer photons reach the solar panel and can induce a current and therefore the short-circuit current density induced decreases with increasing cone size.

In short, the maximum short-circuit current density that is reached for a certain azimuth-elevation occurrence is decreasing with increasing cone size, for an ideal FSLSC. The minimum short-circuit current density from the simulated azimuth-elevation occurrences is increasing between 10 and 30 degrees, shifts from high zenith to low zenith at 30 degrees,

and decreases from 30 degrees onwards. This is due to two counter-acting effects playing a role. On the one hand, the larger the cone size, the larger the area of the FSLSC that is contributing to the short-circuit current density, up to the point where the entire area of the reflector is used at a 45-degree cone size. On the other hand, the smaller the cone size, the higher the photon intensity within the cone, and therefore the higher the induced short-circuit current density.

5.5 Real Properties

The system cannot be fully ideal, which is why real system efficiencies should be taken into account. Figure 5.6 shows the short-circuit current density for different cone sizes, taking into account a quantum yield of luminophores of 95%.

In Figure 5.7, the maximum and minimum short-circuit current densities that are occurring for the given azimuth-elevation instances, as shown in Figure 5.6, are plotted. It can be seen that both the maximum and minimum short-circuit current density increase between 10 and 30 to 40 degrees and decrease again afterwards.

Specifically, when looking at the highest short-circuit current density for varying solar azimuth angles, the short-circuit current densities of a 30-degree cone and 40-degree cone are comparable, being 3.84 and 3.82 mA/cm² respectively. The maximum short-circuit current density of a 50-degree cone is 3.52 mA/cm² and decreases further with increasing cone size. The 20 and 10-degree emission cones reach a maximum of 3.24 and 1.49 mA/cm², respectively. This shows that there is a short-circuit current density optimum of around 30 to 40 degrees.

When taking a closer look at the minimum current densities, the location of the minimum shifts again from a (-) 85-degree azimuth and 88.5-degree zenith (bottom corner in the figure) to the lowest zenith (middle top in the figure) at 40 degrees, similar to the ideal case. Nonetheless, the highest minimum short-circuit current density occurs at a 40-degree cone angle with a value of 1.93 mA/cm² compared to a short-circuit current density of 1.82 mA/cm² for a 30-degree cone.

The trends that can be seen are a combination of three effects. Two effects are similar to the ideal case. First, at a cone angle of 45 degrees, the entire reflector is reflecting towards the module. That means that up to a cone angle of 45 degrees, the reflective area increases with increasing cone size. Second, the ideal photon intensity decreases with increasing cone size. Yet, this now has an additional factor, which is the system efficiency. This means that there is a trade-off between high system efficiency and high concentration factor.

In conclusion, the trends that were seen when assuming an ideal FSLSC alter when taking into account the quantum yield of the luminophores. This is a result of the system efficiency that is taken into account, which is dependent on the cone size. Furthermore, similar to the ideal case, the cone size influences the ideal concentration factor and the area of the reflector that is contributing to the short-circuit current density. The short-circuit current densities increase up to a cone size of around 40 degrees and start to decrease afterwards. The optimal cone angle for the highest and lowest short-circuit current density is a 40-degree cone angle, which would therefore be the most optimal cone angle from the tested cone angles. This 40-degree cone angle will therefore be used in all upcoming

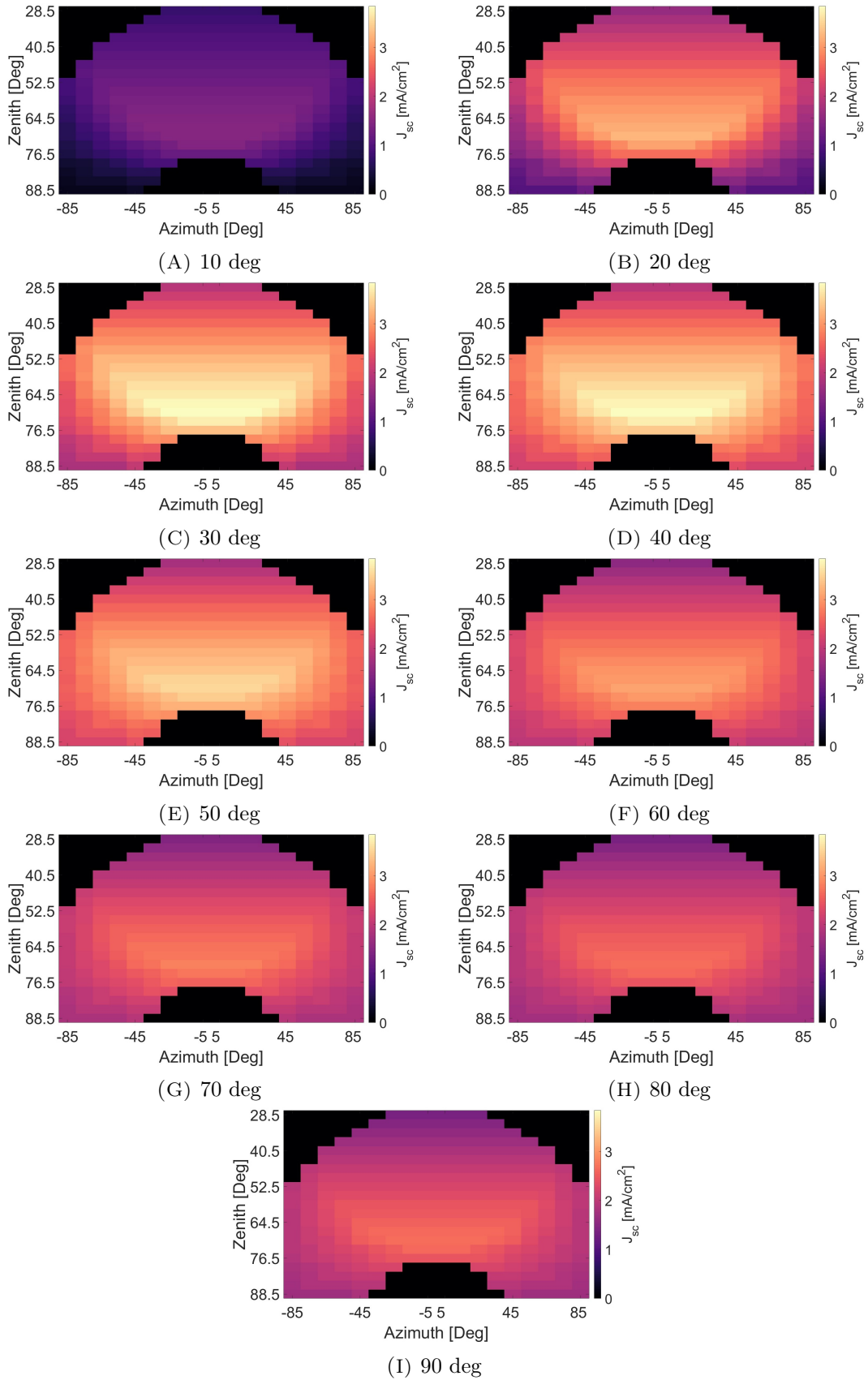


FIGURE 5.6: Emission cone short-circuit current density for a variety of cone angles with a quantum yield of luminophores of 95% in the façade setup.

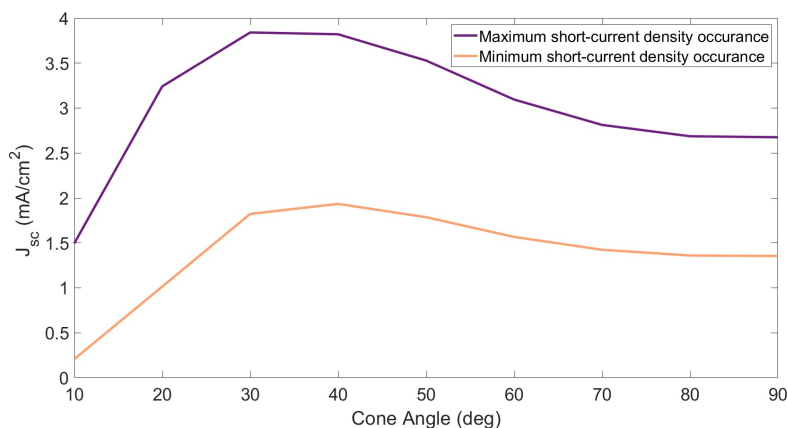


FIGURE 5.7: Maximum and minimum short-circuit current density for all azimuth-elevation occurrences in Enschede, for a variety of cone sizes, given a luminophore quantum yield of 95%.

calculations and comparisons.

5.6 Comparison between Real FSLSC, Specular, and Diffuse Reflector

Given the above, a comparison will be carried out between an FSLSC, a diffuse and a specular reflector with realistic losses. The FSLSC is assumed to have a luminophore quantum yield of 95% and a cone size of 40 degrees, since this cone size has yielded the highest short-circuit current densities. The specular reflection of the FSLSC will be assumed to have an efficiency of 90%. The specular and diffuse reflectors also have an efficiency of 90%. For this comparison, the short-circuit current density from the entire rear of the module is compared, meaning that the specular reflection on the FSLSC and cone emission of the FSLSC are both taken into consideration, but the short-circuit current density of the front is excluded. After the short-circuit current densities have been compared, the yield will be calculated, an MCA analysis will be performed and the reflectors will be compared.

5.6.1 Short-Circuit Current Density Comparison

Figure 5.8 shows the comparison between the short-circuit current densities of a fully diffuse reflector, a fully specular reflector, and a 40-degree FSLSC. A more detailed comparison can be found in Figure 5.9 and Figure 5.10, where the difference between the FSLSC and a diffuse and specular reflector, respectively, are shown. It shows that an FSLSC outperforms a diffuse reflector in 86% of the elevation-azimuth combinations, with an average short-circuit current density of 5.76 mA/cm². The diffuse reflector outperforms the FSLSC in 14% of the cases, with an average short-circuit current density of 0.76 mA/cm². When taking a closer look at the comparison between the specular reflector and the FSLSC, it can be noted that the specular reflector outperforms the FSLSC in 74% of the elevation-azimuth combinations, with an average short-circuit current density of 3.60 mA/cm², whereas the FSLSC outperforms the specular reflector in 26% of the cases with an average short-circuit

current density of 1.22 mA/cm^2 .

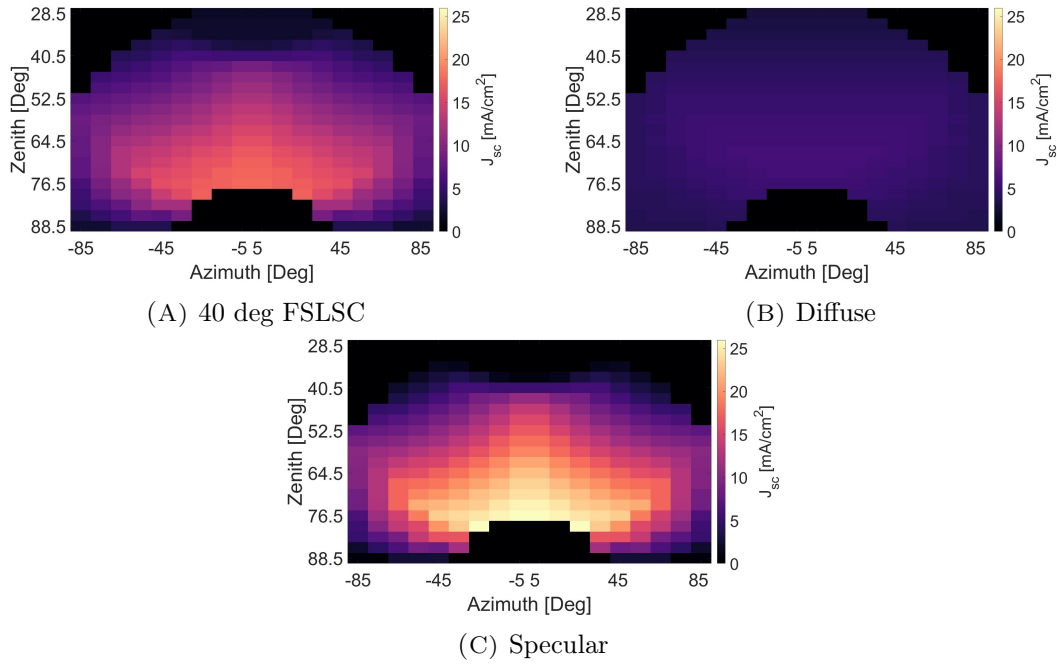


FIGURE 5.8: Comparison of the short-circuit current density reaching the rear of the module for a 40-degree FSLSC, with a luminophore quantum yield of 95% and a reflection efficiency of 90%, and fully diffuse and specular reflectors with an efficiency of 90%.

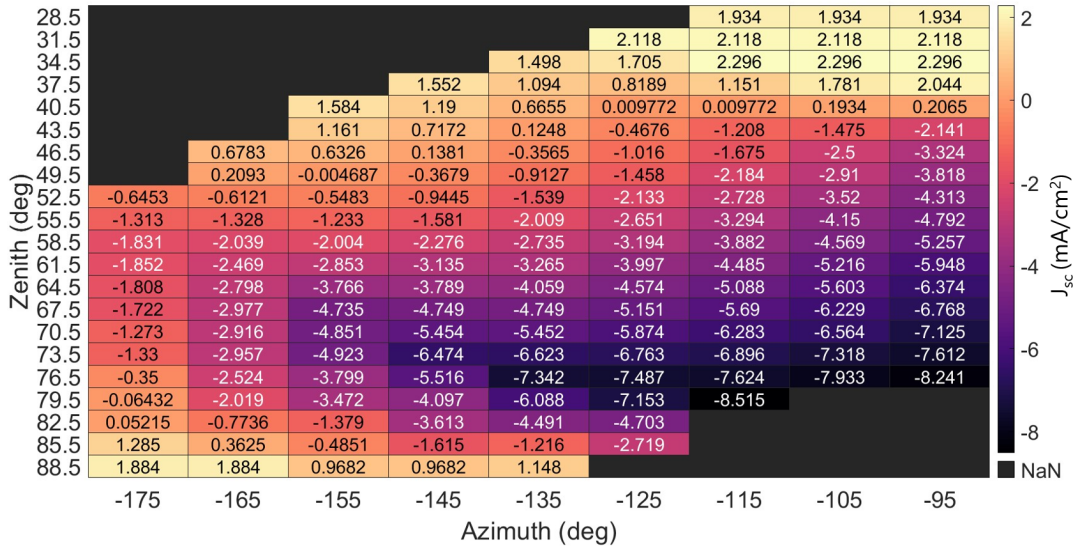


FIGURE 5.9: Comparison between a fully diffuse reflector and a 40-degree FSLSC with a 95% quantum yield of luminophores. In positive cases, the FSLSC outperforms the diffuse reflector. In negative cases, the diffuse reflector outperforms the FSLSC.

Note that not every azimuth-elevation combination occurs at the same frequency and with

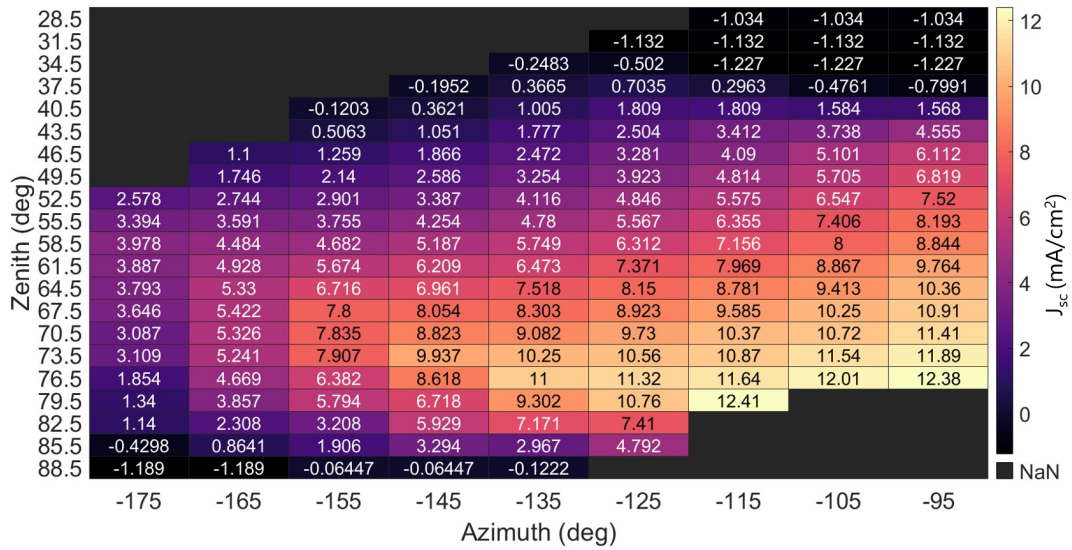


FIGURE 5.10: Comparison between a fully specular reflector and a 40-degree FSLSC with a 95% quantum yield of luminophores. In positive cases, the FSLSC outperforms the specular reflector. In negative cases, the specular reflector outperforms the FSLSC.

the same irradiation. The occurrences of one a day in summer and winter were also shown in Figure 5.2, corresponding to high and low daily irradiance. An exact overview of the number of occurrences of each azimuth-elevation combination can be found in Appendix B.1.

In the comparison between the diffuse reflector and the FSLSC, it can be seen that during the azimuth-elevation occurrences in the summer, the diffuse reflector outperforms the FSLSC. One of the reasons why this is the case, is that the specular reflection on the FSLSC is not reaching the bifacial module for zenith angles below 36.9 degrees. Therefore, in these instances below 36.9-degree zenith, only the cone emission can reach the bifacial spectrum, which is only a part of the spectrum. Nonetheless, the diffuse reflector reflects the entire diffuse spectrum in all directions, thereby outperforming the FSLSC. In addition, the entire non-shaded area of the diffuse reflector is reflecting the spectrum in all directions, among which also to the module. The escape cone is always pointing perpendicular to the reflector, therefore also a large part of this emission cone does not reach the reflector, this can also be seen in a sketch in Appendix B.3. Furthermore, in cases of high zenith angles, the diffuse reflector outperforms the FSLSC, which has to do with shading. The specular reflection of the FSLSC is very sensitive to shading, whereas the diffuse reflector is less since the reflector's area contributing to the short-circuit current density is larger. In all other cases, the FSLSC outperforms the diffuse reflector.

When looking more closely at the comparison between the FSLSC and a specular reflector as shown in Figure 5.10, it can be seen that the FSLSC outperforms the specular reflector during the summer azimuth-elevation occurrences. This is due to the same reason as mentioned before, the specular reflection does not happen for zenith angles below 36.9 degrees. In the case of the FSLSC, there is still an output of the cone emission, whereas there is no output of the specular reflector. In most other cases, the specular reflector outperforms the FSLSC, given that the zenith angle is not very high, i.e. 85.5 or 88.5 degrees. In these

specific cases with high zenith angles the shading plays an important role, as explained before, specular reflection is very sensitive to shading. Even though the FSLSC also has a specular reflection component, it still has the short-circuit current density generated by the emission cone. Therefore, the FSLSC will outperform the specular reflector in these cases.

Concluding, the FSLSC outperforms the diffuse reflector in 86% of the possible azimuth-elevation combinations and is outperformed by a specular reflector in 74% of the cases. Yet, the frequency at which a certain azimuth-elevation combination occur differs and also the irradiance that a certain azimuth-elevation combination receives differs. To consider those effects and to draw a fairer comparison in the actual annual effects, the yield is calculated in the upcoming sections.

5.6.2 Yield Comparison based on Direct Irradiance

In this section, the annual yield from direct irradiance will be shown. As mentioned in Section 3.2.3, the calculation of the yield is for a bifacial heterojunction cell and assumes a constant open-circuit voltage, thereby influences like ambient temperature are not taken into consideration.

In Figure 5.11, the short-circuit current density is calculated based on the irradiation average of three years (2017 to 2019) and displayed as the running average. For example, for the 16th of January, the average has been taken between the 1st of January to the 31st of January and for the 17th of January, the average is taken from the 2nd of January to the 1st of February, and so forth. Figure 5.12 shows the same data, but displayed as a monthly average in a bar diagram. The FSLSC is displayed to be see-through in this graph, so when the FSLSC is outperforming the specular reflector, a line can be seen where the specular reflector is.

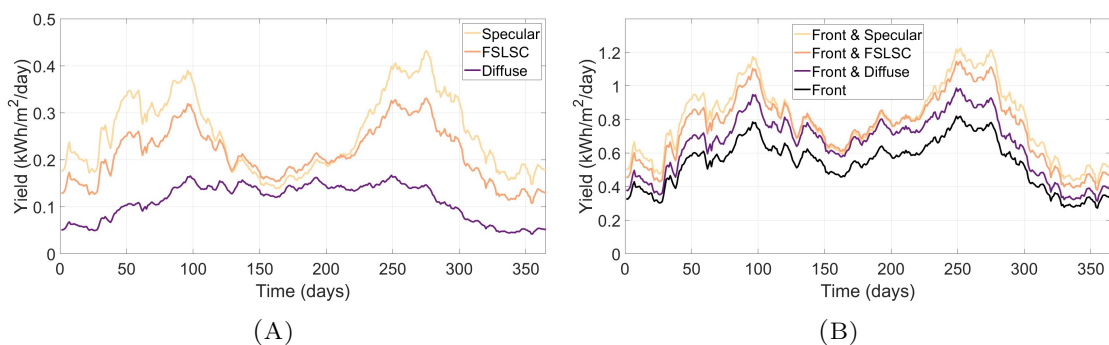


FIGURE 5.11: Running average comparison of the 2017-2019 averaged FSLSC yield, for A) only the rear and B) the front and rear of the module, in the façade setup with direct irradiation for different reflectors.

These two plots show that the yield induced by the diffuse reflector is always lower than the yield induced by the specular reflector and the FSLSC. Additionally, the yield of the diffuse reflector is lowest during winter, increases during spring, is at its optimum in summer and decreases again in autumn. Contrary, the specular reflector and FSLSC have their yield optima during spring and autumn. The additional yield in the summer is higher for the FSLSC than for the specular reflector, and for both higher as in the winter. In other

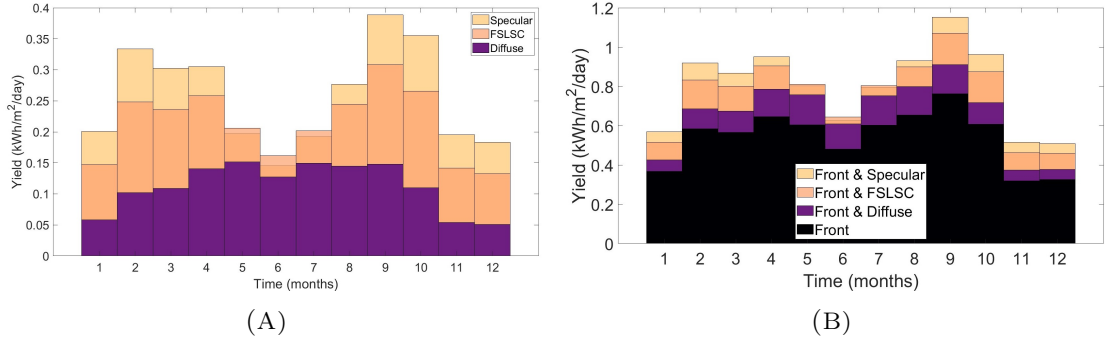


FIGURE 5.12: Monthly averaged comparison of the 2017-2019 averaged FSLSC yield in the façade setup, for A) only the rear and B) the front and rear of the module, with direct irradiation for different reflectors.

periods of the year, the specular reflector outperforms the FSLSC.

The reason why the diffuse reflector is steadily increasing over the first six months is due to the fact that the irradiation is increasing. The diffuse reflector is independent of the solar azimuth and elevation, given that no shade is induced by the module. Therefore, the yield induced by the diffuse reflector follows the trend of the annual irradiation.

The short-circuit current density of the FSLSC and specular reflector are dependent on the solar azimuth and elevation. The azimuth and elevation are most favourable in winter as these angles are close to perpendicular to the module, leading to a relatively high output during these months, even though the irradiation is low. With increasing radiation intensity, the output of the reflectors increases. As the year is progressing, the angles of azimuth and elevation are becoming less and less perpendicular. In the period between 100 to approximately 175 days, the increase in irradiation cannot compensate for the angles getting less perpendicular to the reflector, therefore leading to a reduced short-circuit current density. After summer, this trend repeats itself in the opposite direction. The angles are getting more perpendicular to the module, yet the irradiation gets less intense, leading to a maximum yield in autumn and a minimum yield in winter.

Figure 5.13 shows the daily yield of the rear of the module due to the different reflectors for one year, namely 2018. In the yearly irradiance, all different aspects influencing the irradiation, including weather, are taken into consideration. Note that Figures 5.11 and 5.12 were averaged over approximately 30 days, leading to more visible trends. The daily yield due to the reflectors can be up to 1.41 kWh/m²/day and varies a lot per day. For instance, the yield due to a specular reflector is 1.35 kWh/m² on the 79th day (20th of March 2018) and only 0.02 kWh/m² the next day.

The differences in daily yield can be explained by the weather influence. For example, the 1.35 kWh/m² on the 20th of March 2018 correlates with low cloud coverage [40], whereas the next day there was full cloud coverage [40], which yields only 0.02 kWh/m²/day. Overall, the previously described trends can be seen as well. The days with the highest outputs are between days 40 and 80 as well as days 250 to 330.

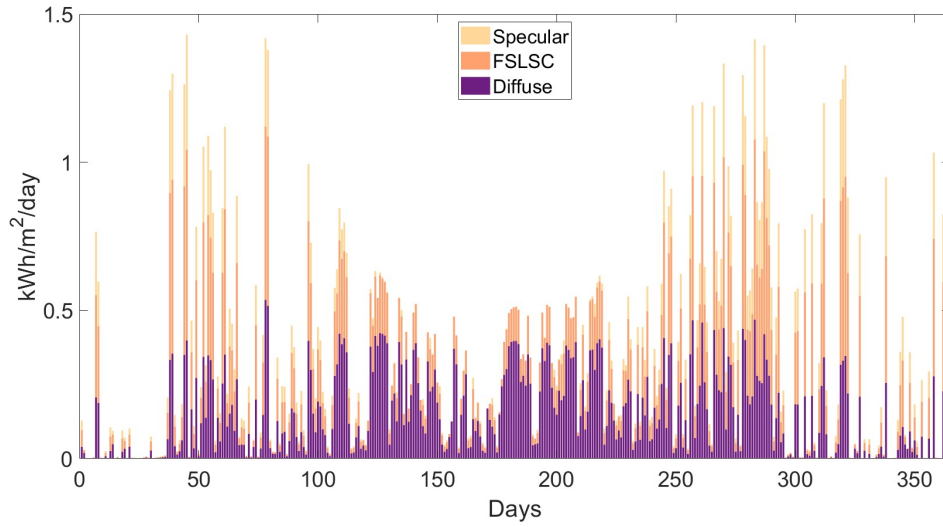


FIGURE 5.13: Yield of the rear of the module in the façade setup from direct radiation in 2018. The FSLSC has a 95% quantum yield of luminophores and a 90% specular reflection efficiency, the diffuse reflector has a 90% efficiency and the specular reflector has a 90% efficiency.

5.6.3 Yield Comparison based on Diffuse Irradiance

This section will look into the yield due to diffuse irradiance. This yield is solely dependent on the amount of irradiance, thereby independent of the solar elevation and azimuth.

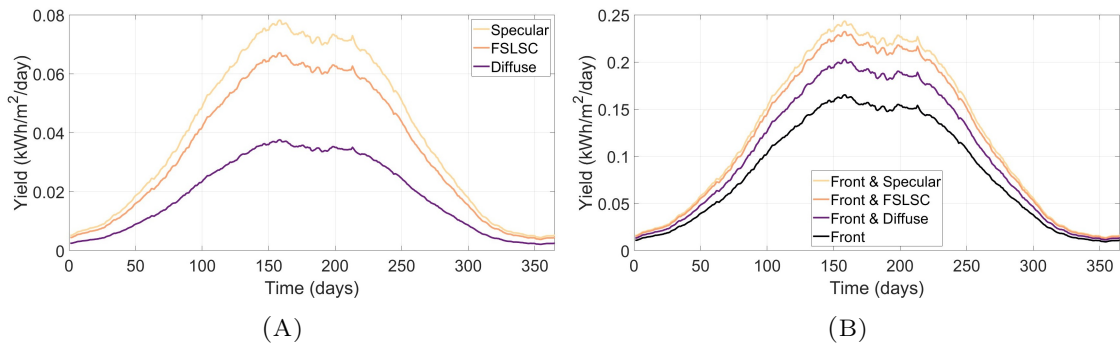


FIGURE 5.14: Running average comparison of the 2017-2019 averaged FSLSC yield, for A) only the rear and B) the front and rear of the module, in the façade setup with diffuse irradiance for different reflectors.

Figure 5.14 shows the running average of the yield over the year, for irradiance data averaged over three years. From now on the monthly bar plots can be found in Appendix B.4. Figure 5.14 shows that the yield in the module increases with time until it reaches its highest point in summer and decreases again afterwards. This is due to the yield being independent of the angle of incidence and solely dependent on the irradiation, which is also lower in winter, increasing in spring and highest in summer.

The specular reflector outperforms the FSLSC, which in its turn outperforms the diffuse reflector. The reason for this was already shown in Figures 5.10 and 5.9 and a

complete overview can be found in Appendix B.5. When looking at all the possible azimuth-elevation combinations, the specular reflector outperforms the FSLSC in 46% of the azimuth-elevation combinations with an average short-circuit current density of 3.69 mA/cm^2 and is outperformed by the FSLSC in 54% of the cases with an average short-circuit current density of 1.16 mA/cm^2 . Overall, the FSLSC is outperformed by the specular reflector for diffuse irradiation, as the yield calculation methodology is averaging over all the different cases. When comparing the diffuse reflector to the FSLSC, the FSLSC is outperforming the diffuse reflector in 54% of the azimuth-elevation combinations with an average short-circuit current density of 5.66 mA/cm^2 . The FSLSC is outperformed by the diffuse reflector in 46% of the cases, with an average short-circuit current density of 0.63 mA/cm^2 . Overall, when using diffuse irradiation, the diffuse reflector is outperformed by the FSLSC.

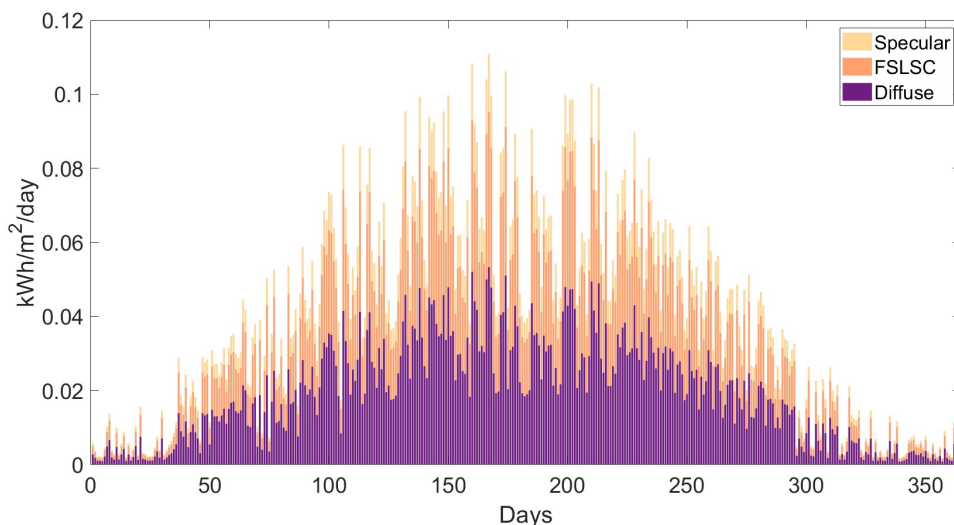


FIGURE 5.15: Yield of the rear of the module in the façade setup from diffuse radiation in 2018. The FSLSC has a 95% quantum yield of luminophores and a 90% specular reflection efficiency, the diffuse reflector has a 90% efficiency and the specular reflector has a 90% efficiency.

Figure 5.15 shows the yield based on the diffuse irradiance in 2018. It shows the same trends as mentioned before, with a clear increase until summer and a decrease afterwards. Compared to the yield from direct irradiance in 2018, as shown in Figure 5.13, the yield from diffuse irradiance is more constant. Whereas drops or increases in yield of 90% per day were happening frequently for direct irradiance, the day-to-day differences for diffuse are maximum around 50% per day, showing a more constant yield from diffuse irradiance.

5.6.4 Annual Yield Comparison

In this section, the total annual yield will be shown, meaning that this is the addition of direct and diffuse yield and thereby the sum of the graphs seen before. As an extra comparison, an optimally tilted monofacial module has been added to the comparison. This module is tilted to 39 degrees elevation and facing south, like could be the case on roofs, and is optimal for Enschede [41].

Figure 5.16 shows the annual yield for a module with the different types of reflectors. It can be seen that the diffuse reflector is outperformed by the FSLSC and specular reflector. The specular reflector's yield exceeds the yield of the FSLSC during most periods of the year, whereas the FSLSC still outperforms the specular reflector in the middle of the summer. This is due to the fact that the specular reflector is outperformed by the FSLSC for direct irradiance, but the specular reflector outperforms the FSLSC for diffuse irradiance, therefore the period at which the FSLSC outperforms the specular reflector has become shorter compared to the direct irradiance case.

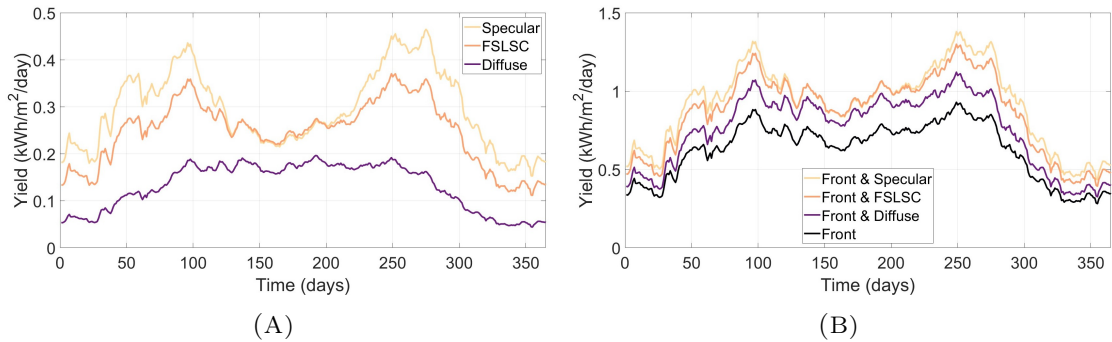


FIGURE 5.16: Running average comparison of the 2017-2019 averaged FSLSC yield in the façade setup, for A) only the rear and B) the front and rear of the module, for different reflectors. The irradiance includes both diffuse and direct irradiation.

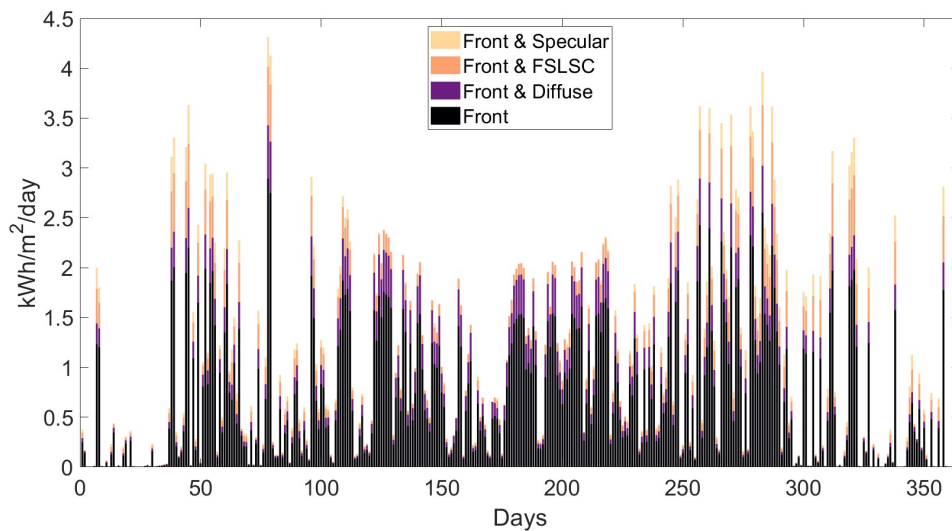


FIGURE 5.17: Yield of the façade setup from total radiation (both diffuse and direct) in 2018. The FSLSC has a 95% quantum yield of luminophores and a 90% specular reflection efficiency, the diffuse reflector has a 90% efficiency and the specular reflector has a 90% efficiency.

When looking at the general trends, the yield of the diffuse reflector increases from winter to summer and starts to decrease again after summer. This effect is more extreme now, as it happens for both diffuse and direct irradiance as was shown in Figures 5.11 and 5.14. For the specular reflector and FSLSC, there are two counter-acting trends in summer, where

there is a peak for diffuse irradiance (as shown in Figure 5.14) and a valley for direct irradiance (as shown in Figure 5.14). Combined, the difference is now less extreme as these effects are cancelling each other out.

Figure 5.17 shows the daily yield for 2018, including the front of the solar panel. It can be seen that there is still a large daily difference and follows the trends as described above.

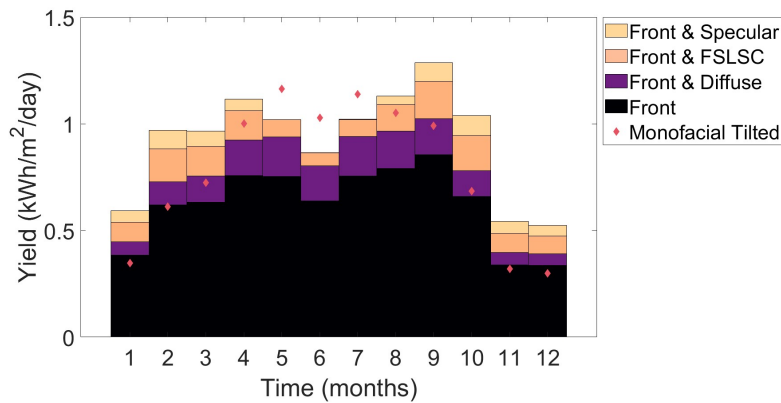


FIGURE 5.18: Monthly averaged comparison of the 2017-2019 averaged FSLSC yield in the façade setup, for both the rear and front of the module, with direct and diffuse irradiation for different reflectors and a 39-degree tilted monofacial solar panel.

Figure 5.18 shows the monthly averaged yield. This includes a monofacial module tilted to 39-degree elevation and 180-degree azimuth, pointing southwards. This is the most optimal installation of solar panels installed on Dutch roofs [41]. It can be seen that the monofacial tilted module outperforms the front of the vertical module from March to October. When adding a diffuse reflector behind the vertical module, this system is only outperformed by the optimally tilted monofacial module between April and August. Having an FSLSC or specular reflector behind the module would shorten this period to May to July. Hence, having a specular or an FSLSC reflector close to a vertical module will enhance the yield to be close to or exceed the yield of an optimal monofacial solar panel throughout the year.

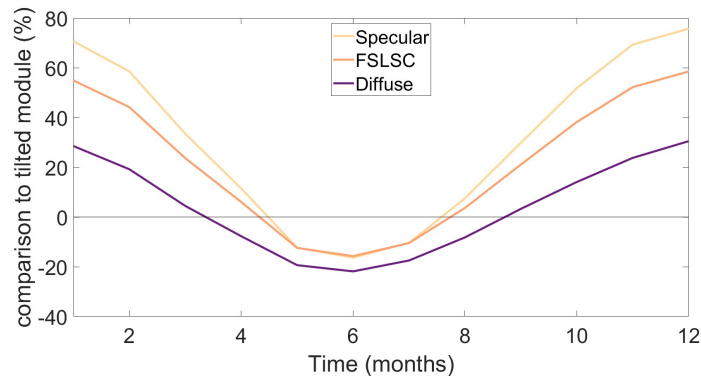


FIGURE 5.19: Comparison of vertical solar panel with specular, FSLSC, or diffuse reflector with 39-degree tilted optimal module for the façade setup.

The monofacial optimal solar module is outperformed by the vertical module with FSLSC in many other cases. Mainly during the winter months, the yield of a vertical panel with FSLSC is significantly higher compared to having an optimal monofacial panel, going from 0.29 kWh/m²/day to 0.47 kWh/m²/day on average in December. This is an increase of 58%. The percentages for all months and reflectors have been plotted in Figure 5.19. This shows that the diffuse reflector outperforms the tilted module by around 25% in January, but is also outperformed by approximately the same percentage in June. The specular reflector outperforms the optimally tilted module by 76% in December and is outperformed by 16 % in June.

Table 5.1 gives an overview of the annual yield per square meter vertical bifacial module with different reflectors compared optimally tilted monofacial module. This shows that the annual yield of a vertical reflector can be enhanced by 47.1%, 39.3%, and 20.9% due to a specular reflector, FSLSC, and diffuse reflector, respectively. The total yield over a year of a vertical bifacial module in combination with a specular reflector or FSLSC exceeds the yield of the optimally tilted monofacial module.

TABLE 5.1: The annual yield that is induced by the reflector (3rd and 4th column) and total yield (5th column) for configurations with a vertical bifacial module and an optimally tilted monofacial module.

Solar Module	Reflector	Yield Enhancement		Total Yield [kWh/m ² /year]
		[kWh/m ² /year]	[%]	
Vertical bifacial module				
	Specular	107.7	47.1	336.4
	FSLSC	89.9	39.3	318.5
	Diffuse	48.0	20.9	276.7
Optimally tilted monofacial module				285.0

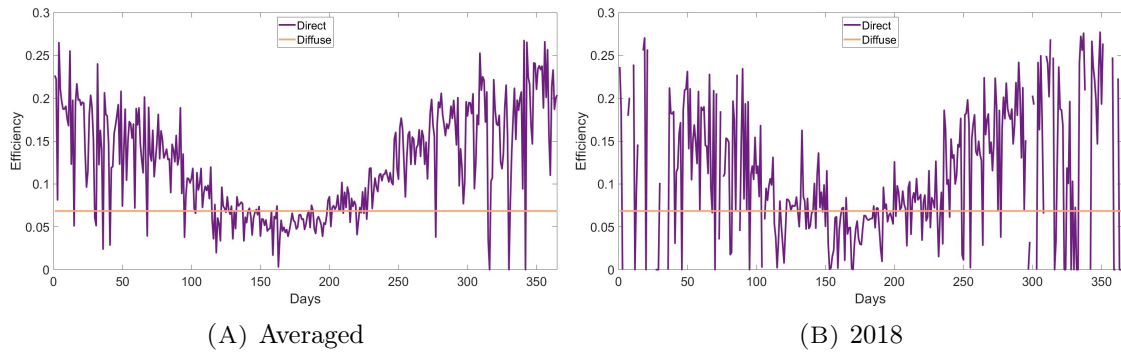


FIGURE 5.20: Efficiency of the front of the module in the façade setup for a) yearly averaged data and b) 2018

To verify the yield calculations that have been done, the efficiency of the front of the vertical solar panel has been calculated and has been shown in Figure 5.20. The efficiency is defined as the energy of the incoming irradiance over the generated energy of the front of the solar module. It shows that the diffuse efficiency is independent of the time of the year, which confirms that it is independent of the azimuth and elevation and only depends on the amount of incoming irradiance. The efficiency of the vertical module has a maximum

26.7%, which occurs in the winter months, due to the optimal azimuth-elevation angles. These angles will get less optimal during summer, leading to a decrease in efficiency. However note that sometimes the efficiency is zero when looking at a plot of one year, as can be seen in Figure 5.20B. This is a limitation of the data that is used, because sometimes the irradiance does time-wise not align with an azimuth-elevation occurrence, therefore having zero efficiency. All in all, the trends of the efficiency are all as expected, thereby supporting the reliability of the previously presented yield calculations.

In conclusion, comparing the yield induced on a vertical solar panel by an FSLSC, a specular and a diffuse reflector shows that the diffuse reflector is outperformed by the FSLSC and specular reflector. The yield generation pattern over the year is similar for the FSLSC and specular reflector, yet the specular reflector outperforms the FSLSC in the period of August to April, whereas the FSLSC outperforms the specular reflector in the other months. In total, the yield of a vertical solar panel can be increased by 20.9%, 39.3%, and 47.1% for a diffuse reflector, an FSLSC, and a specular reflector, respectively. The yield of an optimally tilted monofacial solar module is below the yield of the vertical bifacial fence with either a specular reflector or FSLSC. Specifically, the FSLSC in combination with a vertical fence will outperform an optimally tilted monofacial solar panel on a roof from August to April, up to 58% in December.

5.6.5 Multi-Criteria Analysis

In the previous section, the FSLSC, specular and diffuse reflectors have been compared based on their short-circuit current densities and the annual yield. In this section, the three reflectors will be assessed on the socio-economic criteria of costs, energy mix, safety, social acceptance, and yield in the form of an MCA as described in Section 3.3.

The first considered criterion is the cost. The white paint of the diffuse reflector is a very cheap option and therefore ranked as 'highly favourable'. The mirror, in the case of the specular reflector, is expected to be considerably more expensive than the white paint. Therefore, it is ranked as 'neutral'. Moreover, the FSLSC will be ranked as 'unfavourable', due to relatively high expected production costs, as the nanophotonic coating of multiple dielectric layers and the luminophore-embedded waveguide need to be produced in an exact manner. However, note that the FSLSC is expected to be much cheaper than the solar module itself.

The second criterion that is considered is the energy mix, looking into when the reflector has the highest output compared to the energy generated in the grid. As was already explained in Section 3.3, it would be favourable if the reflector would induce additional yield in the module during the winter months opposite to most of the optimally tilted solar panels. As shown and explained in Figure 5.16, the diffuse reflector follows the trends of the irradiation, generating the highest output in the summer. Due to the reasons mentioned above, the diffuse reflector is ranked as 'highly unfavourable', as it would not contribute to the energy mix and only make the grid congestion problem larger in the Netherlands. In the same figure it can be seen that the specular reflector and FSLSC both induce the most electricity in spring and autumn, thereby contributing to the energy mix. Since the specular reflector also contributes a lot during winter, this will be ranked 'highly favourable' and the FSLSC will be ranked 'favourable', as the yield in the winter is less compared to the specular reflector.

The third criterion is safety, including how safe the technology is for humans and animals. The diffuse reflector includes white paint and no safety risks are associated with this. Contrary, there are safety risks associated with mirrors. First of all, reflecting direct light in urban areas is a potential source of house fires. Firefighters advise keeping reflective items, like mirrors and crystals, out of direct sunlight [42, 43], as they cause house fires throughout the entire year [42, 43, 44, 45]. Second, a façade with a specular reflector is expected to have similar effects as sun glare on road traffic. It is known, that sun glare is one of the major environmental aspects contributing to traffic accidents [46], therefore, a façade with a mirror is not perceived to be safe for the surrounding traffic. Furthermore, redirecting large quantities of direct light, like is done for a specular reflector, could potentially harm humans and animals. Light pollution, which is defined as the alteration of natural light levels due to the introduction of artificial light at night, can alter the individual behaviour of free-living animals [47]. It has drastic and potentially negative effects on biological rhythms, daily activity and reproduction [47]. In this way, light pollution threatens biodiversity through changed night habits, regarding the reproduction and migration, of animals like insects, fish, birds, and bats [48].

In short, using specular reflectors to reflect light would be unsafe due to the risk of fires and traffic accidents and could disturb humans and animals. Therefore the safety aspect of specular reflectors is rated to be 'highly unfavourable'. In the case of an FSLSC, these effects are reduced significantly, since only low-energy photons are reflected in a specular manner. The emission of the cone would also be low-energy photons, leading to a significantly reduced risk. Therefore, the FSLSC ranks 'neutral' on the safety aspect.

The fourth criterion is social acceptance based on its appearance, describing how likely citizens are expected to accept a certain façade. The diffuse reflector is expected to be easily accepted by citizens, therefore having the score of extremely favourable. The reason for this is that the diffuse reflector is comparable to white paint, which is already accepted in the Dutch community. The specular reflector would look like a mirror as the front of a house, it is expected that this is not accepted by Dutch citizens, as this is not something that is currently seen in Dutch cities or villages. Therefore, the specular reflector ranks extremely unfavourable. The FSLSC would absorb wavelengths up to 700 nm, thereby absorbing the entire visible spectrum. The FSLSC would therefore appear as a black surface. Black façades are currently quite common for Dutch houses, therefore the appearance is quite common, yet the choice in materials is not. Therefore, the FSLSC would rank as favourable.

Lastly, the yield is considered for the three different reflectors. As is shown in Table 5.1, the additional annual yield of a diffuse reflector, specular reflector and FSLSC is 47.87 kWh/m², 107.7 kWh/m², and 89.9 kWh/m², respectively. The specular reflector induces the highest additional yield, thereby being 'highly favourable'. The FSLSC also induces a considerable additional yield, thereby being 'favourable'. The diffuse reflector induces about half of the electricity of the FSLSC, thereby being 'unfavourable'.

TABLE 5.2: Multi-criteria analysis comparing the socio-economical effects of an FSLSC, specular and diffuse reflector, ranking five criteria from highly unfavourable (- -) to highly favourable (++) .

Criteria	FSLSC	Specular	Diffuse
Energy Mix	+	++	- -
Costs	-	o	++
Safety	o	- -	++
Social Acceptance	+	- -	++
Yield	+	++	-

An overview of the MCA can be found in Table 5.2. When assessing the results of this comparison, the criterion of safety is considered of major importance. The potential risk of fire and harm to animals and humans eliminates the specular reflector of being a socio-economically accepted option. When comparing the diffuse reflector to the FSLSC, they seem to target a different user group. Whereas a diffuse reflector could be an easy and cheap option to enhance the output of a bifacial solar panel, the FSLSC would be the more expensive, but more durable option, with a large benefit of inducing more yield in the winter.

Chapter 6

Discussion of Model

This chapter will discuss the general limitations of the FSLSC model and the yield calculation approach that has been presented and used throughout this thesis. Additionally, it will provide possible directions to improve and extend the model in the future.

6.1 FSLSC Model

There are several limitations to the FSLSC model that has been developed in this thesis, which are discussed below.

First of all, the FSLSC model is a purely optical model as explained before. Therefore, it does not take the electrical properties of the solar module into account. This means that mismatch losses, i.e. losses caused by the interconnection of solar cells or modules which do not have identical properties or do not experience the same conditions [35], are not taken into consideration. To enhance the realism of the simulations, these effects should be taken into consideration.

Second, the assumptions for the nanophotonic coating have been simplified in the model. Whereas in reality photons could enter within the cone angle for the emission range due to reciprocity (as is shown in Figure 2.6), these photons have been assumed to be specularly reflected in this model (as is shown in Figure 3.2B). The reason for this is that these photons will be emitted in the emission cone, but not red-shifted, adding an extra variable to the code. However, this should be added for more realistic results. Nonetheless, it is also known that the real nanophotonic coatings have a more gradient transition from absorbance to reflectance [20], therefore when realism needs to be enhanced, this should be taken into consideration as well.

Third, when looking into realistic properties of the FSLSC, the system efficiencies are currently taken into account based on Figure 3.5. This is based on simulated data up to a cone angle of 40 degrees and has been extrapolated to a 90-degree cone with an efficiency of 90% afterwards. The model would be improved when simulated data would be extended up to 90 degrees, which is recommended. It is also known that the current assumption of system efficiencies has its limitations, as the efficiency is assumed to be 90% for all luminophore quantum yields. In case the luminophores have a quantum yield of 80% and the total system efficiency is 90%, it is already known that not every photon can be absorbed by the luminophores. Therefore, improving this assumption is also recommended in case the simulated data cannot be extended to 90 degrees.

Lastly, the emission spectrum of the emitting photons is simplified. Currently, it is assumed that the spectrum is either at its maximum or zero, as can be seen in Figure 6.1. Yet, for real materials like Ytterbium, there is a smooth transition towards the maximum emission. For the emission spectrum used in this report, the EQE is in this range independent of the wavelength, so it is expected to not change the results. Yet, when a different emission range is chosen, this effect might become of importance and should be considered.

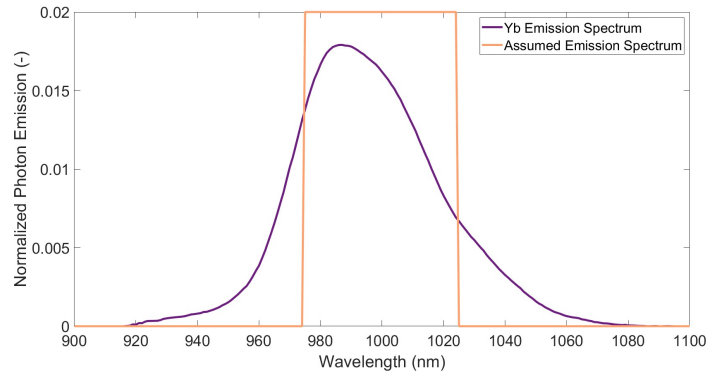


FIGURE 6.1: Comparison between normalized emission spectra of Yb and the assumed emission spectrum in the model

6.2 Yield Calculation

The yield calculation approach that has been used in this thesis also has its limitations, which are elaborated upon below.

As mentioned before, the yield calculation is done based on a very simple calculation approach, where the short-circuit current density is multiplied by the open-circuit voltage and fill factor. To enhance this calculation, it would be advised to take the influence of temperature into consideration, as the electrical efficiency of a solar module is linearly dependent on the operating temperature [49]. Other more detailed models, like the Sandia Model, Normal Operating Cell Temperature Model, or Faiman Model [5] can be considered if more detail is desired.

Furthermore, the FSLSC model is run for a certain irradiance spectrum and afterwards corrected for the actual irradiance throughout the year (as described in Equation 3.4). This assumes that the spectral component stays constant throughout the year. It would be more precise to have the spectral irradiance data for each moment in time and calculate the short-circuit current density for each moment, but this is currently not deemed feasible due to the computational demands. In addition, it is known that diffuse light has a different spectrum compared to direct light, due to scattering depending on wavelength [24]. Therefore, it would be important to have a closer look into the spectral component of diffuse light in the future.

In addition, the current irradiation data and azimuth-elevation occurrences data come from different sources. These are both hourly data but do not align perfectly. Therefore, it can happen that a certain azimuth-elevation occurrence does not receive any irradiance

or that no azimuth-elevation occurrence is attached to irradiance. This was also mentioned as one of the reasons why the efficiency of the solar panel is sometimes zero, as can be seen in Figure 5.20. Therefore, it would be recommended to get data that includes azimuth angle, elevation angle, and irradiance from one source, such that this aligns better.

Lastly, as explained before, diffuse irradiance comes from all different angles. However, in the model, only 540 different angles are taken into consideration, namely at an interval of 3-degree zenith and 10-degree azimuth. This does not take the influence of fully diffuse irradiance into consideration. Therefore to enhance the calculation of the diffuse yield, a smaller interval of angles should be taken.

6.3 Possible Extension of the Model

Up to now, it was assumed that an FSLSC has a cone emission which is normal to the FSLSC. Thermodynamically, it should be possible to tilt the cone emission, meaning that the cone points towards a certain direction. This could be used to enhance the radiance towards the module as could be seen in Figure 6.2. In this optimized case, the upper part of the reflector would still contribute towards the module, whereas this does not happen for the unoptimized case.

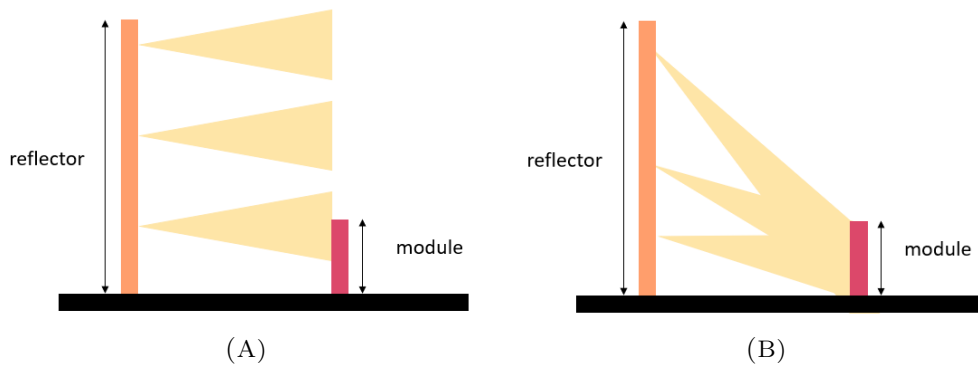


FIGURE 6.2: An unoptimized FSLSC (A) and optimized FSLSC with titled cone (B)

To add the cone tilt to the code, the angle at which the cone emission reaches the module needs to be changed. It is expected that this can be done by using Rodrigues' Rotation Formula to change the angle at which the module receives a ray from the reflector, when adding this in the loop over the pixels of the reflector pixels (mpX and mpY). In this way, the short-circuit current density of the cone will be calculated based on the titled angle between the module and reflector and the optimized cone is taken into consideration.

Chapter 7

Conclusion

Free space luminescent solar concentrators (FSLSC) provide a way to concentrate diffuse light into a cone that can be directed towards a solar module to increase its yield. This thesis presents a methodology for optimizing the cone size and calculating the annual yield of a bifacial module in the presence of an FSLSC.

A generic case is studied to acquire fundamental knowledge on possible use cases and to optimize the cone size, where a solar module is put in front of an FSLSC and the module's tilt and distance are varied. This shows that the optimal short-circuit current density is reached when the module and reflector are parallel to each other. The distance between the two for which the module has the highest output is dependent on the FSLSC's cone size. On the one hand, the distance to the module needs to be optimized such that the entire area of the FSLSC reflects towards the module, which is dependent on the cone size. On the other hand, the distance should be as close as possible, to have the highest possible photon intensity of the emission cone. Assuming ideal properties, the highest achievable short-circuit current density can be reached for a 10-degree cone and decreases with increasing cone size. Taking realistic loss mechanisms into consideration, assuming a 95% quantum yield of the luminophores, the optimal short-circuit current density is reached for a cone angle of approximately 40 degrees.

Based on possible practical configurations, a case has been studied with an FSLSC on a house's façade with a bifacial solar fence in front. It becomes apparent that the optimum cone size is again approximately 40 degrees for an FSLSC in this configuration, taking loss mechanisms with a quantum yield of luminophores of 95% into consideration. Taking a closer look into a 40-degree cone, the possible annual yield that can be generated by the solar fence of 228.6 kWh/m² is increased to 318.5 kWh/m² when implementing an FSLSC façade. An optimally tilted monofacial panel, typically implemented on roofs, has a maximum annual yield of 285.0 kWh/m² and is outperformed by the FSLSC in the months from August to April, up to a yield increase of 58% in December.

The bifacial solar fence can also be surrounded by a specular or diffuse reflector instead of an FSLSC. Hence, a comparison is drawn between the FSLSC and the specular and diffuse reflector. The diffuse reflector would induce an additional 47.87 kWh/m² on the solar fence, the specular reflector 107.7 kWh/m² and the FSLSC 89.9 kWh/m². Yet, the specular reflector has considerable socio-economical disadvantages, like a high fire hazard, posing a risk of traffic accidents, and having negative effects on humans and animals. Therefore, the use of an FSLSC as a reflector would induce the largest increase in yield

while limiting the socio-economical impact.

Future research could be aimed at improving the model by, amongst others, adding the electrical properties of the solar module to the FSLSC model or adding the effect of temperature on the power of the module in the yield calculation. Additionally, the FSLSC and its simulations could be optimized by including cone tilt in the model.

Bibliography

- [1] United Nations. The Sustainable Development Goals Report 2022. Technical report, 2022.
- [2] A.E. Becquerel. Recherches sur les effets de la radiation chimique de la lumieresolaire au moyen des courants electriques. *Comptes Rendus de L'Academie des Sciences*, 9:145–149.
- [3] CBS. Renewable electricity share up by 20 percent in 2022. <https://www.cbs.nl/en-gb/news/2023/10/renewable-electricity-share-up-by-20-percent-in-2022>, 2023. (Accessed on 29-03-2023).
- [4] Rijksdienst voor Ondernemend Nederland. Beleid Zonne-energie. <https://www.rvo.nl/onderwerpen/zonne-energie/beleid#afspraken-voor-voldoende-energie-opwek>, 2023. (Accessed on 23-06-2023).
- [5] W. Gu, T. Ma, S. Ahmed, Y. Zhang, and J. Peng. A comprehensive review and outlook of bifacial photovoltaic (bPV) technology. *Energy Conversion and Management*, 223(May), 2020.
- [6] VDMA. International Technology Roadmap for Photovoltaic. Technical report, 2022.
- [7] A. Cuevas, A. Luque, J. Eguren, and J. D. Alamo. 50 Per cent more output power from an albedo-collecting flat panel using bifacial solar cells. *Solar Energy*, 29(5):419–420, 1982.
- [8] S. Pal. *Tracing the light*. PhD thesis, University of Twente, 2022.
- [9] Rijksdienst voor Ondernemend Nederland. Monitor Zon-PV 2022 in Nederland. Technical report, 2022.
- [10] A.K. Shukla, K. Sudhakar, P. Baredar, and R. Mamat. BIPV based sustainable building in South Asian countries. *Solar Energy*, 170(June):1162–1170, 2018.
- [11] B.P. Jelle and C. Breivik. State-of-the-art building integrated photovoltaics. *Energy Procedia*, 20(1876):68–77, 2012.
- [12] E Saretta, P. Caputo, and F. Frontini. A review study about energy renovation of building facades with BIPV in urban environment. *Sustainable Cities and Society*, 44:343–355, 2019.
- [13] G. Verberne, P. Bonomo, F. Frontini, M.N. van den Donker, A. Chatzipanagi, K. Sinapis, and W. Folkerts. BIPV products for façades and roofs: a market analysis. In *29th European Photovoltaic Solar Energy Conference and Exhibition*, Amsterdam, 2014.

- [14] P. Heinstejn, C. Ballif, and L.E. Perret-Aebi. Building integrated photovoltaics (BIPV): Review, potentials, barriers and myths. *Green*, 3(2):125–156, 2013.
- [15] European Commission. Directive 2010/31/EU of the European Parliament and of the Council of 19 May 2010 on the energy performance of buildings, 2010. (Accessed on 14-06-2023).
- [16] R. Rahman, D.I. Ahmed, M.A. Fahmi, T. Tasnuva, and M.F. Khan. Performance enhancement of PV solar system by diffused reflection. In *2009 1st International Conference on the Developments in Renewable Energy Technology (ICDRET)*, pages 1–4, 2009.
- [17] S. Pal and R. Saive. Experimental Study of the Spectral and Angular Solar Irradiance. In *Conference Record of the IEEE Photovoltaic Specialists Conference*, number 46th, Chicago, USA, 2019.
- [18] L. M. Einhaus. Free-Space Concentration of Diffused Light. Master’s thesis, University of Twente, 2020.
- [19] G. C. Heres. Free-space Luminescent Solar Concentrators. Master’s thesis, University of Twente, 2021.
- [20] L. M. Einhaus, G. C. Heres, J. Westerhof, S. Pal, A. Kumar, J. Zheng, and R. Saive. Free-Space Diffused Light Collimation and Concentration. *ACS Photonics*, 10(2):508–517, 2023.
- [21] J.J. Wang, Y.Y. Jing, C.F. Zhang, and J.H. Zhao. Review on multi-criteria decision analysis aid in sustainable energy decision-making. *Renewable and Sustainable Energy Reviews*, 13(9):2263–2278, 2009.
- [22] Department for Communities and Local Government. Multicriteria Analysis - A manual. Technical report, 2009.
- [23] S. Pal and R. Saive. Output Enhancement of Bifacial Solar Modules under Diffuse and Specular Albedo. *Conference Record of the IEEE Photovoltaic Specialists Conference*, (3):1159–1162, 2021.
- [24] M.Z. Jacobson. *Fundamentals of Atmospheric Modeling*. Cambridge University Press, New York, 2nd editio edition, 2005.
- [25] Y. Zhang, L.O.H. Wijeratne, S. Talebi, and D.J. Lary. Machine learning for light sensor calibration. *Sensors*, 21(18), 2021.
- [26] Paul Quincey. Solid angles in perspective. *Physics Education*, 55(5), 2020.
- [27] ESS Earth Sciences. Different Type of Solar Irradiance. <https://www.esearth.com/solar-irradiance/>, 2020. (Accessed on 09-06-2023).
- [28] PVEducation. Air Mass. <https://www.pveducation.org/pvcdrom/properties-of-sunlight/air-mass>. (Accessed on 04-07-2023).
- [29] F.E. Nicodemus. Directional Reflectance and Emissivity of an Opaque Surface. *Applied Optics*, 4(7):767–775, 1965.

- [30] R. Saive, T.C.R. Russell, and H.A. Atwater. Light Trapping in Bifacial Solar Modules Using Effectively Transparent Contacts (ETCs). In *2018 IEEE 7th World Conference on Photovoltaic Energy Conversion, WCPEC 2018 - A Joint Conference of 45th IEEE PVSC, 28th PVSEC and 34th EU PVSEC*, pages 45–48, 2018.
- [31] OpenStax. Refraction. <https://openstax.org/books/university-physics-volume-3/pages/1-3-refraction>. (Accessed on 27-06-2023).
- [32] OpenStax. Total Internal Reflection. <https://openstax.org/books/university-physics-volume-3/pages/1-4-total-internal-reflection>. (Accessed on 27-06-2023).
- [33] J.R. Albani. *Structure and Dynamics of Macromolecules: Absorption and Fluorescence Studies*. Elsevier B.V., Amsterdam, 1st edition, 2004.
- [34] PVEducation. IV Curve. <https://www.pveducation.org/pvcdrom/solar-cell-operation/iv-curve>. (Accessed on 27-06-2023).
- [35] PVEducation. Mismatch Effects. <https://www.pveducation.org/pvcdrom/modules-and-arrays/mismatch-effects>. (Accessed on 26-06-2023).
- [36] National Renewable Energy Labatory. National Solar Radiation Database. <https://nsrdb.nrel.gov/data-sets/international-data>. (Accessed on 21-06-2023).
- [37] SunEarthTools. Sun Position. https://www.sunearthtools.com/dp/tools/pos_sun.php?lang=en#annual, 2022. (Accessed on 25-05-2023).
- [38] Rijksdienst voor Ondernemend Nederland. Netcapaciteit en netcongestie, 2022. (Accessed on 31-06-2023).
- [39] S. Moghtadernejad, L.E. Chouinard, and M.S. Mirza. Multi-criteria decision-making methods for preliminary design of sustainable facades. *Journal of Building Engineering*, 19(May):181–190, 2018.
- [40] Koninklijk Nederlands Meteorologisch Instituut. Station 260 De Bilt vanaf 1 jan 1901 tot en met 28 jun 2023. <http://knmi.turmin.com/2018-03-20>, 2023. (Accessed on 30-06-2023).
- [41] European Commission. Photovoltaic Geographical Information System. https://re.jrc.ec.europa.eu/pvg_tools/en/#MR, 2022. (Accessed on 11-06-2023).
- [42] Merseyside Fire & Rescue Service. Fire Service warning after two fires started by sunlight reflecting off mirrors. <https://www.merseyfire.gov.uk/media-centre/news-press/latest-news/fire-service-warning-after-two-fires-started-by-sunlight-reflecting-off-mirrors/>, 2022. (Accessed on 30-06-2023).
- [43] London Fire Brigade. Firefighters issue warning after sunlight reflecting off mirror causes fire – Marble Arch. <https://www.london-fire.gov.uk/incidents/2022/may/firefighters-issue-warning-after-sunlight-reflecting-off-mirror-causes-fire-marble-arch/>, 2022. (Accessed on 30-06-2023).
- [44] J. Menheer. Zon in spiegel veroorzaakt brandende handdoek in badkamer aan de Koedood. <https://barendrecht.nl/incidenten/38773/zon-in-spiegel-veroorzaakt-brandende-handdoek-in-badkamer-aan-de-koedood>, 2023. (Accessed on 30-06-2023).

- [45] M. Denton and G. Murray. House completely destroyed by fire sparked by sunlight reflecting off a mirror. <https://www.mirror.co.uk/news/uk-news/house-completely-destroyed-fire-sparked-27185387>, 2022. (Accessed on 30-06-2023).
- [46] S. Das, X. Sun, B. Dadashova, M.A. Rahman, and M. Sun. Identifying Patterns of Key Factors in Sun Glare-Related Traffic Crashes. *Transportation Research Record*, 2676(2):165–175, 2022.
- [47] T. Raap, R. Pinxten, and M. Eens. Light pollution disrupts sleep in free-living animals. *Nature*, 5(1):1–8, 2015.
- [48] F. Hölker, C. Wolter, E.K. Perkin, and K. Tockner. Light pollution as a biodiversity threat. *Trends in Ecology and Evolution*, 25(12):681–682, 2010.
- [49] S. Dubey, J.N. Sarvaiya, and B. Seshadri. Temperature dependent photovoltaic (PV) efficiency and its effect on PV production in the world - A review. *Energy Procedia*, 33:311–321, 2013.

Appendix A

Model

A.1 Tips for running the model

There are two main versions of the model. One version is based on a parameters Excel file where all the running parameters are determined. This version of the model is given in Appendix C.1. Another version of the model requires a separate matrix with azimuths and elevations to run. This version is given in Appendix C.2.

Even though the model is made to represent an FSLSC, it can be changed to a normal diffuse and normal specular reflector easily by making the following changes:

- Specular Reflector: put the absorption wavelength to 300. In this way, the entire surface will become a specular reflector.
- Diffuse Reflector:
 1. Put the absorption wavelength to 1100, such that all the photons are absorbed.
 2. Turn the redshifting off, by adding the line `FinFac_Redshifted = FinFac;`
 3. Set the cone angle to 90 degrees.

Other tips when running the model:

- Always check if the plots represent the situation that you are intending to model!
 - In case you would like to model a vertical reflector, it needs to be modelled in a horizontal way. Make sure you change from elevation to zenith and place the module accordingly.
- When you are running large simulations, turn the plots off. Otherwise, the simulation will crash. However, run a couple of situations beforehand such that you are sure that the situations you intend to model are actually modelled.
- Always run the simulation first for one pixel (even if there are many cases you are simulating), check all the different settings and only run for 10 pixels afterwards.
- Make sure you are running it for the irradiance that you wish to use.
- If you wish to simulate specular reflection, make sure that the reflector is large enough to capture specular reflection.

A.2 Required Files to Run Code

To run part A of the FSLSC code, which equals the code written by Pal, the following functions are required:

- Angle4EQE
- assign
- CoordFinder
- Gridmaker
- SolidAngCalc
- Spacer

To run part B of the FSLSC code, the actual FSLSC model, with azimuth elevation dependence the following functions and data are required:

- AM_Flux_ForSunsolve
- CurrentOneModule
- FluxToCurrentOneModulePixel
- HJT_Bi_Interp_AMSteps
- Illumination
- IncomingUsefulFluxCComputer
- interpolateCone
- Par
- Polygon
- ToRun

To run this code with the complete par file, and not the azimuth-elevation file, the ToRun file can be exchanged with another Par.xlsx, and the EmissionConePlotter.

To run the annual yield calculation file, the following functions and data are required:

- AveragedNRELIrradiance2018
- DiffuseYieldCalculator
- DirectYieldCalculator
- NRELIrradiance2018
- OccurrenceMatrixPerHour

Appendix B

Elaborated Results

B.1 Occurrences Azimuth and Elevation

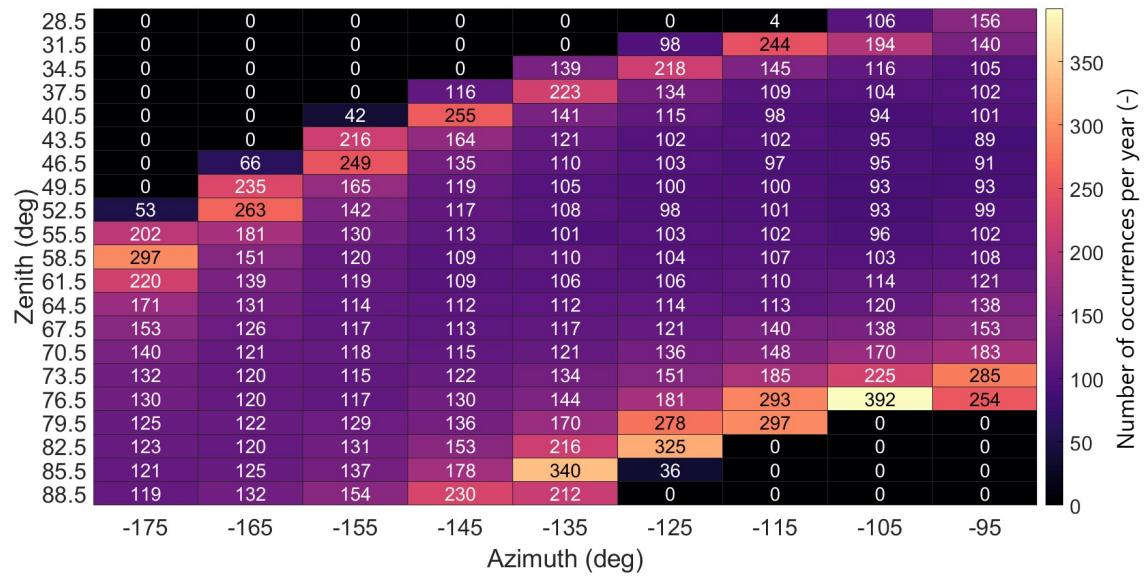


FIGURE B.1: Occurrences of each azimuth and elevation combination based on the parameters defined in the fsisc model

B.2 Façade Case - Angles

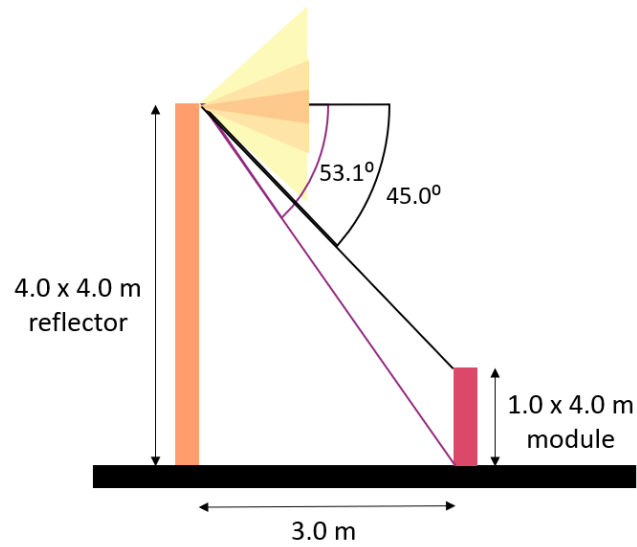


FIGURE B.2: Emission cone angles at which the entire reflector is contributing towards the rear of the module.

B.3 Façade Case - Emission Cone

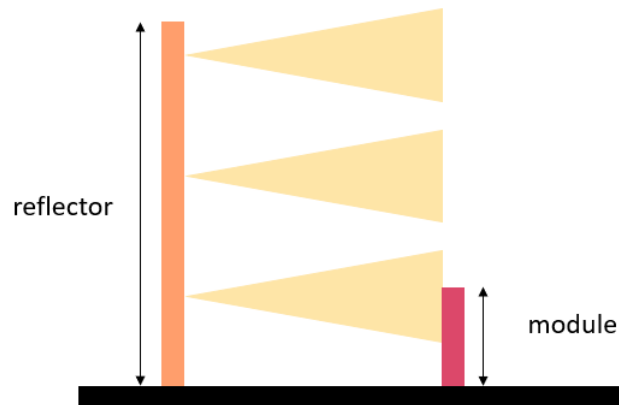


FIGURE B.3: The emission cone is not directed towards the module, therefore the emission cone of the upper part of the reflector is not contributing to the short-circuit current density of the module.

B.4 Monthly Yield

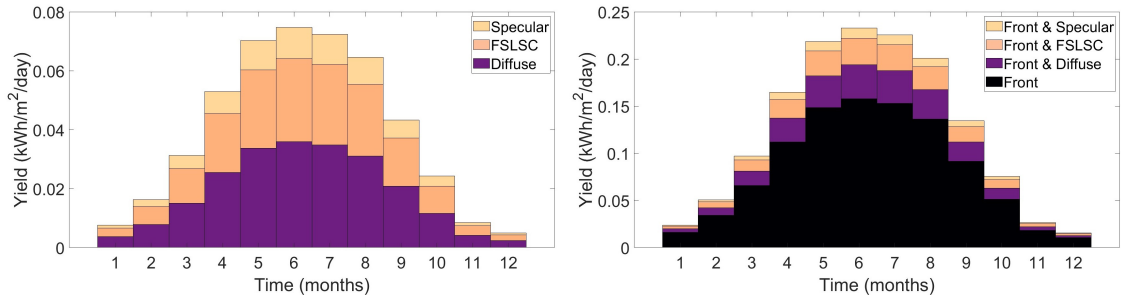


FIGURE B.4: Monthly averaged comparison of the 2017-2019 averaged FSLSC yield in the façade setup, for A) only the rear and B) the front and rear of the module, with diffuse irradiation for different reflectors.

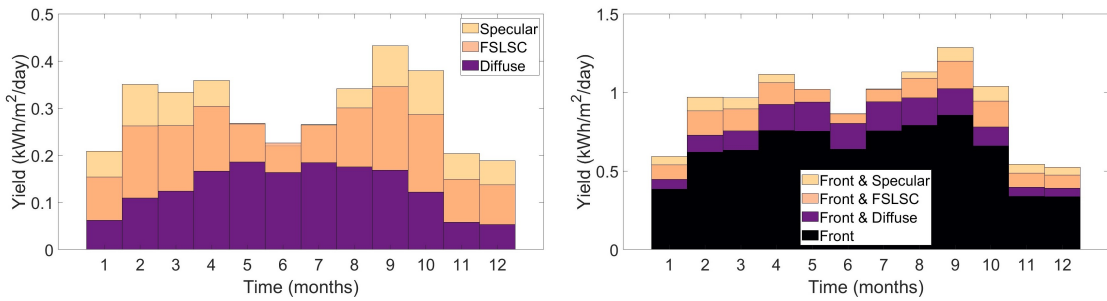


FIGURE B.5: Monthly averaged comparison of the 2017-2019 averaged FSLSC yield, for A) only the rear and B) the front and rear of the module, in the façade setup with diffuse irradiation for different reflectors.

B.5 Comparison Reflectors - Every Angle

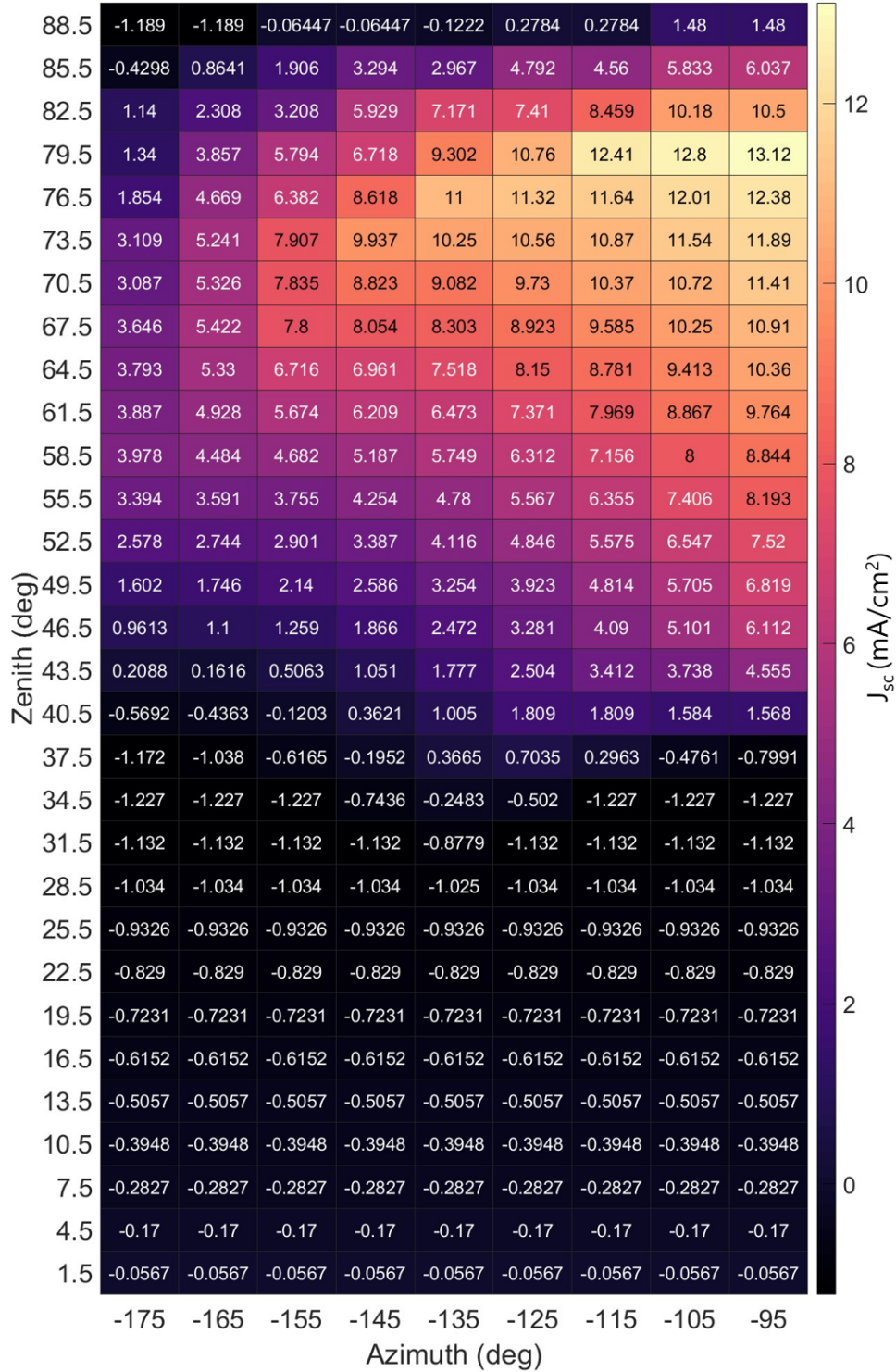


FIGURE B.6: Comparison between a fully diffuse reflector and a 40-degree FSLSC with a 95% quantum yield of luminophores. In positive cases, the FSLSC outperforms the diffuse reflector. In negative cases, the diffuse reflector outperforms the FSLSC.

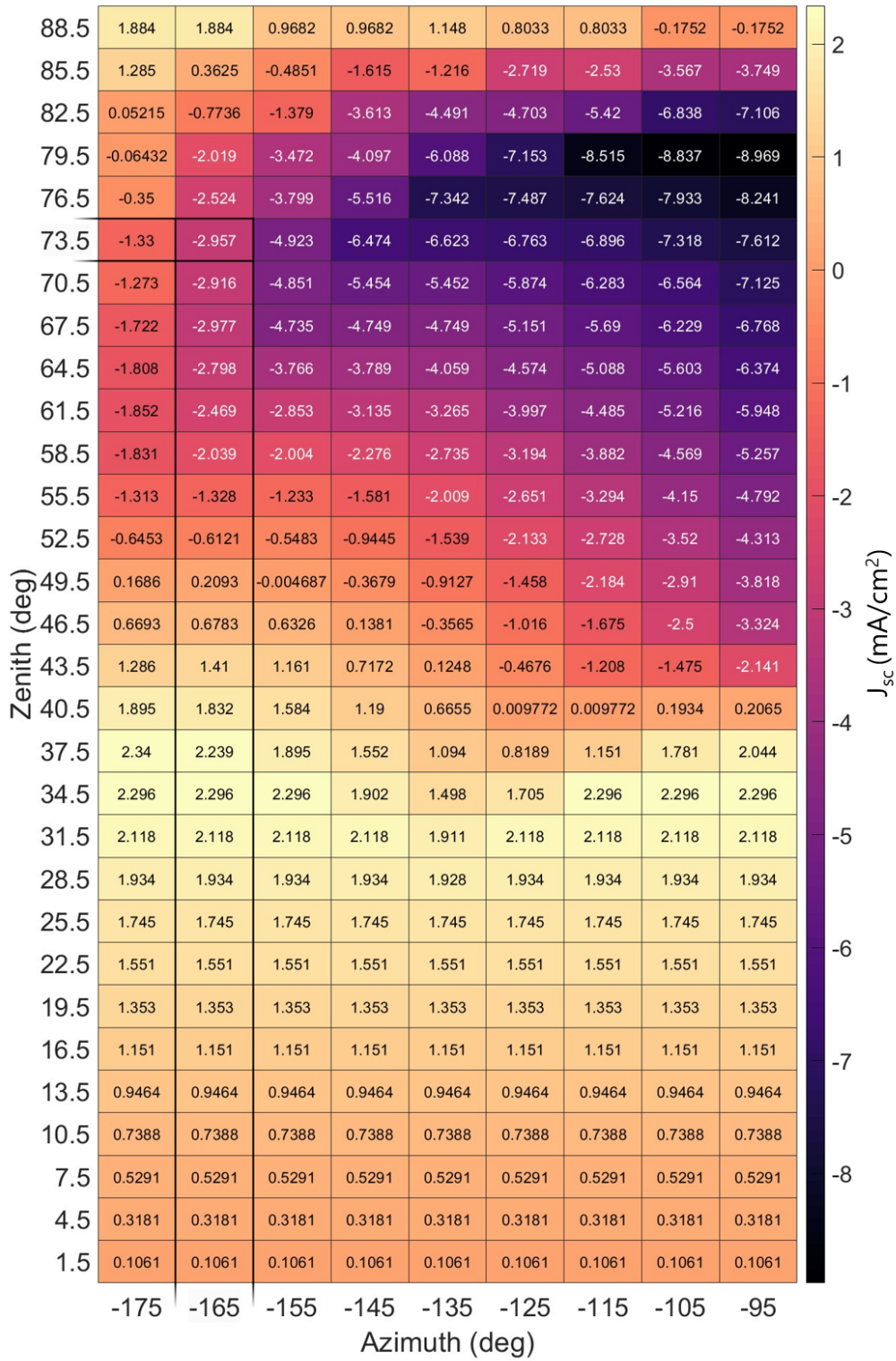


FIGURE B.7: Comparison between a fully specular reflector and a 40-degree FSLSC with a 95% quantum yield of luminophores. In positive cases, the FSLSC outperforms the specular reflector. In negative cases, the specular reflector outperforms the FSLSC.

Appendix C

Code

C.1 FSLSC Code - Parameter Document

```
clear
close all
clc

%% Initialize calculation output
% Explanation of variables from now onwards:
% S, M, R, C: Source, Module, Reflector, Cone
% AoI, Az, El, Zen: Angle of Incidence, Azimuth Angle,
    Elevation Angle, Zenith Angle
% f, j: flux, current density
% F, R, T: Front, Rear, Total
% MM, eqe: MisMatch, External Quantum Efficiency
% s, e, sky: Specular, Emission Cone, Sky

%Define the charge and the table with all the parameters
charge = 1.6*10^-19 ; %define charge
ParametersExcel = readtable('Par.xlsx','ReadRowNames',true); %
    read the parameter sheets from excel
p=assign(ParametersExcel); %transfer table into parameter
tic

% ASSIGN SIZES IN ADVANCE TO SPEED UP
mLength = [p.mL(1):p.mLd(1):p.mL(2)']; %initialize module
    length
mHeight = [p.mH(1):p.mHd(1):p.mH(2)']; %initialize module
    height
mTilt = [p.mT(1):p.mTd(1):p.mT(2)']; %initialize module tilt
rLength = [p.rL(1):p.rLd(1):p.rL(2)']; %initialize reflector
    length
pix = [p.pX(1)']; %initialize number of pixels per unit
sEl = [p.sE(1): p.sEd(1):p.sE(2)']; %initialize source
    elevation
sAz = [p.sA(1): p.sAd(1):p.sA(2)']; %initialize source azimuth
ConeAngles = [p.cA(1):p.cAd(1):p.cA(2)']; %initialize cone
```

```

    angle range
Wavelength_Reflectance_Optimized = p.cWR(1); %Wavelength for
    which the reflectances goes from 0 to 1 in R_in
Wavelength_Emission_Optimized = p.cWE(1); %Wavelength of the
    center of the emission cone from luminophores
Emission_Cone_Width = p.cWEW(1); %width of the emission cone
    in nm

%% Define Idealized Emission
% Parameters for the wavelength range (151, 510, 800 for
    accordance with Albedo code)
Wavelength_Range = 81; %Number of data points into which the
    wavelength range is divided
Wavelength_StartRange = 300; %1st wavelength in wavelength
    range (nm)
Wavelength_EndRange = 1100; %last wavelength in wavelength
    range (nm)
Wavelength_Unit = (Wavelength_EndRange - Wavelength_StartRange
    )/Wavelength_Range; %how many wavelengths are currently in
    one pixel

% Parameters for cone angle range (0,80,81 in accordance with
    albedo code)
Angle_Range = 91; %number of data points
Angle_StartRange = 0; %first angle in degrees
Angle_EndRange = 90; %last angle in degrees

%initialize parameters
lambdas = linspace(Wavelength_StartRange,Wavelength_EndRange ,
    Wavelength_Range); %wavelength range and number of
    intervals
theta_deg = linspace(Angle_StartRange , Angle_EndRange ,
    Angle_Range)'; %range of cone size
theta_rad = deg2rad(theta_deg); %range of cone size tranferred
    to radians

%make emission matrix
Entries_Wavelength_Zeros = ceil((
    Wavelength_Reflectance_Optimized-Wavelength_StartRange)/((
    Wavelength_EndRange-Wavelength_StartRange)/Wavelength_Range
    )); %calculate from which wavelength entry onwards it
    should be one (below zero) -> so from where it is reflected
Emission_Idealized = zeros(length(lambdas),1); % make a matrix
    filled with only zeros
Entries_Wavelength_Emission = ceil((
    Wavelength_Emission_Optimized-Wavelength_StartRange)/((
    Wavelength_EndRange-Wavelength_StartRange)/Wavelength_Range
    )); %the unit of the middle of the emission cone
Emission_Cone_Width_Units = linspace(

```

```

Entries_Wavelength_Emission=floor(Emission_Cone_Width/2/
Wavelength_Unit),Entries_Wavelength_Emission+floor(
Emission_Cone_Width/2/Wavelength_Unit),floor(
Emission_Cone_Width/Wavelength_Unit)); %linspace of pixels
that should be zeros
for i = Emission_Cone_Width_Units
    Emission_Idealized(i,:) = 1.0; %below cone angle and lower
        wavelengths are absorbing, so 0
end

%% Define Illumination
% AM1.5 excel file has extraterrestrial, GHI and DNI in the 2
    nd, 3rd and
% 4th columns respectively, whereas the first is wavelength.
AM_Data = cell2mat(struct2cell(load('AM_flux_ForSunSolve.mat')
    ));
type= 4; %select the column of the preferred radiance
illumIn = strcat('AM',num2str(type));
Fin = Illumination(AM_Data, 1, type) ; %Makes a trimmed input
    flux matrix and prints the maximum possible Jsc for sanity
    check

%eqe0 is the imported data from using SunSolve, it gives the
    eqe for all
%the different wavelengths (first colum) and all the angles (
    next columns)
eqe0 = cell2mat(struct2cell(load('HJT_Bi_Interp_AMsteps.mat'))
    );
eqeParam = eqe0(1,2:end)'; %storing the angular step size in a
    separate variable
eqe = reshape( eqe0(2:end,2:end)', [size(eqe0,2)-1,1,size(eqe0
    ,1)-1]); %move the wavelength to the 3rd dimensions, since
    upcoming calculatings are angle-dependent

%plots the chosen AM spectrum
figure();
plot(Fin(:,1),Fin(:,2),'Linewidth',8 ); xlabel('Wavelength (nm
    )'); ylabel('Flux (#/s/cm^2/nm)'); set(gca, 'FontSize',20);
    xlim([300 1100]); pbaspect([1 0.5 1]) ; hold on

%% Make the BRDF matrix for the emission cone
%Set up the axis
LS_El = linspace(90,0,91); % Initialize Elevation Angles: go
    from 90 to 0
LS_Az = linspace(-180,180,361); % Initialize Azimuth angles:
    go from -180 to 180
Basic_BRDFMatrix = zeros(length(LS_El),length(LS_Az)); %Make a
    matrix with only zeros of the correct shape

```

```

for CA=1:1:size(ConeAngles,1)
    Cone_Angle_deg = ConeAngles(CA,1)
    Cone_Angle_rad = deg2rad(Cone_Angle_deg);
    count=1;
    for AoIAz=1:1:size(sAz,1) %loop over the azimuth angle
        for AoIEl=1:1:size(sEl,1) %loop over the elevation angle
            %for roug=1:1:size(SurfRou,1) %loop over the surface
            roughness range
            if sAz(AoIAz)>=0 %if the source azimuth is
                positive
                %stores incoming angles (1st and 2nd column) and
                outgoing angles (3rd and 4th column)
                [RDir(count,:)] = [sEl(AoIEl,1), sAz(AoIAz,1),
                    sEl(AoIEl,1), -180+sAz(AoIAz,1)];
            else %if the source azimuth is negative
                [RDir(count,:)] = [sEl(AoIEl,1), sAz(AoIAz,1),
                    sEl(AoIEl,1), 180+sAz(AoIAz,1)];
            end
            Refl_Location_sub = Basic_BRDFMatrix; % start
            with the basic zero matrix
            %loop over the angles inside the emission cone
            and set their values to one
            for j = 1:1:Cone_Angle_deg %loop over emission
            cone angles
                for i = 1:1:length(LS_Az) %loop over azimuth
                    Refl_Location_sub(j,i) = 1;
                end
            end
            end

            % normalize BRDF matrix according to the energy
            conservation law
            rad = pi/180; %for conversion from deg to
            radians
            EnergyConservationLaw = abs(trapz( (LS_Az.*rad),
                abs(trapz((LS_El).*rad,abs(Refl_Location_sub
                    .*cosd(90-LS_El')).*sind(90-LS_El')))))); %
            Energy conservation integral
            NormalizationFactor = 1/EnergyConservationLaw; %
            Calculate the normalization factor to get
            energy conservation
            Refl_Location_sub = NormalizationFactor*
                Refl_Location_sub; %Normalize the BRDF Matrix
            EnergyConservationLawCheck = abs(trapz( (LS_Az.*
                rad), abs(trapz((LS_El).*rad,abs(
                    Refl_Location_sub.*cosd(90-LS_El')).*sind(90-
                    LS_El')))))); %Energy conservation integral,
            should equal one
            Refl_Location(:, :, count) = Refl_Location_sub; %
            add it to the matrix for each situation

```

```

%make a plot of the BRDF_Matrix
figure()
imagesc(LS_Az,LS_El,Refl_Location_sub)
xlabel('Azimuth')
ylabel('Elevation')
colorbar()
title('BRDF Matrix')

%Plot the emission cone
EmissionConePlotter(LS_El,LS_Az,sAz,
    Refl_Location_sub)

%end
count=count+1; %to make sure it loops over each
    elevation and azimuth angle
end %AoIEl
end %AoIAz

%% Calculate the current density
for rLong = 1:1:size(rLength,1) %Reflector length
    for pLong = 1:1:size(pix,1) %Pixel
        for mLong = 1:1:size(mLength,1) %Module length
            for ht = 1:1:size(mHeight,1) %Module Height
                for tt= 1:1:size(mTilt,1) %Module Tilt

                    %generate the directory and import the geometry
                    mark = strcat( num2str(rLength(rLong,1)), '_',
                        num2str(pix(pLong,1)), '_', num2str(mLength(
                            mLong,1)), '_', num2str(mHeight(ht,1)), '_',
                            num2str(mTilt(tt,1)) );
                    FileName=strcat(pwd, '\matrices\' , mark);
                    q=load(strcat(FileName, '\M.mat'));

                    %save all the sizes: number of pixels along the
                        module's length
                    %and breadth, reflector's length and breadth,
                        and number
                    %wavelength steps
                    [a(1,1), a(1,2)]=size(q.mAngr); %the number of
                        pixels of the module in x and y direction
                    [a(2,1), a(2,2)]=size(q.mAngr{1,1}); %the number
                        of pixels of the reflector in x and y
                        direction
                    a(3,1)=size(Fin,1); %the number of wavelength
                        points for which the input j is given
                    count=1; %initialize count

                    for AoIAz=1:1:size(sAz,1) %loop over azimuth

```

```

angle
for AoIEl=1:1:size(sEl,1) %loop over
    elevation angle
clear shade SF SR S
disp(strcat(mark, '_', num2str(sEl(AoIEl,1)), '
    _', num2str(sAz(AoIAz,1))));
                                %plot the
                                figures for
                                every angle
figure();
plot3(q.EdgeR
      (:,1), q.
      EdgeR(:,2), q
      .EdgeR(:,3),
      '-k');
hold on;
plot3(q.EdgeM
      (:,1), q.
      EdgeM(:,2), q
      .EdgeM(:,3),
      '-b');
xlim([-15 15]);
ylim([-15 15
]); zlim([-15
15]);
pbaspect([1 1
1]);
hold on
plot3([q.modC
{1,1}(:, :, :)],
[q.modC
{1,2}(:, :, :)], [
q.modC
{1,3}(:, :, :)],
'ob');
hold on;
plot3([q.reflC
{1,1}(:, :, :)],
[q.reflC
{1,2}(:, :, :)],
[q.reflC
{1,3}(:, :, :)],
'ok');
hold on;
xlim([-15 15]);
ylim([-15 15
]); zlim([-15
15]);
pbaspect([1 1

```

```

1]);
hold on

%calculates Flux Incoming Factor
FinFac(:,1) = Fin(:,2).*(1./pix(pLong,1).^2)
.*abs(sind(q.reflN(1,2)).*sind( sEl(AoIEl
,1)) + cosd(q.reflN(1,2)).*cosd(sEl(AoIEl
,1)).*cosd(q.reflN(1,1)-sAz(AoIAz,1)) ) ;

%Changes FinFac to account for redshifting
NumberOfRedshiftedPhotons = trapz(Fin(1:
Entries_Wavelength_Zeros),(FinFac(1:
Entries_Wavelength_Zeros,1)));
NormalizingFactor = Emission_Cone_Width;
FinFac_Redshifted = Emission_Idealized(:,1)
.*NumberOfRedshiftedPhotons./
NormalizingFactor; % the number of
photons that are emitted at the
wavelength
Check_0 = trapz(Fin(1:
Entries_Wavelength_Zeros),(FinFac(1:
Entries_Wavelength_Zeros,1))) - trapz(
lambdas,FinFac_Redshifted)

%CALCULATION FRONT
angcheck1=acosd(sind(mTilt(tt,1)).*sind(RDir
(count,1))+cosd(mTilt(tt,1)).*cosd(RDir(
count,1)).*sind(RDir(count,2))); %
calculating the angle with the module's
normal for the EQE
eqeFront = interp1(eqeParam, eqe0(2:end,2:
end)', angcheck1); %interpolate the data
such that it exists for the given angles
eqeFront=eqeFront';
jSky_1pixel(tt,count) = (charge*trapz( Fin
(1:end,1), abs(FinFac(:,1) .*cosd(
angcheck1).*eqeFront(1:end,1)) ))./( p.mL
(1).*p.mB(1) ) ; %using numerical
integration to calculate J_front for one
pixel
nmb_pixels = p.mL(1) * pix * p.mB(1) * pix;
%calculate the number of pixels
jSky = jSky_1pixel(tt,count).*nmb_pixels; %
calculate the front output for the entire
module

%Calculation of shade
[shade(:,,:), NetShade(:,,:),OnRefl,OnShade ]=
Polygon(q.EdgeM(:,,:), sAz(AoIAz,1), sEl(

```

```

AoIE1,1), q.reflC, 1, '-k', q.modC, RDir(
count,3), RDir(count,4),q.EdgeR) ; %Shade
describes shadow on the reflector,
NetShade is the shadow on the module.
Zero's indicate shade.

%calculation EQE
angcheck2=real(acosd(sind(mTilt(tt,1)).*sind
(-RDir(count,1))+cosd(mTilt(tt,1)).*cosd
(-RDir(count,1)).*sind(RDir(count,2)))));
%calculate the angle with the module's
normal
eqeS = interp1(eqeParam, eqe0(2:end,2:end)',
angcheck2); %interpolate such that the
EQE exists for this angle
EQE=reshape(eqeS(:,:,:),[1,1,a(3,1)]); %
reshape from a 1x81 double to a 1x1x81
double

%CALCULATION SPECULAR REFLECTION
% specular calculation by adapting the eqe
matrix to be zero
% for wavelengths above the '
Wavelength_Reflectance_Optimized'
% and calculate the current density
eqe_specular = eqe0; %make a new eqe matrix
row = find(eqe0(:,1) ==
Wavelength_Reflectance_Optimized); %find
the row which equals the chosen
wavelength
[~, col] = size(eqe0); % the size of the
matrix
emptyrow = zeros(1,col-1); % make an empty
row which can be substituted
for i = 2:1:row
eqe_specular(i,2:end) = emptyrow; %
substitute empty rows below the
selected wavelengths
end
eqe_specular = interp1(eqeParam,
eqe_specular(2:end,2:end)', angcheck2); %
interpolate for the correct angles
EQE_specular=reshape(eqe_specular(:,:,:),
,[1,1,a(3,1)]); %reshape EQE
fS(:,: ,1:a(3,1)) = abs(cosd(90-RDir(count,3)
).*EQE_specular(:,: ,1:a(3,1)).*cosd(
angcheck2).*NetShade(:,:))./abs(cosd(RDir
(count,3)-90));%Calculate flux (photons/s
)

```

```

fmodS(1:a(3,1),:,:) = shiftdim(fS(:,:,:),2);
S=(charge*trapz( Fin(1:end,1),FinFac(:,1) .*
    fmodS(1:end,:,:) ) ) ./ ( p.mL(1).*p.mB(1))
; %numerical integration over
    wavelenghts and multiply by charge to get
    Jsc
S=shiftdim(S(:,:,:),1);

% split the current density in front and
    rear face and calculate totals
if angcheck2 <=90
    SF=S; %front if the angle is below 90 deg
    SR=zeros(size(S));
else
    SR=S; %rear surface if the angle is above
        90 deg
    SF=zeros(size(S));
end
jsFMM=SF; %calculate mismatch for front
jsRMM=SR; %calculate mismatch for rear
jsTMM=S; %calculate total missmatch
jsF(ht,tt,count)=sum(sum(SF));%it calculates
    the sum of the mismatches, this is to
    compare. In reality, you could never add
    them up. But as it is photonics, this
    approach is used.
jsR(ht,tt,count)=sum(sum(SR)); %same for
    rear
jsT(ht,tt,count)=jsF(ht,tt,count)+jsR(ht,tt,
    count); %same for total

for mpY=1:1:a(1,1) %to loop over the module
    pixels in Y-direction
    for mpX=1:1:a(1,2) %to loop over the
        module pixels in X-direction
        for rpY=1:1:a(2,1) % loop over the
            y-pixels from the reflector
            for rpX=1:1:a(2,2) %loop over
                all x-pixels from the
                reflector
                [Cone_BRDF{mpY,mpX}(rpY,
                    rpX)]=interpolateCone(
                    Refl_Location(:,:,count
                    ), q.rAzmAdj{mpY,mpX}(
                    rpY,rpX), q.rThmAdj{mpY
                    ,mpX}(rpY,rpX),LS_El
                    (:,:),LS_Az(:,:)); %to
                    get the BRDF values for
                    certain pixels
            end
        end
    end
end

```

```

        end %x-pixels reflector
    end % y-pixels reflector
R_total = cell2mat(Cone_BRDF(mpY,mpX))
;

flux_wavelength =
    IncomingUsefulFluxComputer(R_total,
        q.rAngmAdj{mpY,mpX}(:, :), q.mAngr{
            mpY,mpX}(:, :), q.dw{mpY,mpX}(:, :), q.
            mEQE{mpY,mpX}(:, :, :), shade, Fin(1:
            end, 1), FinFac_Redshifted(:, 1), RDir,
            count); %caculate flux
[jFMM_pixel, jRMM_pixel] =
    FluxToCurrentOneModulePixel(
        flux_wavelength, Fin(1:end, 1), p.mL
        (1), p.mB(1), charge, q.mAngr{mpY,
            mpX}(:, :)); %calculate flux from
        one module
    results.jFMM(mpY,mpX)= jFMM_pixel; %
        saving value in matrix
    results.jRMM(mpY,mpX)= jRMM_pixel;
end % x-pixels module
end % y-pixels module
[jeF, jeR, jeT] = CurrentOneModule(results.
    jFMM, results.jRMM); %calculate current

%CALCULATION TOTALS & SAVING RESULTS
results.jsF(ht,tt,count) = jsF(ht,tt,count);
results.jsR(ht,tt,count) = jsR(ht,tt,count);
results.jsT(ht,tt,count) = jsT(ht,tt,count);

results.jeF(ht,tt,count) = jeF;
results.jeR(ht,tt,count) = jeR;
results.jeT(ht,tt,count) = jeT;

results.jF(ht,tt,count) = jeF + jsF(ht,tt,
    count);
results.jR(ht,tt,count) = jeR + jsR(ht,tt,
    count);
results.jT(ht,tt,count) = jeT + jsT(ht,tt,
    count);

results.jSky(CA,ht,tt,count) = jSky;

count=count+1;
toc

end %AoIEl
end %AoIAz

```

```

        end %Module Tilt
        end %Module Height
        end %Module length
        end %Pixel
        end %Reflector length
end %Cone Angles
openvar('results')

mark=strcat('lenR', num2str(rLength(rLong,1)),'_pix',num2str(
    pix(pLong,1)),'_lenM',num2str(mLength(mLong,1)),'_Height',
    num2str(p.mH(1)),'_',num2str(p.mHd(1)),'_',num2str(p.mH(2))
    ,'_Tilt',num2str(p.mT(1)),'_',num2str(p.mTd(1)),'_',num2str
    (p.mT(2)),'_CA',num2str(p.cA(1)),'_',num2str(p.cA(2)));
FileName=strcat(pwd, '\matrices\Jsc\' , mark);
mkdir(FileName)
save(strcat(FileName, '\M.mat'), 'results', 'p');

clearvars -except p results Cone_Angle_deg Emission_Cone_Width
    RDir Wavelength_Reflectance_Optimized
    Wavelength_Emission_Optimized %clear variables except the
    ones listed here

```

C.2 FSLSC Code - Looping over azimuths & Elevations

```

clear
close all
clc

%% Initialize calculation output
% Explanation of variables from now onwards:
% S, M, R, C: Source, Module, Reflector, Cone
% AoI, Az, El, Zen: Angle of Incidence, Azimuth Angle,
    Elevation Angle, Zenith Angle
% f, j: flux, current density
% F, R, T: Front, Rear, Total
% MM, eqe: MisMatch, External Quantum Efficiency
% s, e, sky: Specular, Emission Cone, Sky

%Define the charge and the table with all the parameters
charge = 1.6*10^-19 ; %define charge
ParametersExcel = readtable('Par.xlsx','ReadRowNames',true); %
    read the parameter sheets from excel
p=assign(ParametersExcel); %transfer table into parameter
tic

load("ToRun.mat") %load Occurance_Matrix, ElevationsToRun &
    AzimuthsToRun

```

```

% ASSIGN SIZES IN ADVANCE TO SPEED UP
mLength = [p.mL(1):p.mLd(1):p.mL(2)]'; %initialize module
length
mHeight = [p.mH(1):p.mHd(1):p.mH(2)]'; %initialize module
height
mTilt = [p.mT(1):p.mTd(1):p.mT(2)]'; %initialize module tilt
rLength = [p.rL(1):p.rLd(1):p.rL(2)]'; %initialize reflector
length
pix = [p.pX(1)]'; %initialize number of pixels per unit
sEl = Elevations_ToRun'; %initialize source elevation
sAz = Azimuths_ToRun'; %initialize source azimuth
ConeAngles = [p.cA(1):p.cAd(1):p.cA(2)]'; %initialize cone
angle range
Wavelength_Reflectance_Optimized = p.cWR(1); %Wavelength for
which the reflectances goes from 0 to 1 in R_in
Wavelength_Emission_Optimized = p.cWE(1); %Wavelength of the
center of the emission cone from luminophores
Emission_Cone_Width = p.cWEW(1); %width of the emission cone
in nm

%% Define Idealized Emission
% Parameters for the wavelength range (81, 300, 1100 for
accordance with Albedo code)
Wavelength_Range = 81; %Number of data points into which the
wavelength range is divided
Wavelength_StartRange = 300; %1st wavelength in wavelength
range (nm)
Wavelength_EndRange = 1100; %last wavelength in wavelength
range (nm)
Wavelength_Unit = (Wavelength_EndRange - Wavelength_StartRange
)/Wavelength_Range; %how many wavelengths are currently in
one pixel

% Parameters for cone angle range (0,90,91 in accordance with
albedo code)
Angle_Range = 91; %number of data points
Angle_StartRange = 0; %first angle in degrees
Angle_EndRange = 90; %last angle in degrees

%initialize parameters
lambdas = linspace(Wavelength_StartRange,Wavelength_EndRange ,
Wavelength_Range); %wavelength range and number of
intervals
theta_deg = linspace(Angle_StartRange , Angle_EndRange ,
Angle_Range)'; %range of cone size
theta_rad = deg2rad(theta_deg); %range of cone size tranferred
to radians

%make emission matrix

```

```

Entries_Wavelength_Zeros = ceil((
    Wavelength_Reflectance_Optimized-Wavelength_StartRange)/((
    Wavelength_EndRange-Wavelength_StartRange)/Wavelength_Range
)); %calculate from which wavelength entry onwards it
    should be one (below zero) -> so from where it is reflected
Emission_Idealized = zeros(length(lambdas),1); % make a matrix
    filled with only zeros
Entries_Wavelength_Emission = ceil((
    Wavelength_Emission_Optimized-Wavelength_StartRange)/((
    Wavelength_EndRange-Wavelength_StartRange)/Wavelength_Range
)); %the unit of the middle of the emission cone
Emission_Cone_Width_Units = linspace(
    Entries_Wavelength_Emission-floor(Emission_Cone_Width/2/
    Wavelength_Unit),Entries_Wavelength_Emission+floor(
    Emission_Cone_Width/2/Wavelength_Unit),floor(
    Emission_Cone_Width/Wavelength_Unit)); %linspace of pixels
    that should be zeros
for i = Emission_Cone_Width_Units
    Emission_Idealized(i,:) = 1.0; %below cone angle and lower
        wavelengths are absorbing, so 0
end

%% Define Illumination
% AM1.5 excel file has extraterrestrial, GHI and DNI in the 2
    nd, 3rd and
% 4th columns respectively, whereas the first is wavelength.
AM_Data = cell2mat(struct2cell(load('AM_flux_ForSunSolve.mat')
    ));
type= 4; %select the column of the preferred radiance
illumin = strcat('AM',num2str(type));
Fin = Illumination(AM_Data, 1, type) ; %Makes a trimmed input
    flux matrix and prints the maximum possible Jsc for sanity
    check

%eqe0 is the imported data from using SunSolve, it gives the
    eqe for all
%the different wavelengths (first colum) and all the angles (
    next columns)
eqe0 = cell2mat(struct2cell(load('HJT_Bi_Interp_AMsteps.mat'))
    );
eqeParam = eqe0(1,2:end)'; %storing the angular step size in a
    seperate variable
eqe = reshape( eqe0(2:end,2:end)', [size(eqe0,2)-1,1,size(eqe0
    ,1)-1]); %move the wavelength to the 3rd dimensions, since
    upcoming calculatings are angle-dependent

%plots the chosen AM spectrum
figure();
plot(Fin(:,1),Fin(:,2),'Linewidth',8 ); xlabel('Wavelength (nm

```

```

    '); ylabel('Flux (#/s/cm^2/nm)'); set(gca, 'FontSize',20);
    xlim([300 1100]); pbaspect([1 0.5 1]) ; hold on

%% Make the BRDF matrix for the emission cone
%Set up the axis
LS_El = linspace(90,0,91); % Initialize Elevation Angles: go
    from 90 to 0
LS_Az = linspace(-180,180,361); % Initialize Azimuth angles:
    go from -180 to 180
Basic_BRDFMatrix = zeros(length(LS_El),length(LS_Az)); %Make a
    matrix with only zeros of the correct shape

for CA=1:1:size(ConeAngles,1) %loop over cone angles
    Cone_Angle_deg = ConeAngles(CA,1)
    Cone_Angle_rad = deg2rad(Cone_Angle_deg);
    count=1;
    for AoIAz=1:1:size(sAz,1) %loop over the azimuth angle
        for AoIEl=1:1:size(sEl,1) %loop over the elevation angle
            %stores incoming angles (1st and 2nd column) and
            outgoing angles (3rd and 4th column)
            if sAz(AoIAz)>=0 %if the source azimuth is
                positive
                [RDir(count,:) ] = [sEl(AoIEl,1), sAz(AoIAz,1),
                    sEl(AoIEl,1), -180+sAz(AoIAz,1)];
            else %if the source azimuth is negative
                [RDir(count,:) ] = [sEl(AoIEl,1), sAz(AoIAz,1),
                    sEl(AoIEl,1), 180+sAz(AoIAz,1)];
            end

            %make BRDF matrix
            Refl_Location_sub = Basic_BRDFMatrix; % start
                with the basic zero matrix
            %loop over the angles inside the emission cone
            and set their values to one
            for j = 1:1:Cone_Angle_deg %loop over emission
                cone angles
                for i = 1:1:length(LS_Az) %loop over azimuth
                    Refl_Location_sub(j,i) = 1;
                end
            end

            % normalize BRDF matrix according to the energy
            conservation law
            rad = pi/180; %for conversion from deg to
                radians
            EnergyConservationLaw = abs(trapz( (LS_Az.*rad),
                abs(trapz((LS_El).*rad,abs(Refl_Location_sub
                .*cosd(90-LS_El ')).*sind(90-LS_El ')) )))); %
                Energy conservation integral

```

```

NormalizationFactor = 1/EnergyConservationLaw; %
    Calculate the normalization factor to get
    energy conservation
Refl_Location_sub = NormalizationFactor*
    Refl_Location_sub; %Normalize the BRDF Matrix
EnergyConservationLawCheck = abs(trapz( (LS_Az.*
    rad), abs(trapz((LS_El).*rad,abs(
    Refl_Location_sub.*cosd(90-LS_El')).*sind(90-
    LS_El')))))); %Energy conservation integral,
    should equal one

Refl_Location(:,:,count) = Refl_Location_sub; %
    add it to the matrix for each situation
count=count+1; %to make sure it loops over each
    elevation and azimuth angle
end %AoIEl
end %AoIAz

%% Calculate the current density
for rLong = 1:1:size(rLength,1) %Reflector length
    for pLong = 1:1:size(pix,1) %Pixel
        for mLong = 1:1:size(mLength,1) %Module length
            for ht = 1:1:size(mHeight,1) %Module Height
                for tt= 1:1:size(mTilt,1) %Module Tilt

                    %generate the directory and import the geometry
                    mark = strcat( num2str(rLength(rLong,1)), '_',
                        num2str(pix(pLong,1)), '_', num2str(mLength(
                            mLong,1)), '_', num2str(mHeight(ht,1)), '_',
                            num2str(mTilt(tt,1)) );
                    FileName=strcat(pwd, '\matrices\' , mark);
                    q=load(strcat(FileName, '\M.mat'));

                    %save all the sizes: number of pixels along the
                    module's length
                    %and breadth, reflector's length and breadth,
                    and number
                    %wavelength steps
                    [a(1,1), a(1,2)]=size(q.mAngr); %the number of
                    pixels of the module in x and y direction
                    [a(2,1), a(2,2)]=size(q.mAngr{1,1}); %the number
                    of pixels of the reflector in x and y
                    direction
                    a(3,1)=size(Fin,1); %the number of wavelength
                    points for which the input j is given
                    count=1; %initialize count

                    for AoIAz=1:1:size(sAz,1) %loop over azimuth
                        angle

```

```

for AoIEl=1:1:size(sEl,1) %loop over
elevation angle
    if Occurance_Matrix_ToRun(AoIAz ,AoIEl) ~
        0;
        clear shade SF SR S
        disp(strcat(mark, '_', num2str(sEl(
            AoIEl,1)), '_', num2str(sAz(AoIAz
            ,1))));

        %calculates Flux Incoming Factor
        FinFac(:,1) = Fin(:,2).*(1./pix(
            pLong,1).^2).*abs(sind(q.reflN
            (1,2)).*sind( sEl(AoIEl,1)) +
            cosd(q.reflN(1,2)).*cosd(sEl(
            AoIEl,1)).*cosd(q.reflN(1,1)-sAz(
            AoIAz,1)) ) ; % dividing it to be
            per area and cosine correction
            of irradiance

        %Changes FinFac to account for
            redshifting
        NumberOfRedshiftedPhotons = trapz(
            Fin(1:Entries_Wavelength_Zeros),(
            FinFac(1:Entries_Wavelength_Zeros
            ,1))); % calculate number of
            absorbed photons
        FinFac_Redshifted =
            Emission_Idealized(:,1).*
            NumberOfRedshiftedPhotons./
            Emission_Cone_Width; % the number
            of photons that are emitted at
            the wavelength
        Check_0 = trapz(Fin(1:
            Entries_Wavelength_Zeros),(FinFac
            (1:Entries_Wavelength_Zeros,1)))
            - trapz(lambdas,FinFac_Redshifted
            ); %should be small compared to
            10^18 to check if no photons are
            lost

        %CALCULATION FRONT
        angcheck1=acosd(sind(mTilt(tt,1)).*
            sind(RDir(count,1))+cosd(mTilt(tt
            ,1)).*cosd(RDir(count,1)).*sind(
            RDir(count,2))); %calculating the
            angle with the module's normal
            for the EQE
        eqeFront = interp1(eqeParam, eqe0(2:
            end,2:end)', angcheck1); %

```

```

        interpolate the data such that it
        exists for the given angles
eqeFront=eqeFront';
jSky_1pixel(tt,count) = (charge*
    trapz( Fin(1:end,1), abs(FinFac
        (:,1) .*cosd(angcheck1).*eqeFront
        (1:end,1)) ))./( p.mL(1).*p.mB(1)
    ) ; %using numerical integration
        to calculate J_front for one
        pixel
nmb_pixels = p.mL(1) * pix * p.mB(1)
    * pix; %calculate the number of
        pixels
jSky = jSky_1pixel(tt,count).*
    nmb_pixels; %calculate the front
        output for the entire module

%Calculation of shade
[shade(:,,:), NetShade(:,,:),OnRefl,
    OnShade ]= Polygon(q.EdgeM(:,,:),
    sAz(AoIAz,1), sEl(AoIEl,1), q.
    reflC, 1, '-k', q.modC, RDir(
    count,3), RDir(count,4),q.EdgeR)
; %Shade describes shadow on the
    reflector, NetShade is the shadow
    on the module. Zero's indicate
    shade.

%calculation EQE
angcheck2=real(acosd(sind(mTilt(tt
    ,1)).*sind(-RDir(count,1))+cosd(
    mTilt(tt,1)).*cosd(-RDir(count,1)
    ).*sind(RDir(count,2))))); %
    calculate the angle with the
    module's normal
eqeS = interp1(eqeParam, eqe0(2:end
    ,2:end)', angcheck2); %
    interpolate such that the EQE
    exists for this angle
EQE=reshape(eqeS(:,:,:),[1,1,a(3,1)
    ]); %reshape from a 1x81 double
    to a 1x1x81 double

%CALCULATION SPECULAR REFLECTION
% specular calculation by adapting
    the eqe matrix to be zero
% for wavelengths above the'
    Wavelength_Reflectance_Optimized'
% and calculate the current density

```

```

eque_specular = eque0; %make a new eque
matrix
row = find(eque0(:,1) ==
Wavelength_Reflectance_Optimized)
; %find the row which equals the
chosen wavelength
[~, col] = size(eque0); % the size of
the matrix
emptyrow = zeros(1,col-1); % make an
empty row which can be
substituted
for i = 2:1:row
eque_specular(i,2:end) = emptyrow
; %substitute empty rows
below the selected
wavelengths
end
eque_specular = interp1(equeParam,
eque_specular(2:end,2:end)',
angcheck2); %interpolate for the
correct angles
EQE_specular=reshape(eque_specular
(:, :, :), [1,1,a(3,1)]); %reshape
EQE
fS(:, :, 1:a(3,1)) = abs(cosd(90-RDir(
count,3))).*EQE_specular(:, :, 1:a
(3,1)).*cosd(angcheck2).*NetShade
(:, :))./abs(cosd(RDir(count,3)
-90));%Calculate flux (photons/s)
fmodS(1:a(3,1), :, :) = shiftdim(fS
(:, :, :), 2);
S=(charge*trapz( Fin(1:end,1), FinFac
(:,1) .*fmodS(1:end, :, :)) )./( p
.mL(1).*p.mB(1)); %numerical
integration over wavelenghts and
multiply by charge to get Jsc
S=shiftdim(S(:, :, :), 1);

% split the current density in front
and rear face and calculate
totals
if angcheck2 <=90
SF=S; %front if the angle is below
90 deg
SR=zeros(size(S));
else
SR=S; %rear surface if the angle
is above 90 deg
SF=zeros(size(S));

```

```

end
jsFMM=SF; %calculate mismatch for
front
jsRMM=SR; %calculate mismatch for
rear
jsTMM=S; %calculate total mismatch
jsF(ht,tt,count)=sum(sum(SF));%it
calculates the sum of the
mismatches, this is to compare.
In reality, you could never add
them up. But as it is photonics,
this approach is used.
jsR(ht,tt,count)=sum(sum(SR)); %same
for rear
jsT(ht,tt,count)=jsF(ht,tt,count)+
jsR(ht,tt,count); %same for total

%turn comments off for plots
figure();plot3(q.EdgeR(:,1), q.
EdgeR(:,2), q.EdgeR(:,3), '-k'); hold on; plot3(q.EdgeM
(:,1), q.EdgeM(:,2), q.EdgeM(:,3), '-b'); xlim([-15 15]);
ylim([-15 15]); zlim([-15 15]);pbaspect([1 1 1]); hold on
%
plot3([q.modC{1,1}(:,:)],[q.modC
{1,2}(:,:)],[q.modC{1,3}(:,:)], 'ob'); hold on;plot3([q.
reflC{1,1}(:,:)],[q.reflC{1,2}(:,:)], [q.reflC{1,3}(:,:)],
'ok'); hold on;xlim([-15 15]); ylim([-15 15]); zlim([-15
15]);pbaspect([1 1 1]); hold on
%
plot3([q.reflC{1,1}(1,1), q.reflC
{1,1}(1,1)+10*cosd(RDir(count,2)).*cosd(RDir(count,1))],[q
.reflC{1,2}(1,1), q.reflC{1,2}(1,1)+10*sind(RDir(count,2))
.*cosd(RDir(count,1))],[q.reflC{1,3}(1,1), q.reflC
{1,3}(1,1)+10*sind(RDir(count,1))], 'r', 'LineWidth', 2);
hold on
%
plot3([q.reflC{1,1}(1,1), q.reflC
{1,1}(1,1)+10*cosd(RDir(count,4)).*cosd(RDir(count,3))],[q
.reflC{1,2}(1,1), q.reflC{1,2}(1,1)+10*sind(RDir(count,4))
.*cosd(RDir(count,3))],[q.reflC{1,3}(1,1), q.reflC
{1,3}(1,1)+10*sind(RDir(count,3))], '-r', 'LineWidth', 2);
hold on
%
title(strcat(sprintf('Azimuth - %f
',sAz(AoIAz)),sprintf('Elevation - %f', sEl(AoIEl))))
%
for mpY=1:1:a(1,1) %to loop over the
module pixels in Y-direction
for mpX=1:1:a(1,2) %to loop over
the module pixels in X-
direction
for rpY=1:1:a(2,1) % loop
over the y-pixels from

```

```

the reflector
for rpX=1:1:a(2,2) %
loop over all x-
pixels from the
reflector
[Cone_BRDF{mpY,mpX
}(rpY,rpX)]=
interpolateCone
(Refl_Location
(:, :, count), q.
rAzMAdj{mpY,mpX
}(rpY,rpX), q.
rThmAdj{mpY,mpX
}(rpY,rpX),
LS_El(:, :),
LS_Az(:, :)); %
to get the BRDF
values for
certain pixels
end %x-pixels
reflector
end % y-pixels reflector
R_total = cell2mat(Cone_BRDF(
mpY,mpX));

flux_wavelength =
IncomingUsefulFluxComputer(
R_total, q.rAngmAdj{mpY,mpX
}(:, :), q.mAngr{mpY,mpX
}(:, :), q.dw{mpY,mpX}(:, :), q
.mEQE{mpY,mpX}(:, :, :), shade
, Fin(1:end, 1),
FinFac_Redshifted(:, 1), RDir
, count); %caculate flux
[jFMM_pixel, jRMM_pixel] =
FluxToCurrentOneModulePixel
(flux_wavelength, Fin(1:end
, 1), p.mL(1), p.mB(1),
charge, q.mAngr{mpY,mpX
}(:, :)); %calculate flux
from one module
results.jFMM(mpY,mpX)=
jFMM_pixel; % saving value
in matrix
results.jRMM(mpY,mpX)=
jRMM_pixel;
end % x-pixels module
end % y-pixels module
[jeF, jeR, jeT] = CurrentOneModule(

```

```

        results.jFMM, results.jRMM); %
        calculate current

%CALCULATION TOTALS & SAVING RESULTS
results.jsF(AoIEl,AoIAz) = jsF(ht,tt
    ,count);
results.jsR(AoIEl,AoIAz) = jsR(ht,tt
    ,count);
results.jsT(AoIEl,AoIAz) = jsT(ht,
    tt,count);

results.jeF(AoIEl,AoIAz) = jeF;
results.jeR(AoIEl,AoIAz) = jeR;
results.jeT(AoIEl,AoIAz) = jeT;

results.jF(AoIEl,AoIAz) = jeF + jsF(
    ht,tt,count);
results.jR(AoIEl,AoIAz) = jeR + jsR
    (ht,tt,count);
results.jT(AoIEl,AoIAz) = jeT + jsT
    (ht,tt,count);

results.jSky(AoIEl,AoIAz) = jSky;
else
    disp(sAz(AoIAz))
    disp(sEl(AoIEl))
%CALCULATION TOTALS & SAVING RESULTS
results.jsF(AoIEl,AoIAz) = 0.00;
results.jsR(AoIEl,AoIAz) = 0.00;
results.jsT(AoIEl,AoIAz) = 0.00;

results.jeF(AoIEl,AoIAz) = 0.00;
results.jeR(AoIEl,AoIAz) = 0.00;
results.jeT(AoIEl,AoIAz) = 0.00;

results.jF(AoIEl,AoIAz) = 0.00;
results.jR(AoIEl,AoIAz) = 0.00;
results.jT(AoIEl,AoIAz) = 0.00;

results.jSky(AoIEl,AoIAz) = 0;
end % if statement

count=count+1;
toc

    end %AoIEl
end %AoIAz

end %Module Tilt

```

```

        end %Module Height
    end %Module length
end %Pixel
end %Reflector length
end %Cone Angles
openvar('results')

mark=strcat('lenR', num2str(rLength(rLong,1)), '_pix', num2str(
    pix(pLong,1)), '_lenM', num2str(mLength(mLong,1)), '_Height',
    num2str(p.mH(1)), '_', num2str(p.mHd(1)), '_', num2str(p.mH(2))
    , '_Tilt', num2str(p.mT(1)), '_', num2str(p.mTd(1)), '_', num2str
    (p.mT(2)), '_CA', num2str(p.cA(1)), '_', num2str(p.cA(2)));
FileName=strcat(pwd, '\matrices\Jsc\' , mark);
mkdir(FileName)
save(strcat(FileName, '\M.mat'), 'results', 'p');

clearvars -except p results Cone_Angle_deg Emission_Cone_Width
    RDir Wavelength_Reflectance_Optimized
    Wavelength_Emission_Optimized %clear variables except the
    ones listed here

```

C.3 FSLSC Code - Subfunctions

C.3.1 CurrentOneModule

```

function [jF,jR,jT] = CurrentOneModule(current_front_pixel ,
    current_rear_pixel)
% Computes the current density on one module pixel.
%
% =====
% Input:      - current_front_pixel matrix      current density
%              generated on
%
%              the front of the
%              module per
%              module pixel
%              - current_rear_pixel matrix      current density
%              generated on
%
%              the front of the
%              module per
%              module pixel
%
% -----
% Output:     - jF float the current generated on the front
%              of the module
%              - jR float the current generated on the rear of
%              the module

```

```

%           - jT float the current generated on the front +
%           rear of the module
%
=====

jF = sum(current_front_pixel(:,:),[1,2]);
jR = sum(current_rear_pixel(:,:),[1,2]);

jT = jR+ jF;

end

```

C.3.2 EmissionConePlotter

```

function [] = EmissionConePlotter(LS_El,LS_Az, sAz,
    Refl_Location)

elevation_angle = LS_El;
azimuth_angle = LS_Az;

if sAz> 0 % for az 0 - 180
    azimuth_angle_2 = azimuth_angle - 90;
    elevation_angle_2 = 90-elevation_angle;
else % for az 0 - -180
    azimuth_angle_2 = 90 - azimuth_angle;
    elevation_angle_2 = 90+elevation_angle;
end

c = [0.45 0.65 0.85]; %defining color according to other plots

figure()
%plotting axes
plot_origin_line_z = plot3(zeros(11,1),zeros(11,1), [-5:5], '
    color', c );
hold on
plot_origin_line_x = plot3([-5:5],zeros(11,1), zeros(11,1),'
    color', c); %color can be 'r' for clarity
hold on
plot_origin_line_y = plot3(zeros(11,1),[-5:5], zeros(11,1),'
    color', c ); %color can be 'm' for clarity
hold on

%labelling axes
xlabel('X')
ylabel('Y')
zlabel('Z')
xlim([-2,2])
ylim([-2,2])

```

```

zlim([0,2])

% setting all angles
theta = [90:-0.5:-90];
phi = [-90:0.5:90];
pbaspect([1 1 1])

% Sphere
hold on

[reflectance_to_plot_x,reflectance_to_plot_y,
 reflectance_to_plot_z] = sph2cart(deg2rad( azimuth_angle_2)
 ,deg2rad( flip(elevation_angle_2 ')),Refl_Location(:,:)); %
 cosd(elevation_angle)*

surf_reflectance = surf(reflectance_to_plot_x,
 reflectance_to_plot_y,reflectance_to_plot_z, 'EdgeAlpha',0)
;
colormap([0.79 0.85 0.93]);
xlabel( 'X' )
ylabel( 'Y' )
zlabel( 'Z' )
pbaspect([1 1 1])
hold on

end

```

C.3.3 FluxToCurrentOneModulePixel

```

function [jFMM_pixel,jRMM_pixel] = FluxToCurrentOneModulePixel
(flux,wavelengths, module_length, module_breadth, charge,
 angle_module_reflector )
% Computes the current density on one module pixel.
%
=====

% Input:      - flux          matrix    flux
              incoming on the
%
              reflector,
%
              per wavelength
%
              - wavelengths   matrix    wavelengths
              in the code
%
              - module_length float     length of
              the module
%
              - module_breadth float     breadth of
              the module
%
              - charge        float     charge
              produced by one photon

```

```

%           - angle_module_reflector   matrix   angle
%           between the module pixel
%
%           center and
%           reflector pixels center
%
% -----

% Output:   - jFMM_pixel   the current generated on the front
%           of the module pixel
%           - jRMM_pixel   the current generated on the rear
%           of the module pixel
%
% =====

j_total(:,:)= (charge*trapz(wavelengths , flux ))./(
    module_length.*module_breadth ) ;

%split results into front and rear reflection
j_front = j_total; % front reflection
j_front(angle_module_reflector(:,:)>90) = 0;

j_rear = j_total; % rear reflection
j_rear(angle_module_reflector(:,:)<=90) = 0;

% sum over contributions of every reflector pixel
jFMM_pixel=sum(sum(j_front(:,,:)));
jRMM_pixel=sum(sum(j_rear(:,,:)));
end

```

C.3.4 Illumination

```

function [f] = Illumination(input , flux, ColSelect)

if flux ~= 1 %if the flux does not(!) equal to 1, the units
    are not correct
    input2 = FluxConverter( input(:,[1 ColSelect])) ; %
        irradiance to flux converter -> to number of photon
else
    input2 = input(:, [1 ColSelect]) ; %it is already always in
        flux
end
input2(:,2) = input2(:,2)./1000 ; %for unit correction
f = input2;

disp(strcat( 'AM Jsc = ',num2str((1.6*10^-19).*trapz(f(:,1),f
    (:,2))), ' mA/cm2' ))

```

end

C.3.5 IncomingUsefulFluxComputer

```
function flux_wavelength = IncomingUsefulFluxComputer(brdf,
    angle_reflector_module, angle_module_reflector,dw,mEQE,
    shade,wavelengths,flux,RDir,count)
% Multiplies all factors which, multiplied by the flux, will
% lead to the
% current density
%
=====

% Input:      - flux          matrix   flux
%              incoming on the
%
%              reflector,
% per wavelength
%              - brdf         matrix   contains
%              brdf (R) values.
%              - wavelengths  matrix   wavelengths
%              in the code
%              - angle_reflector_module  matrix   angle
%              between the module pixel
%
%              center and
% reflector pixels center
%              - angle_module_reflector  matrix   angle
%              between the reflector pixel
%
%              center and
% module pixels
%              - dw           float    solid angle
%              - mEQE         matrix   external
%              quantum
%
%              efficiency
%              - shade        matrix   0/1
%              depending on
%
%              whether
% reflector is in shade
%
-----

% Output:     - flux_wavelength  matrix   reflected
%              flux (incoming
%
%              in the
% module) per
%
%              wavelength
%
=====
```

```

% computing the useful flux factor
flux_factor(:,:,:) = abs(brdf.*cosd(angle_reflector_module).*
    dw.*mEQE.*cosd(angle_module_reflector).*shade) ;%
    distribution of reflected light + taking into account
    efficiencies

%reorganize matrix to get the flux factor per wavelength
flux_factor_wavelength(1:length(wavelengths),:,:) = shiftdim(
    flux_factor(:,:,:),2) ; %reorganize per wavelength

% multiply the flux by its distribution
flux_wavelength = flux .* flux_factor_wavelength(1:end,:,:) ;
end

```

C.3.6 interpolateCone

```

function [val] = interpolateCone(data,xq,yq,axis_El , axis_Az)
[dim1,dim2]=size(data);
y=repmat(axis_El ', 1,dim2); %make NGRID
x=repmat(axis_Az ,dim1, 1); %make NGRID
v=data;

val=interp2(x,y,v,xq,yq); %interpolate data

end

```

C.3.7 Polygon

```

function [Shading,IllS,InRef1, InShade] = Polygon(eM,sPhi, sEl
    ,rC,cond,colr,SpecC, reflTh, reflAz, eR)

r = abs(eM(:,3)./sind(-sEl));
spoly(:,1:3) = [ eM(:,1)+r.*cosd(180+sPhi).*cosd(-sEl), eM
    (:,2)+r.*sind(180+sPhi).*cosd(-sEl), eM(:,3)+ r.*sind(-sEl)
    ] ;
spoly(5,1:3) =spoly(1,1:3) ;

Shading = 1-inpolygon( rC{1,1}(:,:), rC{1,2}(:,:), spoly(:,1),
    spoly(:,2) ) ; % the function gives '1' for the point
    inside the polygon and '0' for others.
%We make the inside(or shaded) points '0', and others '1'

%Plot the black lines indicating the shadow on the reflector
r(1,1)=10;
if cond==1
    plot3([spoly(:,1)], [spoly(:,2)], [spoly(:,3)], colr, '
        LineWidth', 3); hold on
    plot3([spoly(4,1), spoly(4,1)+r(1,1)*cosd(sPhi).*cosd(sEl)],
        [spoly(4,2), spoly(4,2)+r(1,1)*sind(sPhi).*cosd(sEl)], [

```

```

        spoly(4,3), spoly(4,3)+r(1,1)*sind(sEl)], '--', 'Color'
        ,[0.8500 0.3250 0.0980], 'LineWidth', 4); hold on
r(1,1)=1.4;
plot3([spoly(4,1), spoly(4,1)+r(1,1)*cosd(180+sPhi).*cosd(
    sEl)], [spoly(4,2), spoly(4,2)+r(1,1)*sind(180+sPhi).*
    cosd(sEl)], [spoly(4,3), spoly(4,3)+r(1,1)*sind(sEl)], '
    -', 'Color',[0.8500 0.3250 0.0980], 'LineWidth', 4); hold
    on
% plot3([eM(1,1), eM(1,1)+r(1,1)*cosd(180+sPhi).*cosd(sEl)],
    [eM(1,2), eM(1,2)+r(1,1)*sind(180+sPhi).*cosd(sEl)], [eM
    (1,3), eM(1,3)+r(1,1)*sind(sEl)], ':r', 'LineWidth', 2);
    hold on
% plot3([eM(1,1), spoly(1,1)], [eM(1,2), spoly(1,2)], [eM
    (1,3), spoly(1,3)], '-r', 'LineWidth', 2); hold on
end

clear r
sEl=-reflTh; sPhi=180+reflAz;
z=SpecC{1,3}(:, :) ; r=z./sind(-sEl);
x=SpecC{1,1}(:, :)+r.*cosd(sPhi).*cosd(-sEl); y=SpecC
    {1,2}(:, :)+r.*sind(sPhi).*cosd(-sEl);
if cond==1
    plot3([x], [y], [zeros(size(x))], 'o', 'MarkerEdgeColor',[0
        0 0] , 'MarkerFaceColor', [0.9290 0.6940 0.1250], '
        MarkerSize', 5, 'LineWidth',0.5 ); hold on
end

%check if they lie on the reflector and then check if they
    are shaded.
%This gives an warning that the results from the INPOLYGON may
    not be
%reliable, if the angle of elevation equals the angle of the
    module (parallel),
%meaning that due to the infinitely small thickness of the
    panel, no shadow
%will exist
InRef1 = inpolygon(x,y,eR(:,1),eR(:,2)) ;
InShade = inpolygon(x,y,spoly(:,1),spoly(:,2)) ;
InShade = 1-InShade;
IllS = InShade&InRef1;

end

```

C.4 Yield Calculation Code

```

%% Define Parameters
Efficiency_Cone = 0.634202919215434; % -> based on 40 deg cone

```

```

    size
Efficiency_Spec_FSLSC = 0.90; % -> based on specular
    reflection
Efficiency_SpecDiff = 0.90;%efficiency

FF = 0.85; %[-] -> assumption
Voc = 0.730; %[V] -> based on Rebecca's paper

load("OccuranceMatrixPerHour_newEveryHour.mat") %load
    occurance matrix
load("NRELIrradiance2018.mat"); % irradiance data for 2018 (
    one year)
Daily_DNI = Daily_DNI';
Daily_DHI = Daily_DHI';
load("AveragedNRELIrradiance2018.mat") % irradiance data as an
    average for 2017-2019
Daily_DNI = Averaged_Daily_DNI';
Daily_DHI = Averaged_Daily_DHI';
Daily_DNI(366,24) = 0;
Daily_DHI(366,24) = 0;

%% Calculate Yield from Diffuse Irradiance
% FSLSC
load(strcat(pwd, '\EveryAngle_FSLSC_10pix\M.mat'))
results_FSLSC.jsF = results.jsF.*Efficiency_Spec_FSLSC;
results_FSLSC.jsR = results.jsR.*Efficiency_Spec_FSLSC;
results_FSLSC.jsT = results.jsT.*Efficiency_Spec_FSLSC;
results_FSLSC.jeF = results.jeF.*Efficiency_Cone;
results_FSLSC.jeR = results.jeR.*Efficiency_Cone;
results_FSLSC.jeT = results.jeT.*Efficiency_Cone;
Dif_FSLSC = DiffuseYieldCalculator(FF,Voc,results_FSLSC,
    Daily_DHI); %[kW/m2/year]

% Diffuse
load(strcat(pwd, '\EveryAngle_Diffuse_10pix\M.mat'))
results_Diff.jeF = results.jeF.*Efficiency_SpecDiff;
results_Diff.jeR = results.jeR.*Efficiency_SpecDiff;
results_Diff.jeT = results.jeT.*Efficiency_SpecDiff;
Dif_Diff = DiffuseYieldCalculator(FF,Voc,results_Diff,
    Daily_DHI); %[kW/m2/year]

% Diffuse
load('strcat(pwd, '\EveryAngle_Specular\M.mat'))
results_Spec.jsF = results.jsF.*Efficiency_SpecDiff;
results_Spec.jsR = results.jsR.*Efficiency_SpecDiff;
results_Spec.jsT = results.jsT.*Efficiency_SpecDiff;
Dif_Spec = DiffuseYieldCalculator(FF,Voc,results_Spec,
    Daily_DHI); %[kW/m2/year]

```

```

% Sky
results_Sky.jSky = results.jSky;
Dif_Sky = DiffuseYieldCalculator(FF,Voc,results_Sky,Daily_DHI)
    ; %[kW/m2/year]

% Optimized Front Solar Panel
load('strcat(pwd,'\EveryAngle_NormalSolarPanel2\M.mat'))
results_NormalsolarPanel.jSky = results.jSky;
Dif_NSP = DiffuseYieldCalculator(FF,Voc,
    results_NormalsolarPanel,Daily_DHI);

%% Calculate Yield from Direct Irradiance
% FSLSC
load(strcat(pwd,'\40DegCone\M.mat'))
results_FSLSC.jsF = results.jsF.*Efficiency_Spec_FSLSC;
results_FSLSC.jsR = results.jsR.*Efficiency_Spec_FSLSC;
results_FSLSC.jsT = results.jsT.*Efficiency_Spec_FSLSC;
results_FSLSC.jeF = results.jeF.*Efficiency_Cone;
results_FSLSC.jeR = results.jeR.*Efficiency_Cone;
results_FSLSC.jeT = results.jeT.*Efficiency_Cone;
Direct_FSLSC = DirectYieldCalculator(FF,Voc,results_FSLSC,
    Daily_DNI,Occurance_Matrix_PerHour); %[kW/m2/year]

% Diffuse
load(strcat(pwd,'\Diffuse_Shweta2\M.mat'))
results_Diff.jeF = results.jeF.*Efficiency_SpecDiff;
results_Diff.jeR = results.jeR.*Efficiency_SpecDiff;
results_Diff.jeT = results.jeT.*Efficiency_SpecDiff;
Direct_Diff = DirectYieldCalculator(FF,Voc,results_Diff,
    Daily_DNI,Occurance_Matrix_PerHour); %[kW/m2/year]

% Diffuse
load(strcat(pwd,'SpecularShweta\M.mat'))
results_Spec.jsF = results.jsF.*Efficiency_SpecDiff;
results_Spec.jsR = results.jsR.*Efficiency_SpecDiff;
results_Spec.jsT = results.jsT.*Efficiency_SpecDiff;
Direct_Spec = DirectYieldCalculator(FF,Voc,results_Spec,
    Daily_DNI,Occurance_Matrix_PerHour); %[kW/m2/year]

% Sky
results_Sky.jSky = results.jSky;
Direct_Sky = DirectYieldCalculator(FF,Voc,results_Sky,
    Daily_DNI,Occurance_Matrix_PerHour); %[kW/m2/year]

% Optimized Front Solar Panel
load(strcat(pwd,'NormalSolarCell2\M.mat'))
results_NormalsolarPanel.jSky = results.jSky;
Direct_NSP = DirectYieldCalculator(FF,Voc,

```

```

    results_NormalsolarPanel ,Daily_DNI ,Occurance_Matrix_PerHour
); %[kW/m2/year]

%% Defining Totals
Plot_Dif_FSLSC = sum(Dif_FSLSC.jeT')+sum(Dif_FSLSC.jsT');
Plot_Dif_Diffuse = sum(Dif_Diff.jeT');
Plot_Dif_Specular = sum(Dif_Spec.jsT');
Plot_Dif_Sky = sum(Dif_Sky.jSky');
Plot_Dif_NSP = sum(Dif_NSP.jSky');

Plot_Dir_FSLSC = sum(Direct_FSLSC.jeT')+sum(Direct_FSLSC.jsT')
;
Plot_Dir_Diffuse = sum(Direct_Diff.jeT');
Plot_Dir_Specular = sum(Direct_Spec.jsT');
Plot_Dir_Sky = sum(Direct_Sky.jSky');
Plot_Dir_NSP = sum(Direct_NSP.jSky');

Plot_Total_FSLSC = Plot_Dif_FSLSC + Plot_Dir_FSLSC;
Plot_Total_Diffuse = Plot_Dif_Diffuse + Plot_Dir_Diffuse;
Plot_Total_Specular = Plot_Dif_Specular + Plot_Dir_Specular;
Plot_Total_Sky = Plot_Dif_Sky + Plot_Dir_Sky;
Plot_Total_NSP = Plot_Dif_NSP + Plot_Dir_NSP;

c1 = [ 1.46159096e-03, 4.66127766e-04, 1.38655200e-02];
c2 = [ 4.32967001e-01, 1.17854987e-01, 5.06159754e-01];
c3 = [ 9.95121854e-01, 6.31696376e-01, 4.31951492e-01];
c4 = [ 9.94523666e-01, 8.41386618e-01, 5.98982818e-01];

%% Efficiency Plot
figure()
plot(sum(Direct_Sky.jSky') .*1000./(2.*sum(Daily_DNI')),
    LineWidth=3,Color=c2)
hold on
%plot(sum(Direct_Sky.jSky') .*1000./(2.*sum(
    HourlyDirectIrradiance_vert')),LineWidth=3,Color=c2)
plot(sum(Dif_Sky.jSky') .*1000./sum(Daily_DHI'),LineWidth=3,
    Color=c3)
xlabel('Days');
ylim([0 0.3])
ylabel('Efficiency');
xlim([0 365])
legend('Direct','Diffuse','Location','north')
set(gca,"FontSize",22)

%% histogram with averages per month
ToBePlotted = Plot_Total_Sky;
DaysPerMonth = [31 28 31 30 31 30 31 31 30 31 30 31 0 0];
BinnedToBePlotted = [];
NuOBins = length(DaysPerMonth);

```

```

index1 = 1;
index2 = 31;
for i=1:1:12
    BinnedToBePlotted(i) = sum(ToBePlotted(1,index1:index2))/
        DaysPerMonth(i);
    index1 = index1 + DaysPerMonth(i);
    index2 = index2 + DaysPerMonth(i+1);
end

figure()
bar(1:1:12,BinnedToBePlotted,'FaceColor',c3, 'BarWidth',1)
xlabel('Months')
ylabel('kWh/m^2/day')
set(gca,'FontSize',22)

%% Running Average Plots
ToBePlotted = Plot_Total_Sky;
Days = length(ToBePlotted);
ToBePlotted = [ ToBePlotted ToBePlotted ToBePlotted];
AveragedTobePlotted = [];
AverageValues_OneSide = 15;
index1 = Days - AverageValues_OneSide;
index2 = Days + AverageValues_OneSide;
for i=1:1:Days
    AveragedTobePlotted(i) = sum(ToBePlotted(1,(i+index1):(i+
        index2)))/(AverageValues_OneSide.*2+1);
end

figure()
plot(AveragedTobePlotted,linewidth=3, Color=c3)

```

C.4.1 DiffuseYieldCalculator

```

function [DiffuseYield] = DiffuseYieldCalculator(FF,Voc,
    Results,DailyIrradiance_Hor)
%Voc [mW]

ResultNames = fieldnames(Results);
days = 366;
[xlen, ylen] = size(Results.(string(ResultNames(1))));
NormalizationFactor_Diffuse = xlen.*ylen; % the number of
    possible elevation-azimuth combinations
NormalizationFactor_AssumedCurrentDensity = 0.7052; %[kW/m2]
    based on type of irradiance (DNI)
DailyIrradiance_Hor_corrected = DailyIrradiance_Hor./1000; %kW
    /m2

for i=1:length(ResultNames)
    DailyYield = [];

```

```

Power_Calculated = [];
HourlyYield = [];
ResultName = string(ResultNames(i)); %retrieve name
r = Results.(ResultName); %[mA/cm2] select matrix
Power_Calculated = r .* Voc .* FF; %[mW/cm2] calculate
    power
Power_Calculated = Power_Calculated./1000.*10000./1000; %[
    kW/m2/year]
Power.(ResultName) = Power_Calculated;
for j = 1:1:days
    Yield = sum(sum(Power_Calculated)) ./
        NormalizationFactor_Diffuse; %[kW/m2/year]
    DailyYield = [DailyYield ; Yield];
end
for h =1:1:24 %hours
    HYield = DailyYield.*DailyIrradiance_Hor_corrected(:,h
        ).*NormalizationFactor_AssumedCurrentDensity;
    HourlyYield(:,h) = HYield;
end
DailyYield_Irradiance.(ResultName) = HourlyYield; %.[kW/m2
/year] corrected for irradiance
end

DiffuseYield = DailyYield_Irradiance;

end

```

C.4.2 DirectYieldCalculator

```

function [DirectYield] = DirectYieldCalculator(FF,Voc,
    Results,DailyIrradiance_Hor,Occurance_Matrix)

ResultNames = fieldnames(Results);
days = 366;
NormalizationFactor_AssumedCurrentDensity = 0.7052; %[kW/m2]
    based on type of irradiance (DNI)
DailyIrradiance_Hor_corrected = DailyIrradiance_Hor./1000; %kW
/m2

%flip the occurance matrix for each day
for i=1:1:days
    for j=1:1:24
        Occurance_Matrix_Flipped(:,:,j,i)= (Occurance_Matrix
            (:,:,j,i)');
    end
end

%calculate the yield
for i=1:length(ResultNames)

```

```

DailyYield = [];
Power_Calculated = [];
HourlyYield = [];
ResultName = string(ResultNames(i)); %retrieve name
r = Results.(ResultName); %[mA/cm2]
Power_Calculated = r .* Voc .* FF; %[mW/cm2] calculate
power
Power_Calculated = Power_Calculated./1000.*10000./1000; %[
kW/m2/year]
Power.(ResultName) = Power_Calculated;
for j = 1:1:days
    for i = 1:1:24
        Occurances = sum(sum(Occurance_Matrix_Flipped(:, :,
            i, j)));
        Yield = Occurance_Matrix_Flipped(:, :, i, j) .*
            Power_Calculated .* 2; %[kW/m2/year]
        Yield = sum(sum(Yield));
        if Occurances ~ 0;
            Norm_Yield = Yield/Occurances; % this
                averaging also makes sure that it is kWh
        else
            Norm_Yield = 0; %make sure that no division by
                0
        end
        HourlyYield(j,i) = Norm_Yield;
    end
end
DailyYield_Irradiance.(ResultName) = HourlyYield.*
    DailyIrradiance_Hor_corrected./
    NormalizationFactor_AssumedCurrentDensity; %[kWh/m2/
    year] corrected for irradiance
end
DirectYield = DailyYield_Irradiance;

end

```

C.5 Data Analysis Codes

C.5.1 Extracting Occurance Matrix

```

clear all
clc

%% Import Data from Excel File

Data = readcell("AnnualSunPath_2022_Enschede_5min.csv"); %read
file
[xlen,ylen] = size(Data); % calculate size

```

```

for i=1:1:xlen
    for j=1:1:ylen
        if isequal(Data(i,j), {'--'})
            Data(i,j) = {NaN}; %delete empty values
        end
    end
end

Data_Mat = cell2mat(Data(2:end,2:end)); % make matrix
Axis_Mat = Data(1,2:end); % make variable with axis
[days,~] = size(Data_Mat);

%% Make one column with all the elevation and azimuth data
% make one column with all elevations
count = 1; % to start with first column

for i = 1:1:days
    Data_Day = Data_Mat(i,:);
    Elevations = [];
    count =1;
    while (count < (ylen-1))
        col = Data_Day(:,count);
        Elevations = [Elevations ; col];
        count = count+2;
    end
    Elevations_PerDay(:,i) = Elevations;

    %make one column with all azimuths
    count = 2; % to start at second column
    Azimuths = [];
    while (count < (ylen))
        col = Data_Day(:,count);
        Azimuths = [Azimuths ; col];
        count = count+2;
    end
    Azimuths_PerDay(:,i) = Azimuths;
end

%% Make a histogram for every hour

% loop over the hours
XBinEdges = [40 50 60 70 80 90 100 110 120 130 140 150 160 170
    180 190 200 210 220 230 240 250 260 270 280 290 300 310
    320];
YBinEdges = [0 3 6 9 12 15 18 21 24 27 30 33 36 39 42 45 48 51
    54 57 60 63];

for j=1:1:days
    indexI = 1;

```

```

indexII = 12;
for i= 1:1:12
    figure()
    h = histogram2(Azimuths_PerDay(indexI:indexII,j),
        Elevations_PerDay(indexI:indexII,j),XBinEdges,
        YBinEdges,'DisplayStyle','tile');
    % calculating values general
    Occurance_Matrix = h.Values;
    Azimuths = h.XBinEdges;
    Elevations = h.YBinEdges;
    BinWidth = h.BinWidth;
    Azimuths = Azimuths(:,1:end-1) + BinWidth(1,1)/2; %
        every azimuth (except last) + half the bin width
    Elevations = Elevations(:,1:end-1) + BinWidth(1,2)/2;
        %every elevation (except last) + half the bin width

    %saving values facade case -> meaning that the azimuth
        and
    %elevation align with the other code
    Occurance_Matrix_ToRun = Occurance_Matrix;
    Elevations_ToRun = 90 - Elevations; %switch to zenith
    Azimuths_ToRun = Azimuths -270; %switch to new
        coordinate system
    indices = find(Azimuths_ToRun<-180); %delete indices
        below -180
    Azimuths_ToRun(indices) = [];
    Occurance_Matrix_ToRun(indices,:) = [];
    indices = find(Azimuths_ToRun>-90); %delete indices
        above -90
    Azimuths_ToRun(indices) = [];
    Occurance_Matrix_ToRun(indices,:) = [];

    %
    Occurance_Matrix_PerHour(:,:,i,j) =
        Occurance_Matrix_ToRun;
    indexI = indexI+12;
    indexII = indexII + 12;%due to five minute interval

    figure()
    imagesc(Occurance_Matrix_PerHour(:,:,i,j))
    title(sprintf('hour - %f',i))
end
disp(j)
end

%% storing results
mkdir(pwd);
save(strcat(pwd, '\OccuranceMatrixPerHour_new.mat'), '

```

```

    Occurance_Matrix_PerHour');

%% Make Histogram & Plot Data
figure;
XBinEdges = [40 50 60 70 80 90 100 110 120 130 140 150 160 170
             180 190 200 210 220 230 240 250 260 270 280 290 300 310
             320];
YBinEdges = [0 3 6 9 12 15 18 21 24 27 30 33 36 39 42 45 48 51
             54 57 60 63];

DayToBePlotted = 300; %which day you would like to plot
for i=DayToBePlotted:100:days
    figure()
    histogram2(Azimuths_PerDay(:,i),Elevations_PerDay(:,i),
               XBinEdges,YBinEdges,'DisplayStyle','tile')
    xlabel('Azimuth [deg]')
    ylabel('Elevation [deg]')
    fancy = magma(100);
    colormap(fancy)
    colorbar()
    set(gca,'color',[0 0 0])
    set(gca,'FontSize',22)
    xlim([0 360])
    ylim([0 90])
end

```

C.5.2 Extracting Irradiance Data

```

    Data = readcell('526386_52.25_6.90_2019.csv'); %read the
    data file

%% Extract Data from CSV file
Month = cell2mat(Data(4:end,2));
Day = cell2mat(Data(4:end,3));
Hour = cell2mat(Data(4:end,4));
DHI = cell2mat(Data(4:end,6));
GHI = cell2mat(Data(4:end,7));
DNI = cell2mat(Data(4:end,8));

%% Convert Irradiance to Hourly Irradiance
%DHI
indexI = 1;
indexII = 4; %everything is steps of four, since the data is
             for 15 minutes
Daily_DHI = ones(365,24);

for d = 1:1:365
    for h = 1:1:24

```

```

        Daily_DHI(d,h) = sum(DHI(indexI:indexII,1));
        indexI = indexI+4;
        indexII = indexII + 4;
    end
end

%GHI
indexI = 1;
indexII = 4;
Daily_GHI = ones(365,24);

for d = 1:1:365
    for h = 1:1:24
        Daily_GHI(d,h) = sum(GHI(indexI:indexII,1));
        indexI = indexI+4;
        indexII = indexII + 4;
    end
end

%DNI
indexI = 1;
indexII = 4;
Daily_DNI = ones(365,24);

for d = 1:1:365
    for h = 1:1:24
        Daily_DNI(d,h) = sum(DNI(indexI:indexII,1));
        indexI = indexI+4;
        indexII = indexII + 4;
    end
end

Daily_DNI = Daily_DNI './4; %correction for having 4 data
           points per hour
Daily_GHI = Daily_GHI './4; %correction for having 4 data
           points per hour
Daily_DHI = Daily_DHI './4; %correction for having 4 data
           points per hour

%% Figures
c1 = [ 1.46159096e-03,    4.66127766e-04,    1.38655200e-02];
c2 = [ 4.32967001e-01,    1.17854987e-01,    5.06159754e-01];
c3 = [ 9.95121854e-01,    6.31696376e-01,    4.31951492e-01];
c4 = [ 9.94523666e-01,    8.41386618e-01,    5.98982818e-01];

figure()
plot(sum(Daily_DHI),LineWidth=3,Color=c1)
hold on

```

```

%plot(sum(Daily_GHI),LineWidth=3,Color=c2)
plot(sum(Daily_DNI),LineWidth=3,Color=c3)
legend('DHI','DGI','DNI')
xlim([0 365])
set(gca,'FontSize',22)

%% Check - Average for each month
indexI = 1;
indexII = 30;
for m = 1:1:12
    Monthly_DNI(m) = sum(sum(Daily_DNI(:,indexI:indexII)))/30;
    indexI = indexI + 30;
    indexII = indexII + 30;
end

%%
kWhPerYear = sum(sum(Daily_GHI)./1000)

%%
%mkdir(pwd);
%save(strcat(pwd,'\NRELirradiance2018.mat'),'Daily_DNI','
    Daily_DHI'); %SAVE CORRECT ONES!

%% averaging over years
%Daily_DNI2019 = Daily_DNI;
%Daily_DHI2019 = Daily_DHI;

Averaged_Daily_DNI = (Daily_DNI2017 + Daily_DNI2018 +
    Daily_DNI2019) ./3;
Averaged_Daily_DHI = (Daily_DHI2017 + Daily_DHI2018 +
    Daily_DHI2019) ./3;
save(strcat(pwd,'\AveragedNRELirradiance2018.mat'),'
    Averaged_Daily_DNI','Averaged_Daily_DHI'); %SAVE CORRECT
    ONES!

```